Doctoral Dissertations   Graduate School

8-1978

Nonlinear Dynamic Modeling of a Once-Through Steam Generator

Ming-Huei Lee
University of Tennessee - Knoxville

To the Graduate Council:

I am submitting herewith a dissertation written by Ming-Huei Lee entitled "Nonlinear Dynamic Modeling of a Once-Through Steam Generator." I have examined the final electronic copy of this dissertation for form and content and recommend that it be accepted in partial fulfillment of the requirements for the degree of Doctor of Philosophy, with a major in Nuclear Engineering.

T. W. Kerlin, Major Professor

We have read this dissertation and recommend its acceptance:

J. E. Mott, James C. Robinson, P. F. Pasqua, Chia Chang Shih

Accepted for the Council:
Dixie L. Thompson

Vice Provost and Dean of the Graduate School

(Original signatures are on file with official student records.)

To the Graduate Council:
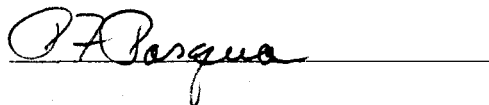
I am submitting herewith a dissertation written by Ming-Huei Lee entitled "Nonlinear Dynamic Modeling of a Once-Through Steam Generator." I recommend that it be accepted in partial fulfillment of the requirements for the degree of Doctor of Philosophy, with a major in Nuclear Engineering.

_____
T. W. Kerlin, Major Professor
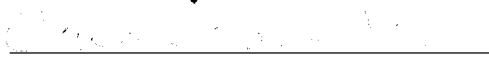
We have read this dissertation and recommend its acceptance:

_____

_____

_____

Accepted for the Council:

_____
Vice Chancellor
Graduate Studies and Research

NONLINEAR DYNAMIC MODELING OF A

ONCE-THROUGH STEAM GENERATOR

A Dissertation

Presented for the

Doctor of Philosophy

Degree

The University of Tennessee, Knoxville

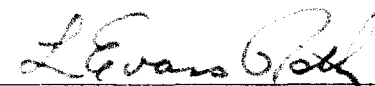Ming-Huei Lee

August 1978

ACKNOWLEDGMENTS

ABSTRACT

A detailed, nonlinear, many lump, moving boundary dynamic model for a helical coiled once-through steam generator with nonuniform tube cross section is developed. Six flow regimes are employed in the model; each regime may consist of more than one section. The responses for two lumping cases (i.e., two sets, each with a different number of sections in the model) are compared with the same perturbations. Bases for selection of the number of sections and the calculational time step are suggested.

The steady state calculation for generating the state variable distributions along the tube coordinate is developed. Information obtained from the steady state distributions is compared with transient response at the final observation time. The comparisons for all individual steam generator input perturbations are satisfactory. Confidence in the correctness of the steady state calculation is obtained from the comparison of the steady state results with a set of design data.

Nonlinearity of the steam generator responses is studied. Comparison of the transient responses with two other models is given. The Fort St. Vrain 330 MW(e) steam generator is used as the reference design for this study.

TABLE OF CONTENTS

LIST OF TABLES

LIST OF FIGURES

NOMENCLATURE

$\overline{A}$	average cross section area for a section in fluid flow or tube
$A_a(t)$	area of a closed surface moving in space
A_g	free flow cross section area for helium in the shell side
A_i	tube or fluid flow cross section area for section i
$\overline{A}_i$	average cross section area for section i in fluid flow or tube
A_{in}	tube or fluid flow cross section area at the entrance of a section
$\overline{A}_{mi}$	average tube metal cross section for tube section i
A_o	tube or fluid flow cross section area at the outlet of a section
A_{sg}	tube outer surface area in a section of the primary fluid
A_{ss}	tube inner surface area in a section of the secondary fluid
B	a constant in equation (5-13)
C_m	tube heat capacity
C_{mi}	tube heat capacity for section i
C_p	fluid heat capacity
CPA1	factor defined by equation (3-32-8)
CPA2	factor defined by equation (3-32-9)
C_{pf}	heat capacity of liquid
C_{pg}	heat capacity for helium
C_1	unit conversion factor, .1250 $(BTU/ft^3)/psi$
C_2	unit conversion factor, 4632.48 $(lb\text{-}ft/sec^2)/(ft^2\text{-}psi)$
C_3	shell length/tube length

C_{6gi}	model correction factor for momentum for helium section i
C_{6i}	model correction factor for momentum for steam/water section i
C_{7gi}	model correction factor for energy for helium section i
C_{7i}	model correction factor for energy for steam/water section i
C_9	unit conversion factor, 1/14.5038 bar/psi
D	tube diameter
$\overline{D}$	average diameter of a fluid flow cross section
$\dfrac{D}{Dt}$	differential operator, $\dfrac{\partial}{\partial t} + \vec{v} \cdot \nabla$
$\dfrac{d}{dt}$	total differentiation with respect to time
DA1	factor defined by equation (3-45-8)
DA2	factor defined by equation (3-45-9)
DD1	factor defined by equation (3-45-6)
DD2	factor defined by equation (3-45-7)
d_i	tube inner diameter
$\overline{D}_i$	average diameter of a fluid flow cross section for section i
DID1	tube inner diameter
DID2	tube inner diameter
DPR	factor given by equation (3-47-2)
DPU	factor given by equation (3-47-1)
dV	differential volume element
DX_{Lb}	factor defined by equation (3-45-5)
DX_{Lf}	factor defined by equation (3-45-4)
DX_{pc}	factor defined by equation (3-45-2)
DX_{Tm}	factor defined by equation (3-45-1)

Dx_w factor defined by equation (3-45-3)

$EK_{g \to m}$ heat conductance defined as the rate of heat transfer from gas side to tube metal per unit temperature difference between gas and tube metal

$EK_{gs \to m}$ heat conductance defined as the rate of heat transfer from gas side to tube metal per unit temperature difference between tube outer surface temperature and tube metal

$EK_{g \to 1}$ heat conductance defined as the rate of heat transfer from gas side to tube subsection 1 per unit temperature difference between gas and tube subsection 1

$EK_{m \to s}$ heat conductance defined as the rate of heat transfer from tube metal to secondary fluid per unit temperature difference between tube metal and secondary fluid

$EK_{m \to ss}$ heat conductance defined as the rate of heat transfer from tube metal to secondary fluid per unit temperature difference between tube metal and tube inner surface temperature

$EK_{1 \to 2}$ heat conductance defined as the rate of heat transfer from tube subsection 1 to tube subsection 2 per unit temperature difference between subsection 1 and 2

$EK_{2 \to s}$ heat conductance defined as the rate of heat transfer from tube subsection 2 to secondary fluid per unit temperature difference between tube subsection 2 and secondary fluid

E_p factor given by equation (3-15)

E_s a constant in equation (3-15)

f	friction factor
F	factor defined by equation (5-9)
f_c	friction factor for coiled tube
f_{eff}	effective friction factor for fluid flow in the tube bundle in the shell side
f_i	friction factor for section i
f_s	friction factor for straight tube
$f_{T.P.}$	two phase flow friction factor
F_1	a function for F
F_2	a function for suppression factor
G	mass flux, mass flow rate per unit area
$\vec{g}$	gravitational acceleration
g	$= \lvert \vec{g} \rvert$
G_{NR}	number of rows in flow direction in a tube bank
h	specific enthalpy of fluid
h_c	convective heat transfer coefficient
h_f	specific enthalpy of liquid water at saturation
h_g	specific enthalpy of water vapor at saturation
h_{fg}	$h_g - h_f$
h_{gi}	specific enthalpy of helium for section i
h_i	specific enthalpy of steam/water for section i
h_{in}	specific enthalpy of fluid at the entrance of a section
h_{NCB}	nucleate boiling heat transfer coefficient
h_o	specific enthalpy of fluid at the outlet of a section
h_p	heat transfer coefficient on the primary fluid (helium) side

h_s heat transfer coefficient on the secondary fluid (steam/water) side

h_t heat transfer coefficient

$\overline{\overline{I}}$ unit matrix

i_b index for the beginning section of a region represented by a flow regime

i_ℓ index for the last section of a region represented by a flow regime

I_p relative index for a section in a given region

k thermal conductivity

k_f thermal conductivity of liquid

k_g thermal conductivity of vapor

ℓ tube length

ℓ^* tube length measured from the entrance of water to where tube cross section change takes place

$\Delta\ell$ $\ell_o - \ell_i$, length of a tube section

L_b lower boundary location of a region represented by a flow regime (see Figure 3.7.2, 3.7.3)

L_f upper boundary location of a region represented by a flow regime (see Figure 3.7.2, 3.7.3)

ℓ_i tube length measured from the water entrance to one end of section i (see Figure 3.7.2 and Figure 3.7.3)

$\Delta\ell_i$ tube length for section i

ℓ_{in} tube length measured from the entrance of water to the inlet of a section

ℓ_o tube length measured from the water entrance to the outlet of a section

L1   location for onset of nucleate boiling

L2   location for zero steam quality

L3   location where steam quality equals to X_{DNB}

L4   location where steam quality equals to 1

M   Mach number

Min(,)   the minimum value of two quantities in (,)

$\hat{n}$ unit vector of a surface

n   a constant defined in equation (5-13)

NDI   number of sections in a region

P   pressure

PA1   factor defined by equation (3-32-8)

PA2   factor defined by equation (3-32-9)

P_c pressure at departure from nucleate boiling

PCT   factor given by equation (3-49-4)

P_{gi} helium pressure for section i

PHX   factor defined by equation (3-42-8)

P_i pressure for section i

P_{in} pressure at the entrance of a section

P_o pressure at the outlet of a section

P_r Prandtl number

PRMB   factor defined by equation (3-42-3)

PRMF   factor defined by equation (3-42-4)

PRUB   factor defined by equation (3-42-5)

PRUF	factor defined by equation (3-42-6)
PRU1	factor defined by equation (3-42-1)
PRU2	factor defined by equation (3-42-2)
ΔP_{sat}	difference in saturation pressures corresponding to ΔT_{sat}
P_{s1}	pressure at the location where the change of tube cross section takes place
PVX	factor defined by equation (3-42-7)
Q	heat flux
$\vec{q}$	heat flux vector
$\hat{q}$	heat flux unit vector
Q_{gi}	heat transfer per unit time from helium section i to a tube section
Q_r	rate of heat transfer in the radial direction of a tube cross section
Q_{rg}	rate of heat transfer from helium to tube metal for a section
Q_{rs}	rate of heat transfer from tube metal to steam/water for a section
Q_{si}	heat transfer per unit time from a tube section to section i on steam/water side
$\hat{r}$	unit vector in the radial direction in a tube cross section
R	factor defined by equation (3-42-9), gas constant
R_c	radius of tube coil
RAG1	factor defined by equation (3-32-10)
RAG2	factor defined by equation (3-32-11)
RAH1	factor defined by equation (3-32-5)

RAH2	factor defined by equation (3-32-7)
RAUM1	factor defined by equation (3-32-14)
RAUM3	factor defined by equation (3-32-15)
RAU1	factor defined by equation (3-32-4)
RAU2	factor defined by equation (3-32-6)
RA1	factor defined by equation (3-32-1)
RA2	factor defined by equation (3-32-2)
RA21	factor defined by equation (3-52-1)
RA3	factor defined by equation (3-32-3)
RA31	factor defined by equation (3-52-2)
Re	Reynolds number of fluid
Re_f	Reynolds number of liquid phase
$Re_{T.P.}$	two phase Reynolds number
r_{in}	tube inner radius
r_o	tube outer radius
R_u	gas constant
$\bar{r}_1$	average radius for tube subsection 1
$\bar{r}_2$	average radius for tube subsection 2
S	factor defined by equation (3-42-10)
S_R	suppression factor
S_v	state variable
SXG1	factor given by equation (3-32-16)
SXG2	factor given by equation (3-32-17)
SXG3	factor given by equation (3-32-18)
SXG4	factor given by equation (3-32-19)

$\bar{\bar{T}}$	stress tensor
T_g	primary fluid (helium) temperature
$\bar{T}_g$	helium average temperature of a section
T_{gb}	base temperature for helium
T_{gin}	helium temperature at the entrance of a section
T_{go}	helium temperature at the outlet of a section
T_{gs}	tube surface temperature on the primary fluid (helium) side
T_m	tube metal temperature
$\bar{T}_m$	tube metal average temperature
T_{mi}	tube metal average temperature for section i
T_s	secondary fluid (steam/water) temperature
T_{sat}	saturation temperature
ΔT_{sat}	tube wall superheat ($T_{ss} - T_{sat}$)
T_{ss}	tube surface temperature on the secondary fluid (steam/water) side
T_{ssi}	tube surface temperature on the secondary fluid (steam/water) side for section i
$<T>_1$	tube average temperature for subsection 1
$<T>_2$	tube average temperature for subsection 2
u	specific internal energy
$\bar{u}$	average specific internal energy of fluid in a section
u_i	specific internal energy for section i
u_{gi}	helium specific internal energy for section i
URAG12	factor given by equation (3-32-12)
URAG2	factor given by equation (3-32-13)

V	fluid speed
$\vec{V}$	fluid velocity
v	specific volume
$V_a(t)$	a volume moving in space
V_e	sonic speed in fluid
$\vec{V}_e$	sonic velocity in fluid
v_f	specific volume of liquid water at saturation
v_{fg}	$v_g - v_f$
v_g	specific volume of water vapor at saturation
W	fluid mass flow rate
$\overline{W}$	average fluid mass flow rate for a section
ΔW	variation in mass flow rate
W_F	tube length fraction occupied by cross section XA2 in a section
W_{gi}	helium mass flow rate for section i
W_i	steam-water mass flow rate for section i
$\vec{W}_i$	fluid mass velocity at the entrance of a section
W_{in}	fluid mass flow rate at the entrance of a section
W_o	fluid mass flow rate at the outlet of a section
$\vec{W}_o$	fluid mass velocity at the outlet of a section
X	steam quality
XA1	fluid flow cross section area
XA2	fluid flow cross section area
X_{DNB}	steam quality at which departure from nucleate boiling occurs
X_i	steam quality for section i

X_{tt}	factor given by equation (5-10)
γ_1	factor defined by equation (3-49-1)
γ_2	factor defined by equation (3-49-2)
γ_3	factor defined by equation (3-49-3)
ϵ	average tube roughness
ϵ_1	width of tube subsection 1 in radial direction
ϵ_2	width of tube subsection 2 in radial direction
μ	fluid viscosity
μ_f	liquid viscosity
μ_{fg}	difference in viscosity between liquid and vapor phases
μ_g	viscosity of water vapor
π	3.14159
ρ	density
$\bar{\rho}$	average density for a section
ρ_f	density of liquid phase
ρ_g	density of vapor phase
ρ_{gi}	helium density for section i
ρ_i	density for section i
ρ_{in}	density of a fluid or tube at the fluid entrance of a section
ρ_{mi}	tube metal density for section i
ρ_{m1}	tube metal density in subsection 1
ρ_{m2}	tube metal density in subsection 2
ρ_o	fluid or tube density at the outlet of a section
σ	surface tension of water
$\bar{\bar{\tau}}$	viscous stress tensor

ϕ	gravitational potential function
$\hat{\omega}$	velocity of a volume surface
Ω	total energy per unit mass

Superscripts

$=$	matrix, tensor
$\hat{}$	unit vector
$>$	vector
$-$	denotes average property

Subscripts

c	coiled tube or at DNB
eff	effective
f	liquid phase
g	primary fluid (helium) or vapor phase
gi	helium section i
gs	denotes at tube outer surface in a section of the primary fluid
i	section i or at inner
in	at entrance
m	tube
mi	tube section i
m1	tube subsection 1
m2	tube subsection 2
NCB	nucleate boiling
o	out, outlet or outer

rg	from helium to a section in radial direction
rs	to steam/water in radial direction
s	secondary fluid or straight tube
sg	denotes at tube outer surface in a section of the primary fluid
si	secondary fluid (steam/water) section i
ss	denotes at tube inner surface in a section of the secondary fluid
T.P.	two phase

Mathematical Notation

∇	gradient operator, $\hat{i}\dfrac{\partial}{\partial x} + \hat{j}\dfrac{\partial}{\partial y} + \hat{k}\,\dfrac{\partial}{\partial z}$
$\dfrac{\partial}{\partial t}$	partial derivative
$\lvert\;\rvert$	scalar of a vector or absolute value of a variable which is not a vector
$\langle\;\rangle$	volume averaged quantity
Δ	difference or variation

CHAPTER 1

INTRODUCTION

The dynamic behavior in once-through steam generators is inherently distributed—parameter and nonlinear. The research presented here deals with the development of a very detailed, many lump, nonlinear once-through steam generator model for studying its nonlinear dynamics.

Because of its compact size, high thermal efficiency and fast response to loads, the once-through steam generator is being utilized increasingly in the nuclear industry. However a major disadvantage of this type steam generator is the complexity of its dynamics. This presents control and design problems. Nonlinearities, large variations in properties along spatial coordinates, complex two phase phenomena and instability[1,2,3,4] of the flow system are the major factors that contribute to the complexity. Dynamic studies are quite necessary for providing information for designing and improving control systems in the once-through steam generator system.

Dynamic modeling is a means of studying system dynamic and control. The research on dynamic modeling also extends to system parameter identification.[5,6] The model can be based on a theoretical approach or an empirical approach. The latter requires the operating system to be tested while the former can be performed before system testing. Both linear and nonlinear modeling formulations are used for dynamic studies. The linear model employs linearized differential equations, which means the resulting simulation is suitable only for small

1

perturbations about a preset operating level. The nonlinear model uses nonlinear differential equations, which describes the nonlinearities of the system behavior and does not limit the simulation to small perturbations. In this research, the theoretical nonlinear modeling approach is adopted.

Previous researches on once-through steam generator modeling were reviewed by C. W. Savery et al.[7] In the following, recently published articles on nonlinear modeling for once-through steam generators are reviewed.

Ray and Bowman[8] developed a nonlinear, lumped parameter, moving boundary model for a once-through steam generator used in a gas cooled power plant. Their model consisted of three sections: the economizer, the evaporator and the superheater. Six differential equations derived from the conservation equations were employed to describe time derivatives of moving boundaries, internal energy and density in the secondary fluid. The mass flow rates were calculated either through quasistatic momentum equations without a velocity head term or by using algebraic relationships. Other variables were obtained from thermodynamic property equations or algebraic equations. For the primary fluid, only energy equations were described; the mass and momentum balances were ignored since steady flow and constant pressure in the primary coolant were assumed.

Chen[9] developed a nonlinear once-through steam generator model for use in the pressurized water reactor system. It was a lumped parameter model with moving boundaries, which consisted of subcooled, saturated

and superheated regions. Each region was further divided into two subregions except the saturated region which was treated with one section. Fourteen state variables, including ten temperatures, two levels, and two pressures were selected in his work. Some important treatments for his model formulation included employing compressibility-adjusted ideal gas state equations for superheated steam, using the critical flow relationship and the orifice flow equation for evaluating mass flow rates, linear variation of steam quality along the axial coordinate and using a zero time constant formulation for calculating boiling rate. The quasi-static momentum equation was also employed.

The once-through steam generator model developed by Kwatny and Konopacki[10] was a nonlinear moving boundary model. It was used to represent a prototypical 1160 MW(e) HTGR steam generator. Their model had two sections in the economizer, and one section in the evaporator and superheater each. In the steam/water side, all friction effects were lumped at the inlet to the respective sections and quasi-static momentum equations or equivalent orifice equations were used to calculate mass flow rates. The evaporator was modeled by two elements. The first represented a lumped frictional resistance. The second was a frictionless heated section. The pressure drop across the heated section was assumed negligible so that pressure, temperature and densities of liquid and vapor were independent of length and dependent on time only. Therefore their mass balance and energy balance equations appeared similar in form to those in the fixed boundary model. Furthermore, the liquid velocity at a characteristic length in the evaporator was made identical to the

equilibrium liquid velocity at 0.5 steam quality and the mass flow rate
at the outlet of the evaporator was made equal to that at a characteristic
length. These two assumptions together with an orifice equation were
used to determine the mass flow rates in the evaporator. An orifice
equation was also used to calculate the superheater length. The primary
fluid flow was considered to be quasi-static, which resulted in zero
time derivatives in the mass balance and energy balance equations in
their model.

Bruens et al.[11] developed models within one basic modeling concept
for LMFBR, MSBR and PWR once-through steam generators. A distributed
parameter approach was employed. Compressibility and spatial variations
in velocity of the single-phase heating fluids were neglected and only
energy conservation was considered. A homogeneous flow model was assumed
for the two phase flow region. In the treatment of the momentum equation,
a quasi-static form without the acceleration term was used. For the tube
wall, two first-order differential equations for two surface temperatures
were used. Except for the MSBR steam generator model, the specific
enthropy was used instead of the enthalpy as one of the state variables
in their model.

Blast,[12] a digital computer program developed by Hedrick and
Cleveland, simulated the high temperature gas cooled reactor reheater-
steam generator module with a multimode, fixed boundary, homogeneous
flow model. This model accepted as many as twenty nodes for steam/water,
tube and helium regions respectively to represent the reheater,
economizer, evaporator and superheater sections in the reheater-steam

generator module. The flow regimes included the subcooled convection, nucleate boiling, transition boiling, film boiling and the superheated convection regimes. The differential equations derived from the conservation of energy, mass and momentum were developed for each node using their nodal description. An implicit technique[13,14,15] was employed to solve these differential equations. Linear interpolation and iteration techniques were applied to calculate pressure, temperature and other thermodynamic properties.

From the above literature review, the following conclusions are drawn:

Increasing the number of sections in dynamic models is a trend for studying dynamic behavior for once-through steam generator. However in the case of many section modeling, the complexity increases and the computing time becomes of great concern. An adequate treatment for section division in the model has not yet been suggested.

Assumptions and simplifications are generally used in the model for circumventing difficulties encountered in nonlinear modeling and obtaining an effective model. But inconsistent assumptions and simplifications are found in many models. This may arise because of different steam generator characteristics and different purposes of the simulation studies. In many models, some formulations in the quasi-static form are accepted.

In this study, a more generalized modeling technique for a many lump, moving boundary model will be presented. It is a nonlinear model which consists of the subcooled convection region, subcooled nucleate

boiling region, saturated nucleate boiling region, film boiling region, and superheater I and II regions. Each region may be divided into multiple sections. An adequate treatment for the section division in the model will be suggested. In addition, a detailed method for determining moving boundaries and a new method for evaluating heat transfer conductances and tube surface temperatures is described. Most of the major difficulties in the nonlinear modeling of the once-through steam generator are solved in detail.

A Fort St. Vrain 330 Mw(e) High Temperature Gas Cooled Reactor steam generator[16] is used in this study. The modeling techniques for the special features of this steam generator such as nonuniformity in tube diameters, coexistence of the counter flow and the parallel flow in the superheater region and effects of the helical coil geometry are included. Even though the Fort St. Vrain system steam generator was used to demonstrate the method the computer program is suitable for analyzing other steam generators of similar design.

CHAPTER 2

DESCRIPTION OF THE FORT ST. VRAIN HIGH

TEMPERATURE GAS COOLED REACTOR

330 MW(e) STEAM GENERATOR

The Fort St. Vrain 330 MW(e) steam generator module is a helical
coil, once-through type, which is designed to produce superheated steam
at 2400 psig and 1000°F at the main steam stop valves of the high pressure
turbine and to reheat steam to 1000°F before it enters the intermediate
turbines.

Two identical steam generating units are employed in two primary
coolant loops. Each unit contains six identical modules. In each module,
the reheater section is located at the top, then followed by the steam
generator containing the superheater II, superheater I, evaporator and
economizer sections in succession. The hot primary coolant, helium,
from the reactor enters the top of the module then flows downward in the
shell side and leaves the steam generator at the bottom of the economizer
section. The secondary coolant loops are made of helically coiled tubes.
In the economizer-evaporator-superheater I section, water flows upward to
produce steam in countercurrent flow. In superheater II, the steam
coming from superheater I enters at the top and flows downward to form
cocurrent flow. The steam from superheater II enters the high pressure
turbine and the exhausted steam enters the reheater after driving the
helium circulator turbines. In the reheater section, steam flows upward

7

to produce countercurrent flow then enters an intermediate pressure turbine.

The lengths of helically wound tube bundles are designed to produce equal heat transfer to each tube. Therefore the bundles are neither in staggered or in-line arrays. The tube dimensions and material used are shown in Table 2.1. In this table, other important physical characteristics are also shown. The schematic diagram of a Fort St. Vrain 330 MW(e) steam generator module is shown in Figure 2.1. The arrangement of the steam generator in the Fort St. Vrain nuclear power plant reactor is shown in Figure 2.2. A set of design conditions is given in Table 2.2.

TABLE 2.1

FORT ST. VRAIN 330 MW(e) STEAM GENERATOR PHYSICAL
CHARACTERISTICS (SINGLE MODULE DATA)[17,18]

	EES[a]	SH2[b]
Number of tube	54	54
Effective heat transfer area without leads (ft^2)		
Installed	2480	850
Ideal	2120	704
Superficial gas flow area (ft^2)	18.634	15.569
Area occupied by:		
Tubing	11.657	9.367
Support structure	0.435	0.420
Effective transverse tube spacing (pitch) (inches)	1.42	1.48
Effective longitudinal tube spacing (pitch) (inches)	1.47	1.44
Tube outside diameter (inches)	1.00	1.00
Tube wall thickness (inches)	.138/.138/.225	.205
Tube material	SA-213 T2/T22/T22	SB-163-GR2 NI-FE-CR
Effective tube length (ft)		
Installed	175.	60.
Ideal	149.99	49.81
Cross-sectional free flow area (ft^2)	6.542	5.782
Coil diameter[c] (ft)	3.88	3.88

TABLE 2.1 (continued)

	EES	SH2
Tube relative roughness[d]	5.6×10^{-3}	$.41 \times 10^{-3}$
Friction factor in shell[e]	.12	.12

[a]EES = Economizer-Evaporator-Superheater I.

[b]SH2 = Superheater 2.

[c]Average values estimated from data in reference 18.

[d]Values obtained from reference 18.

[e]Values obtained by using Figure 5.1.
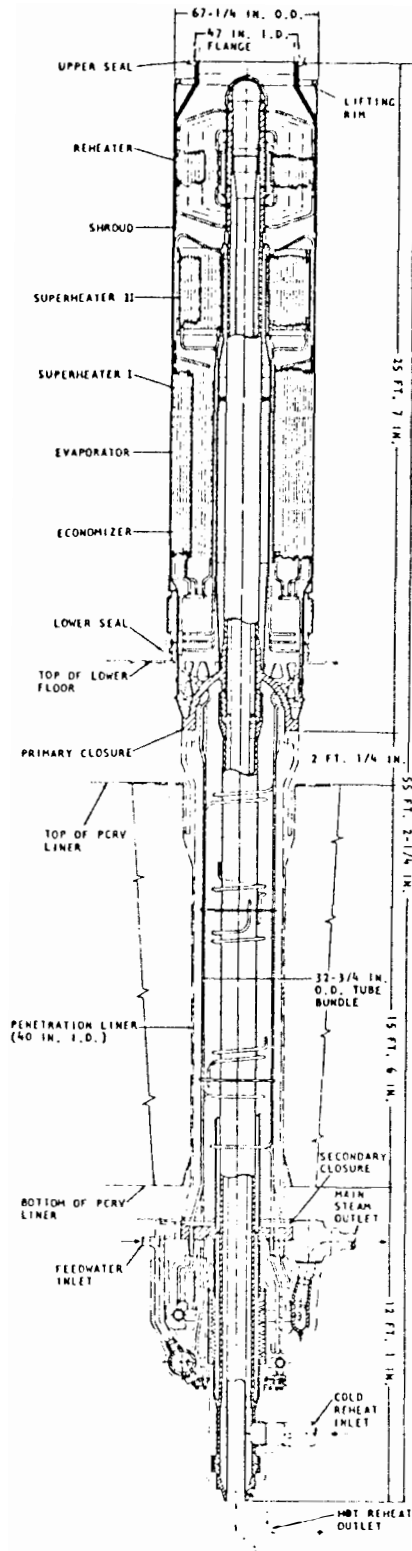
Figure 2.1. Fort St. Vrain Nuclear Power Plant Steam Generator Module.

Helium
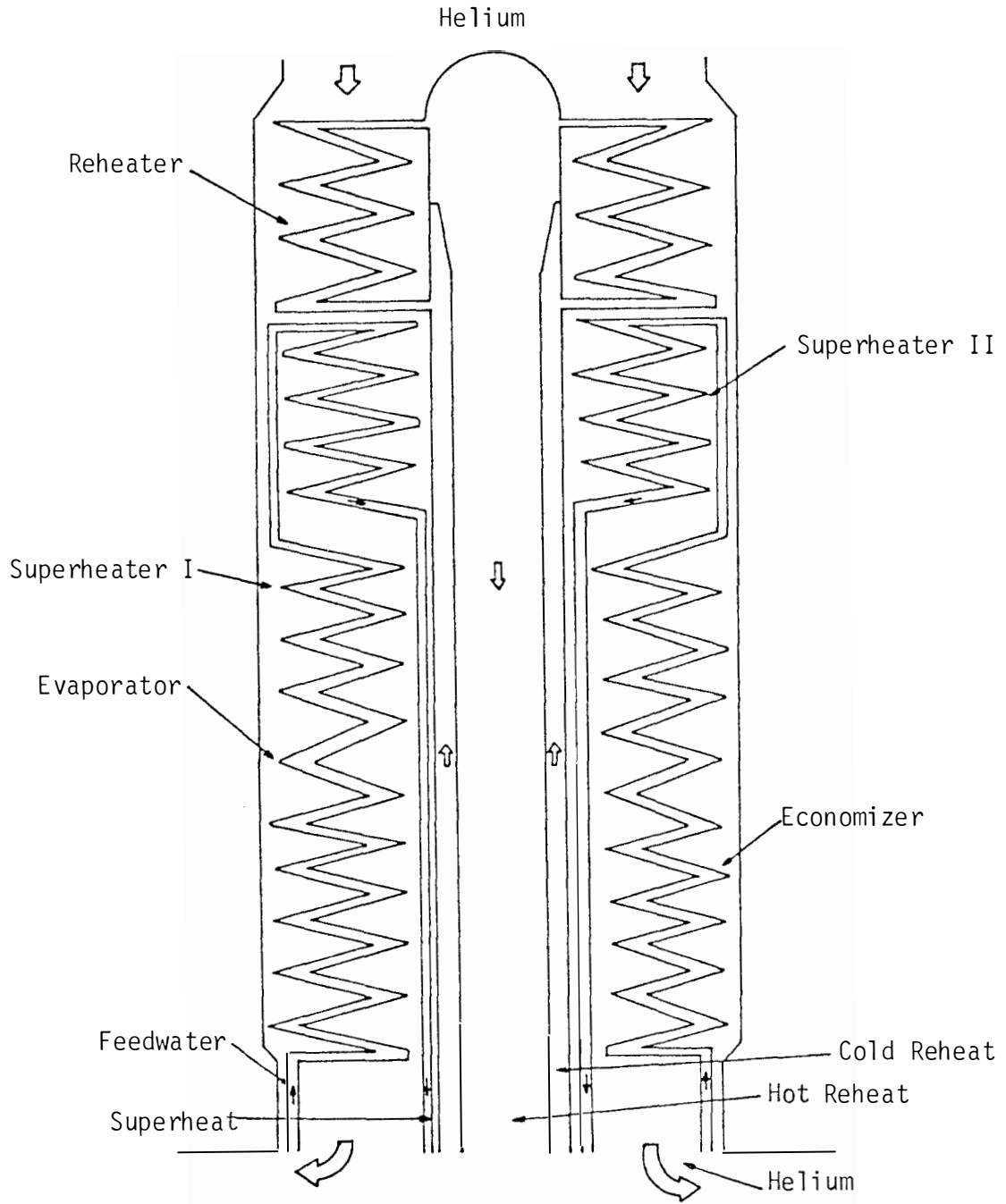
STEAM GENERATOR SCHEMATIC DIAGRAM

Figure 2.1 (continued)
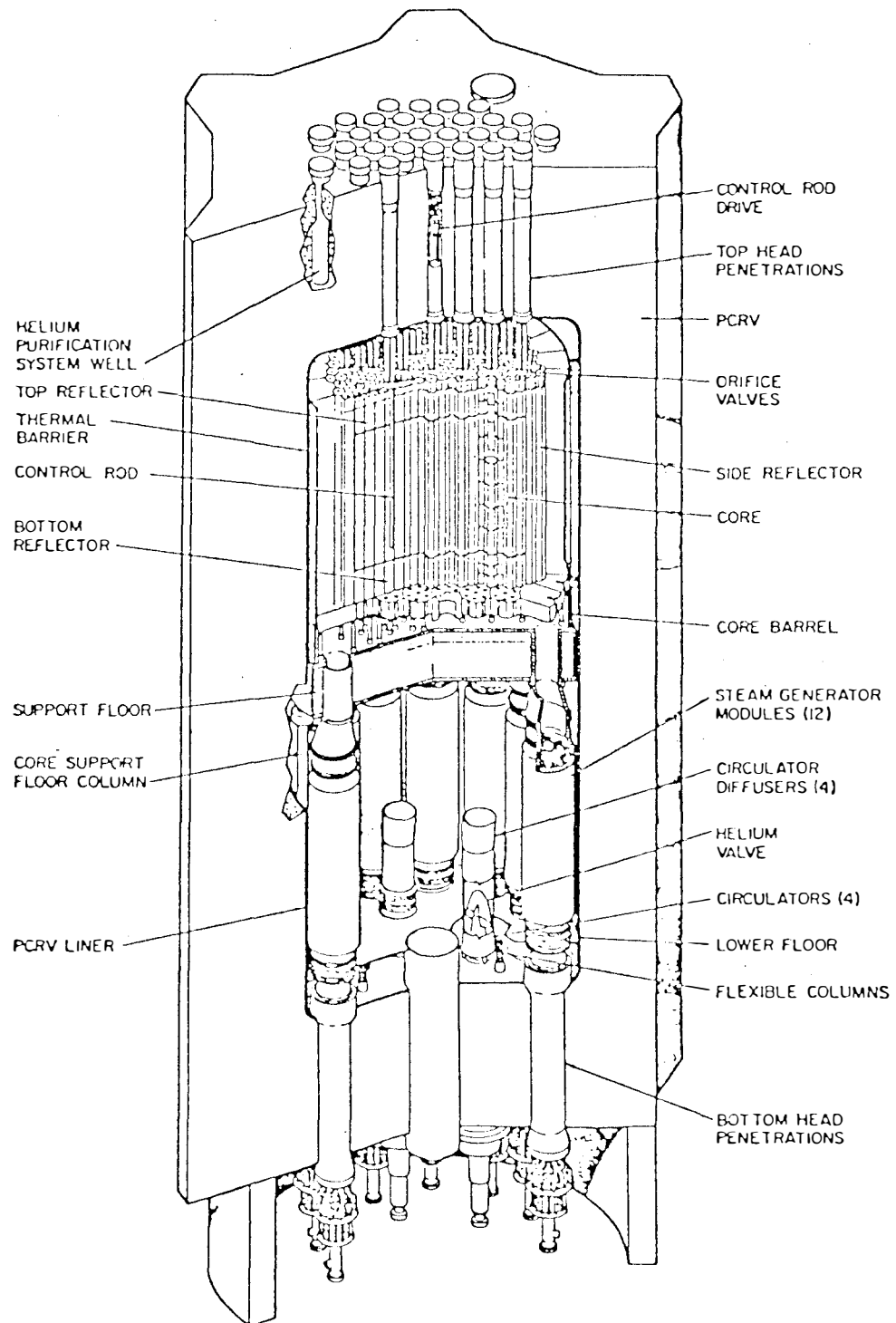
Figure 2.2. Fort St. Vrain 330 MW(e) High Temperature Gas Cooled
Reactor Arrangement.

TABLE 2.2

FORT ST. VRAIN 330 MW(e) NUCLEAR POWER PLANT STEAM
GENERATOR DESIGN CONDITIONS (SINGLE MODULE
DATA FOR 100% STEAM FLOW)[19]

	Helium	Feedwater/Main Steam
Flow (lbm/hr)	284170	192110
Inlet pressure (psia)	690	2980
Outlet pressure (psia)	686	2640
Inlet temperature (°F)	1331	415
Outlet temperature (°F)	741	1030

CHAPTER 3

DEVELOPMENT OF THE DYNAMIC MODEL

In this chapter, the development of the nonlinear model using the lumped parameter approach is described.

3.1 Flow Regimes and Their Boundary Conditions

The water in the once-through steam generator is forced to circulate through the continuous piping system, which experiences various flow patterns. Each flow pattern is associated with a hydrodynamic or heat transfer theory. Despite difficulties in designating the flow pattern for a specified local flow condition, the following regions are considered in this model:

1. subcooled convective region
2. subcooled nucleate boiling region } economizer

3. saturated nucleate boiling region
4. film boiling region } evaporator

5. superheated region } superheater I and II

Each region is characterized by a heat transfer and hydrodynamic correlation, which is described in Chapter 4.

The conditions for separating one region from another are listed below:

(1) $T_{ss} = T_{sat} (P)$

where

T_{ss} = tube wall temperature

T_{sat} (P) = saturation temperature at pressure P

This condition (that the tube wall temperature is equal to the saturation temperature determined by the local pressure) is used to separate the pure convective region and the nucleate boiling region in the subcooled region.

(2) X = 0

where X = steam quality

The zero steam quality condition (evaluated from the averaged enthalpy) determines the boundary between the subcooled and the saturated regions.

(3) The departure of the nucleate boiling is determined
     from the empirical equation[20]:

$$X_{DNB} = 1.565 \times 10^{-3} \ Q^{0.719} \ G^{-0.212} \ exp \ (1.724 \times 10^{-4} P)$$

where Q is the heat flux in $Btu/(hr\text{-}ft^2)$, G is the mass flux in $lbm/(ft^2\text{-}hr)$ and the pressure, P, is in psi.

(4) X = 1

The 100% steam quality point determines the boundary between the saturated region and the superheated region.

In the Fort St. Vrain steam generator, heat transfers through both counterflow and parallel flow in the superheater. The fifth condition is the location where the flow type changes. It is the boundary for superheater I and the superheater II.

(5) ℓ = 149.99 ft measured along the coiled tube from the

  entrance of water into the steam generator.

Incorporation of the above conditions into the dynamic modeling is shown in Section 3.8 of this chapter.

3.2 Two Phase Flow Model

In a two phase flow system, two basic models are discussed, the homogeneous model and the separated flow model. Regardless of the detailed flow patterns, these two models are generally used in engineering design and applications. However the most valid patterns for the homogeneous model are the bubbly and wispy-annuler flow patterns at high linear velocity and pressures and the separated model is best for the annular flow pattern. The homogeneous model assumes equality of the vapor and liquid linear velocity (i.e. slip ratio equal to one), thermodynamic equilibrium between two phases and a suitably defined single phase friction factor for the two phase flow. In the separated flow model, thermodynamic equilibrium between two phases is also assumed. However, the vapor and the liquid velocities are not necessarily equal and the two phase friction factor which is obtained from empirical correlations or simplified concepts is in terms of flow variables related to the void fraction. Depending on the pressure, mass flow rate, steam quality and other factors, the differences of the correlation values, such as the two phase friction multipliers, resulting from these two models may be significant, especially at lower pressure. At higher pressure, the differences are smaller. On the mass flow rate effect, it is suggested[21] that for systems with a low mass velocity (G < 1.002 x

10^6 lbm/ft^2-hr), the separated flow model using the Martinelli-Nelson correlation provides more accurate pressure drop estimates. In the higher mass velocity ranges (G > 1.475 x 10^6 lbm/ft^2-hr), the homogeneous model gives better results.

For the operating ranges of the Fort St. Vrain steam generator, the homogeneous model is adopted, which is essentially based on the evaluations in Table 3.2.1.

TABLE 3.2.1

SECONDARY FLUID MASS VELOCITY AT SEVERAL TUBE
CROSS SECTIONS IN FORT ST. VRAIN
STEAM GENERATOR

Designed mass flow rate per tube (lb/hr)			3557.59
Tube inside diameter (ft)	0.06033	0.04583	0.04917
Mass velocity, G (lb/ft^2-hr)	1.2439 x 10^6	2.1561 x 10^6	1.8724 x 10^6

3.3 Compressibility of the Working Fluids

Evaluation of the compressibility of the working fluids is helpful in the development of the dynamic model. An important measure of the compressibility effects is the Mach number which is defined as the ratio of the fluid velocity to the velocity of sound.

The flow regimes (designated according to the Mach number) are as follows:

$$M << 1 \qquad\qquad\qquad \text{incompressible flow}$$

$$1/2 < M < 1, \qquad\qquad\qquad \text{subsonic flow}$$

$$M \simeq 1, \qquad\qquad\qquad \text{transonic flow}$$

$$M > 1, \qquad\qquad\qquad \text{supersonic flow}$$

If the fluid velocity is much smaller than the sound velocity, compressibility effects are usually small.[22] For the Fort St. Vrain steam generator, the Mach numbers for the primary fluid, helium and the secondary fluid, steam/water are shown in Table 3.3.1.

It is noted from the Mach numbers indicated above that the properties of the working fluids of the Fort St. Vrain steam generator are close to incompressible.

In the application of the conservation equations to the working fluid, it must be noted that the nature of the conservation equations for compressible fluid flow contains the wave propagation phenomenum at sonic velocity.[23] A very short time step (less than the acoustic propagation, e.g. 10^{-4} sec) must be used for achieving numerical stability in the direct numerical integration. Such a short time step process is not practical in nuclear power plant system dynamics modeling. To obtain the dynamic behavior with a larger time step (e.g. 10^{-2} sec), the method used in this research is to evaluate the mass flow rate variation from a combination of the first order momentum and mass equations. The resultant equation[24] is

$$\Delta W(\ell, t) = \Delta W \left(0, \; t - \frac{|\ell|}{|\vec{V}_e + \vec{V}|}\right) \qquad\qquad (3\text{-}1)$$

TABLE 3.3.1

FLUID SPEED, SPEED OF SOUND AND MACH NUMBER FOR THE WORKING FLUIDS
IN THE FORT ST. VRAIN 330 MW(e) STEAM GENERATOR

Fluid	Pressure (Psia)	Temperature (°F)	Fluid Speed (Ft/Sec)	Speed of Sound (Ft/Sec)	Mach Number, M
Helium	688.97	734.28	56.07	4980.83	0.0113
Superheated steam	2640.0	1026.94	154.48	2501.73	0.0617
Superheated steam	2869.7	709.16	67.73	1968.79	0.0344
Saturated water (X = 1.0)	2922.15	691.37	31.86	660.90[a]	0.0482
Saturated water (X = 0.543)	2935.98	692.08	22.33	676.78[a]	0.0330

[a]Homogeneous model.

where $\overset{>}{V}_e$ = sonic velocity in the fluid

$\overset{>}{V}$ = fluid velocity

$\Delta W(\ell,t)$ = variation of the mass flow rate at tube length

ℓ, and time t

In the above equation, $\ell = 0$ represents the location of the perturbation source. Equation (3-1) can be written as

$$\Delta W(\ell,t) = \Delta W[0,t - \frac{|\ell|}{V_e(1\pm M)}]$$ (3-2)

where (1+M) is for $\ell > 0$ and (1-M) is for $\ell < 0$.

Using the Mach number and sonic velocity shown above, it is found that, for helium and subcooled water

$$\Delta W(\ell, t) \simeq \Delta W(0,t)$$ (3-3)

which leads to assumption (3) in Section 3.5.

Equation (3-2) and equation (3-3) are obtained based on the first order variations in a combination of momentum and mass equations. Effects of higher order variations neglected in the derivation of equation (3-2) and equation (3-3) require further investigation.

3.4 Fixed Node Boundary and Moving Node Boundary Models

Two models are generally used, the fixed boundary model and the moving boundary model. In the fixed boundary model, the coordinate along the tube length is divided to produce a selected number of fixed-length sections. Each section may contain one or more than one flow regime. The length of a section in the theoretical equations used is

therefore a parameter and not a variable. The fixed boundary model (with dynamic equations relatively simple in the spatial coordinate) is suitable for representing a complicated geometry system such as the steam generator containing nonuniform tube cross sections. However the number of sections required for describing the dynamics may be large.

In the moving boundary model, the theoretical equations are applied to describe the dynamics for each region which is represented by a single flow regime. Since the boundary between two regimes is a function of load and thermodynamic properties, the length of a region is treated as a variable in the dynamic equations. Because of the single characteristic in a region, the dynamic modeling is simplified. In addition, the transition from one regime to another, such as the appearance or disappearance of a regime can be expressed more easily and accurately.[25]

For the modeling of the Fort St. Vrain steam generator, the fixed boundary model is employed for the superheater II region because of the single phase steam and the moving boundary model is employed for the economizer-evaporator-superheater I region.

3.5 Assumptions

The assumptions used for the development of the Fort St. Vrain steam generator model consist of:

1. The dynamic behavior of all of the tubes in a module can be represented by a single characteristic tube.

2. The dynamic behavior is essentially one dimensional in the direction of the main flow. Effects of the secondary flow in

the radial direction of the coil are considered using correction factors on heat transfer, and pressure drop.

3. The mass flow rate for the helium or subcooled water region is determined by equation (3-3) and that for the saturated region or superheated region is determined by equation (3-2).

4. The heat transfer along the axial direction is neglected.

5. A homogeneous model for two phase flow is used.

6. Other assumptions used for developing the dynamic equations (see Section 3.6).

3.6 Conservation Equations

In general, the theoretical model is based on the following equations:

conservation of mass,

$$\frac{D\rho}{Dt} + \rho \nabla \cdot \vec{V} = 0 \qquad\qquad (3-4)$$

conservation of momentum,

$$\rho \frac{D\vec{V}}{Dt} = \rho \vec{g} + \nabla \cdot \overline{\overline{T}} \qquad\qquad (3-5)$$

and conservation of energy,

$$\rho \frac{D\Omega}{Dt} = - \nabla \cdot \vec{q} + \nabla \cdot (\overline{\overline{T}} \cdot \vec{V}) \qquad\qquad (3-6)$$

where

$$\frac{D}{Dt} = \frac{\partial}{\partial t} + \vec{V} \cdot \nabla \tag{3-7}$$

$$\overline{\overline{T}} = -P\overline{\overline{I}} + \overline{\overline{\tau}} \tag{3-8}$$

$$\Omega = u + \frac{1}{2}v^2 + \phi \tag{3-9}$$

$$\vec{q} = \text{heat flux vector}$$

Considering a geometry as shown in Figure 3.6.1, the above differential equations are integrated over a volume $V_a(t)$ with a surface area $A_a(t)$. Each region with $V_a(t)$ in Figure 3.6.1 is actually associated with a flow regime described in Section 3.1. The general transport theorem,

$$\int_{V_a(t)} \frac{\partial S_v}{\partial t} \, dV = \frac{d}{dt} \int_{V_a(t)} S_v \, dV - \int_{A_a(t)} S_v \, \vec{\omega} \cdot \hat{n} \, dA \tag{3-10}$$

where S_v = state variable

$\vec{\omega}$ = velocity of the volume surface

is applied to the integral term containing the partial time derivative and the following set of macroscopic balance equations for each region is developed:

mass balance equation,

$$\frac{d}{dt} (\overline{\rho} \, \overline{A} \, \Delta \ell) = W_{in} - W_o - \rho_{in} \, A_{in} \, \frac{d\ell_{in}}{dt} + \rho_o \, A_o \, \frac{d\ell_o}{dt} \tag{3-11}$$

momentum balance equation,
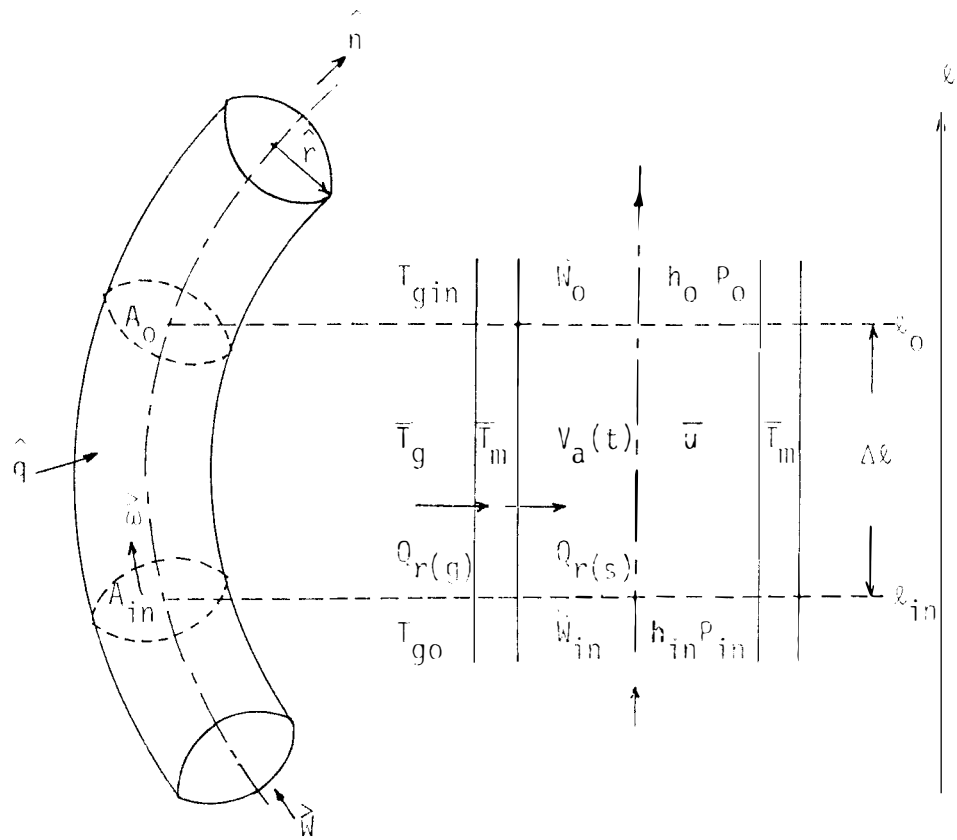
Figure 3.6.1.   A Diagram for Developing Macroscopic Balance Equations.

$$\frac{d}{dt}(\overline{W}\Delta\ell) = \frac{W_{in}^2}{\rho_{in}A_{in}} - \frac{W_o^2}{\rho_o A_o} - W_{in}\frac{d\ell_{in}}{dt} + W_o\frac{d\ell_o}{dt} + C_2(P_{in}A_{in} - P_o A_o)$$

$$- \frac{f}{8}\pi \cdot \overline{D} \cdot \Delta\ell \frac{\overline{W}^2}{\overline{\rho A}^2} + (A_o - A_{in})\, C_2\, P_{s1} \tag{3-12}$$

energy balance equation,

$$\frac{d}{dt}(\overline{\rho u A}\,\Delta\ell) = -(\hat{r} \cdot \hat{q})\, Q_r + (W_{in} - \rho_{in}\, A_{in}\frac{d\ell_{in}}{dt})\, h_{in}$$

$$- (W_o - \rho_o\, A_o\frac{d\ell_o}{dt})\, h_o + C_1\, P_{in}\, A_{in}\frac{d\ell_{in}}{dt} - C_1\, P_o\, A_o\frac{d\ell_o}{dt} \tag{3-13}$$

where P_{s1} is the pressure at the location where the change of tube cross section takes place.

P_{s1} and the average flow area, $\overline{A}$, for a region containing a change of tube cross section, are approximated by equation (3-14) and equation (3-16).

$$P_{s1} = \left[(\frac{\ell^* - \ell_{in}}{\Delta\ell})\, P_o + (\frac{\ell_o - \ell^*}{\Delta\ell})\, P_{in} \right] \cdot E_p \tag{3-14}$$

where

$$E_p = 1 + E_s \cdot \text{Min}\,(\frac{\ell_o - \ell^*}{\Delta\ell}, \frac{\ell^* - \ell_{in}}{\Delta\ell}) \tag{3-15}$$

Equation (3-15) is a correction factor for the linear estimation for pressure P_{s1}, in which E_s is an empirical constant.

$$\overline{A} = (\frac{\ell_o - \ell^*}{\Delta\ell})\, A_o + (\frac{\ell^* - \ell_{in}}{\Delta\ell})\, A_{in} \tag{3-16}$$

If $A_o > A_{in}$, the fluid flow experiences a sudden expansion in a pipeline; if $A_o < A_{in}$, the fluid flow suffers a sudden contraction. If $A_o = A_{in}$, the fluid flow is in a constant cross section pipe.

Derivation of the above balance equations is achieved with the following further assumptions:

The energy flux due to the dissipative term in the stress tensor, i.e.,

$$\int_{A_{a(t)}} (\hat{n} \cdot \bar{\bar{\tau}}) \cdot \vec{V} dA$$

is negligible.

The gravitational effect on momentum is negligible due to the small angle of tube inclination or the small helium density.

The kinetic energy and the potential energy in the total energy per unit mass are negligible.

Differentiation of the left-hand term of each balance equation leads to the following set of transient equations:

$$\frac{d\bar{\rho}}{dt} = [W_{in} - W_o - (\rho_{in} - \bar{\rho}) A_{in} \frac{d\ell_{in}}{dt} + (\rho_o - \bar{\rho}) A_o \frac{d\ell_o}{dt}]$$

$$/[A_o(\ell_o - \ell*) + A_{in} (\ell* - \ell_{in})] \qquad (3-17)$$

$$\frac{d\bar{W}}{dt} = [\frac{W_{in}^2}{\rho_{in}A_{in}} - \frac{W_o^2}{\rho_o A_o} + (\bar{W} - W_{in}) \frac{d\ell_{in}}{dt} + (W_o - \bar{W}) \frac{d\ell_o}{dt} + C_2 P_{in} A_{in}$$

$$- C_2 P_o A_o - \frac{f}{8} \pi \bar{D} \cdot \Delta\ell \frac{\bar{W}^2}{\rho \bar{A}^2} + (A_o - A_{in}) C_2 P_{sl}]/(\ell_o - \ell_{in}) \qquad (3-18)$$

$$\frac{d\overline{u}}{dt} = [-(\hat{r} \cdot \hat{q}) \; Q_r + (W_{in} - \rho_{in} \; A_{in} \; \frac{d\ell_{in}}{dt})(h_{in} - \overline{u})$$

$$- (W_o - \rho_o \; A_o \; \frac{d\ell_o}{dt})(h_o - \overline{u}) + C_1 \; P_{in} \; A_{in} \; \frac{d\ell_{in}}{dt} - C_1 \; P_o \; A_o \; \frac{d\ell_o}{dt}]$$

$$/[\overline{\rho}(A_o \; (\ell_o - \ell^*) + A_{in} \; (\ell^* - \ell_{in}))] \tag{3-19}$$

Equation (3-17) through equation (3-19) are the dynamic equations for determining a state of a region at each instant. However, these equations are not ready to be solved since the differential equations involve too many dependent variables. First, the number of state variables must be equal to the number of equations. Second, the moving boundary derivatives must be determined from those conditions described in Section 3.1. Third, the inputs and outputs for an isolated steam generator must be specified. To achieve the first purpose, a model structure is proposed; the resultant model equations and the necessary relationships for thermodynamic properties are presented in Section 3.7. In Section 3.8, determination of the moving boundaries is described. The inputs and outputs of the steam generator studied are given below.

Input variables are water inlet enthalpy or temperature, water inlet mass flow rate, steam outlet pressure, helium inlet temperature, helium inlet mass flow rate and helium inlet pressure.

Output variables include water inlet pressure, steam outlet temperature, steam outlet mass flow rate, helium outlet pressure, helium outlet temperature, and helium outlet mass flow rate.

3.7 A Model Structure and Model Equations

A model diagram for the Fort St. Vrain steam generator is shown in Figure 3.7.1. In this diagram, the region representing a single flow regime is defined by two boundary conditions. Each region can be further divided as shown in the diagram. In order to obtain a generalized formulation for the many section dynamic model, the detailed division for a typical region is drawn and shown in Figure 3.7.2 and Figure 3.7.3. Figure 3.7.2 and Figure 3.7.3 are employed to develop the model equations. The difference between Figure 3.7.2 and Figure 3.7.3 is that the last section in Figure 3.7.2 can be used to represent the outlet conditions while in Figure 3.7.3, the beginning section is used to represent the outlet conditions. Therefore for the output variables of the steam generator given in Section 3.6, it is selected to use Figure 3.7.2 for the steam/water flow and Figure 3.7.3 for the helium flow. In Figure 3.7.2, a state variable as a function of tube coordinate is shown for a region. Along the tube coordinate, the region is further divided into a number of subregions of equal tube length. For each typical subregion i, where boundaries are denoted by ℓ_i and ℓ_{i+1}, the properties of this subregion (two thermodynamic variables and one mass flow rate) are taken as the same values as the properties at ℓ_{i+1}. Figure 3.7.3 is applied to the primary coolant. In Figure 3.7.3, the properties of a subregion i are taken as the same as the properties at boundary i.

If a change of tube cross section takes place in a subregion i, then the average cross sectional area of that subregion is calculated as:

$$\overline{A}_i = [A_i \ (\ell_{i+1} - \ell^\star) + A_{i-1} \ (\ell^\star - \ell_i)]/(\ell_{i+1} - \ell_i) \qquad (3\text{-}20)$$
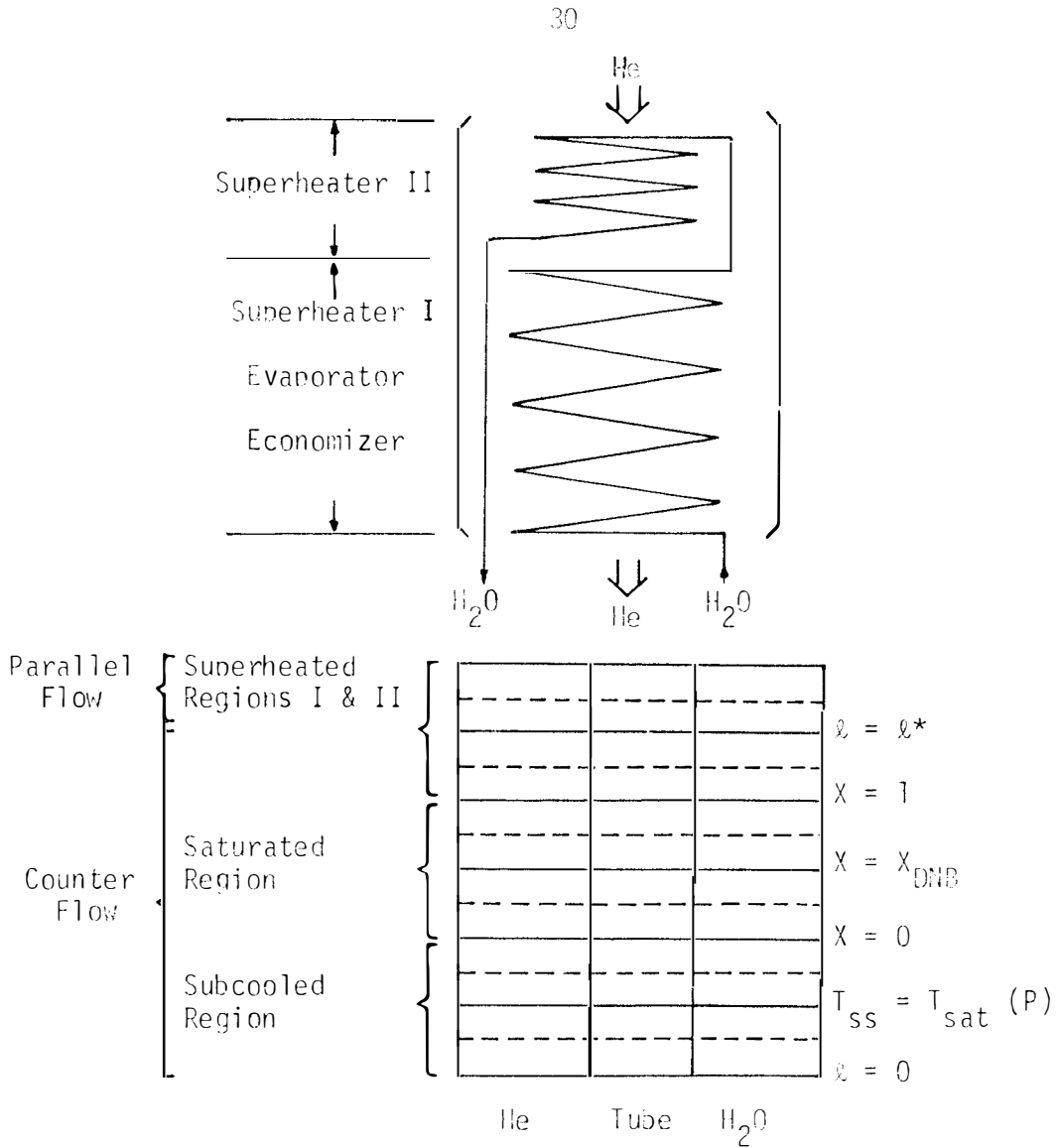
ℓ = tube length; ℓ*, a fixed tube length

P = pressure

T = temperature; T_{sat}, saturation temperature; T_{ss}, tube surface temperature on H_2O side

X = steam quality; X_{DNB}, steam quality at DNB

Figure 3.7.1.   Schematic Diagram of a Fort St. Vrain Once-through Steam Generator and Its Model Diagram.
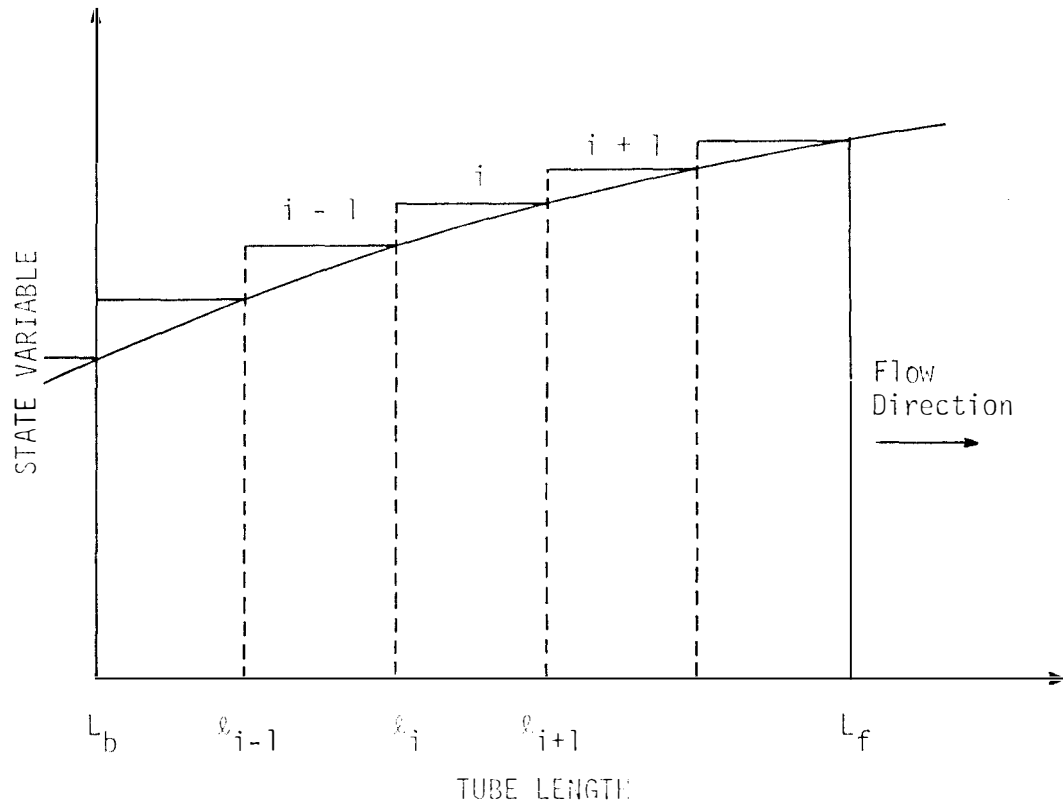
Figure 3.7.2. The Model Diagram for a Typical Region in Steam/Water Flow.
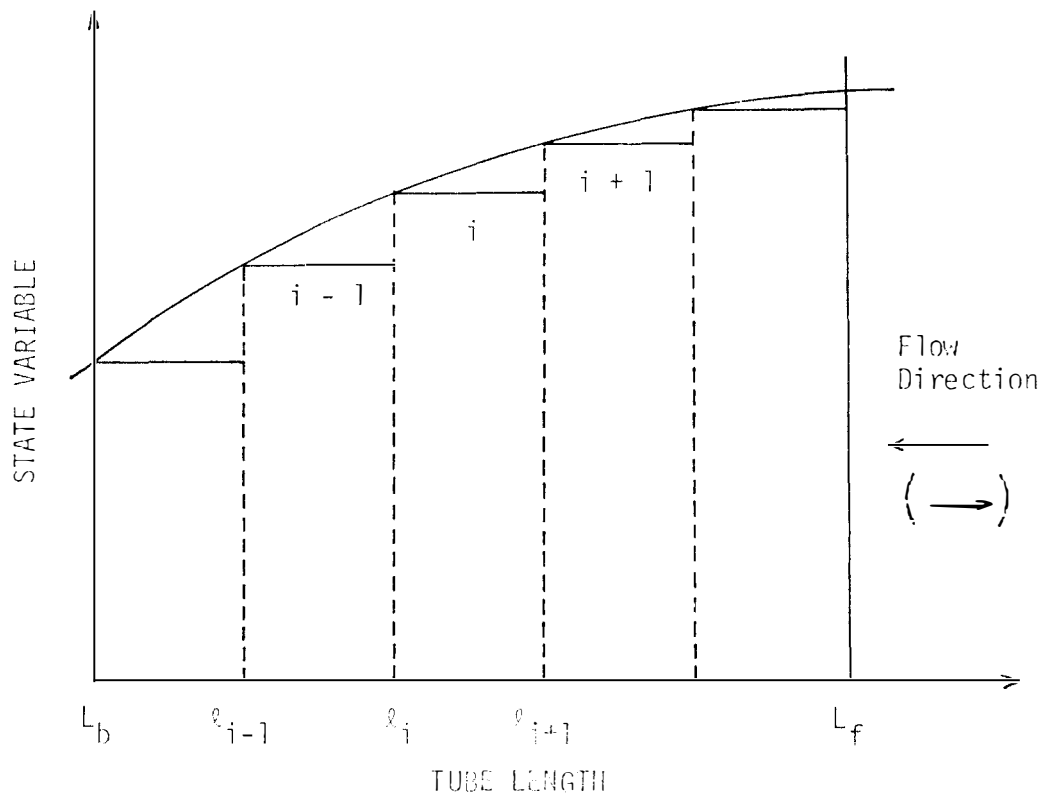
Figure 3.7.3.   The Model Diagram for a Typical Region in Helium Flow.

The model equations developed according to Figure 3.7.2 and
Figure 3.7.3 are given below:

1. On the steam/water side:

Mass balance equation:

$$\frac{d\rho_i}{dt} = [W_i - W_{i+1} + (-RA1 \cdot SXG3 + RA2 \cdot SXG1 - RA1 \cdot SXG1 + RA3$$

$$\cdot SXG3) \frac{d}{dt} L_b + (-RA1 \cdot SXG4 + RA2 \cdot SXG2 - RA1 \cdot SXG2 + RA3$$

$$\cdot SXG4) \frac{d}{dt} L_f]/(\overline{A}_i \cdot \Delta\ell_i) \qquad (3-21)$$

Energy balance equation:

$$\frac{du_i}{dt} = [Q_{si} + W_{i-1} h_{i-1} - W_i h_i - u_i (W_i - W_{i+1}) + ((RAH2 - RAU2)$$

$$\cdot SXG1 - (RAH1 - RAU1) \cdot SXG3 + CPA1 \cdot SXG3 - CPA2 \cdot SXG1) \frac{d}{d_t} L_b$$

$$+ ((RAH2 - RAU2) \cdot SXG2 - (RAH1 - RAU1) \cdot SXG4 + CPA1 \cdot SXG4$$

$$- CPA2 \cdot SXG2) \frac{d}{dt} L_f]/(\rho_i \overline{A}_i \Delta\ell_i) \qquad (3-22)$$

Momentum balance equation:

$$\frac{dW_i}{dt} = [\frac{W_{i-1}^2}{\rho_{i-1} A_{i-1}} - \frac{W_i^2}{\rho_i A_i} + C_2 (P_{i-1} A_{i-1} - P_i A_i) - C_{6i} \frac{f_i}{8} \pi\overline{D}_i$$

$$\cdot \Delta\ell_i \frac{W_i^2}{\rho_i \overline{A}_i^2} + C_2 (A_i - A_{i-1})((\ell^* - \ell_i) P_i + (\ell_{i+1} - \ell^*) P_{i-1})$$

$$\cdot E_p/\Delta\ell_i + (-W_{i-1} SXG3 + W_i \cdot SXG1 + W_i/NDI) \cdot \frac{d}{dt} L_b + (-W_{i-1}$$

$$\cdot SXG4 + W_i \cdot SXG2 - W_i/NDI) \cdot \frac{d}{dt} L_f]/\Delta\ell_i \qquad (3-23)$$

These balance equations are applied to each subregion except the region at the steam outlet.

At the steam outlet region where the pressure is an input condition, the following mass and energy equations are used.

$$\frac{d\rho_i}{dt} = (\frac{dP_i}{dt} - \frac{dP_i}{du_i} \cdot \frac{du_i}{dt})/\frac{dP_i}{d\rho_i} \qquad (3\text{-}24)$$

and

$$\frac{du_i}{dt} = (Q_{si} + W_{i-1} \ h_{i-1} - W_i \ h_i)/(\rho_i \ \overline{A}_i \cdot \Delta\ell_i) - u_i \frac{d\rho_i}{dt}/\rho_i \qquad (3\text{-}25)$$

i = steam outlet section index

2. On the gas side:

Mass balance equation:

$$\frac{d\rho_{gi}}{dt} = [W_{gi+1} - W_{gi} + (RAG2 \cdot SXG1 - RAG1 \cdot SXG3 + RAG1/NDI)$$

$$\cdot \ C_3 \cdot \frac{d}{dt} L_b + (RAG2 \cdot SXG2 - RAG1 \cdot SXG4 - RAG1/NDI) \cdot C_3$$

$$\cdot \ \frac{d}{dt} L_f]/(A_g \cdot C_3 \cdot \Delta\ell_i) \qquad (3\text{-}26)$$

Momentum balance equation:

$$\frac{dW_{gi}}{d_t} = [C_2 \ A_g \ (P_{gi+1} - P_{gi}) + (\frac{W_{gi+1}}{\rho_{gi+1} \ A_g} - \frac{W_{gi}}{\rho_{gi} \ A_g}) + (W_{gi+1}$$

$$\cdot \ SXG1 - W_{gi} \cdot SXG3 + W_{gi}/NDI) \cdot C_3 \cdot \frac{d}{dt} L_b + (W_{gi+1} \cdot SXG2$$

$$- W_{gi} \cdot SXG4 - W_{gi}/NDI) \cdot C_3 \cdot \frac{d}{dt} L_f + \rho_{gi} \cdot g \cdot A_g \cdot C_3 \cdot \Delta\ell_i$$

$$- C_{6gi} \ A_g \ f_{eff} \cdot G_{NR} \cdot (W_{gi}/A_g)^2/(2 \cdot \rho_{gi})]/(C_3 \cdot \Delta\ell_i) \qquad (3\text{-}27)$$

Energy balance equation:

$$\frac{du_{gi}}{dt} = [-Q_{gi} + W_{gi+1} h_{gi+1} - W_{gi} h_{gi} - u_{gi} (W_{gi+1} - W_{gi})$$

$$+ (URAG2 \cdot SXG1 - URAG12 \cdot SXG1) \cdot C_3 \cdot \frac{d}{dt} L_b + (URAG2 \cdot SXG2$$

$$- URAG12 \cdot SXG2) \cdot C_3 \cdot \frac{d}{dt} L_f]/(A_g \cdot \rho_{gi} \cdot C_3 \cdot \Delta \ell_i) \qquad (3-28)$$

3. For the tubes:

The energy equation is

$$\frac{dT_{mi}}{dt} = [Q_{gi} - Q_{si} + (RAUM3 - RAUM1) \cdot (SXG3 \cdot \frac{d}{dt} L_b + SXG4$$

$$\cdot \frac{d}{dt} L_f)]/(\rho_{mi} \cdot (\overline{A}\Delta\ell)_{mi} \cdot C_{mi}) \qquad (3-29)$$

In the above equations, Q_{gi} and Q_{si} represent the heat transfer from the primary coolant to the tube and from the tube to the secondary coolant respectively for a section with index i. Q_{gi} and Q_{si} may be written as

$$Q_{gi} = C_{7gi} \cdot EK_{g \rightarrow m,i} (T_{gj} - T_{mi}) \qquad (3-30)$$

$$Q_{si} = C_{7i} \cdot EK_{m \rightarrow s,i} (T_{mi} - T_{si}) \qquad (3-31)$$

where j = i if counter flow

j = i_b + i_ℓ -i if parallel flow

$EK_{g \rightarrow m,i}$ and $EK_{m \rightarrow s,i}$ are conductances for a division i, which are in terms of properties of a subsection. The evaluation of the conductances is given in Chapter 4.

C_{7gi} and C_{7i}, the model correction factors for energy, are used in order to satisfy the energy balance since the distributed parameter properties of the steam generator are represented by using a fewer number of sections in the model. In a section with an infinitesimal tube length, Q_{gi} is equal to $EK_{g \to m,i}$ $(T_{gj} - T_{mi})$ and Q_{si} is equal to $EK_{m \to s,i}$ $(T_{mi} - T_{si})$. But in a section with large tube length, $EK_{g \to m,i}$ $(T_{gj} - T_{mi})$ and $EK_{m \to s,i}$ $(T_{mi} - T_{si})$ are not accurate enough to represent Q_{gi} and Q_{si}. Therefore, C_{7gi} and C_{7i} must be used for corrections.

For the same reason, C_{6gi} and C_{6i} in the momentum equations are the model correction factors for the momentum, which are employed to satisfy the momentum balance.

Other notation used in the above equations is given below:

$$RA1 \quad = \rho_i \, A_i \tag{3-32-1}$$

$$RA2 \quad = \rho_{i+1} \, A_{i+1} \tag{3-32-2}$$

$$RA3 \quad = \rho_i \, A_{i-1} \tag{3-32-3}$$

$$RAU1 \quad = \rho_i \, A_i \, u_i \tag{3-32-4}$$

$$RAH1 \quad = \rho_{i-1} \, A_{i-1} \, h_{i-1} \tag{3-32-5}$$

$$RAU2 \quad = \rho_{i+1} \, A_{i+1} \, u_i \tag{3-32-6}$$

$$RAH2 \quad = \rho_i \, A_i \, h_i \tag{3-32-7}$$

$$CPA1 \quad = C_1 \cdot PA1 = C_1 \, P_{i-1} \, A_{i-1} \tag{3-32-8}$$

$$CPA2 \quad = C_1 \cdot PA2 = C_1 \, P_i \, A_i \tag{3-32-9}$$

$$RAG1 \quad = \rho_{gi} \, A_g \tag{3-32-10}$$

$$RAG2 \quad = \rho_{gi+1} \, A_g \tag{3-32-11}$$

$$URAG12 = A_g \, \rho_{gi+1} \, u_{gi} \tag{3-32-12}$$

$$\text{URAG2} \quad = A_g \ \rho_{gi+1} \ u_{gi+1} \tag{3-32-13}$$

$$\text{RAUM1} \quad = \rho_{mi-1} \ A_{mi-1} \ C_{mi-1} \ T_{mi-1} \tag{3-32-14}$$

$$\text{RAUM3} \quad = \rho_{mi-1} \ A_{mi-1} \ C_{mi} \ T_{mi} \tag{3-32-15}$$

$$\text{SXG1} \quad = 1 - I_p/\text{NDI} \tag{3-32-16}$$

$$\text{SXG2} \quad = I_p/\text{NDI} \tag{3-32-17}$$

$$\text{SXG3} \quad = 1 - (I_p - 1)/\text{NDI} \tag{3-32-18}$$

$$\text{SXG4} \quad = (I_p - 1)/\text{NDI} \tag{3-32-19}$$

$\text{NDI} \quad = $ number of sections in a region

$I_p \quad = $ relative index for a section in a given region

3.8 Moving Boundaries

This section deals with the mathematical formulation for the time derivatives of the locations at $X = 1$, $X = X_{DNB}$, $X = 0$ and at the onset of nucleate boiling.

a. The time derivatives of the locations for $X = 1$, $X = X_{DNB}$ and $X = 0$.

In the two phase region, the following equations are valid for the homogeneous model:

$$h = h_f + X \ h_{fg} \tag{3-33}$$

$$v = v_f + X \ v_{fg} \tag{3-34}$$

$$\rho = 1/v \tag{3-35}$$

$$u = h - C_1 \ P/\rho \tag{3-36}$$

Differentiating the above equations, one obtains the following equations:

$$\frac{dh}{dt} = (\frac{dh_f}{dp} + X\frac{dh_{fg}}{dp}) \frac{dp}{dt} + h_{fg} \frac{dX}{dt} \tag{3-37}$$

$$\frac{dv}{dt} = (\frac{dv_f}{dp} + X\frac{dv_{fg}}{dp}) \frac{dp}{dt} + v_{fg} \frac{dX}{dt} \tag{3-38}$$

$$\frac{d\rho}{dt} = - \frac{1}{v^2} \frac{dv}{dt} \tag{3-39}$$

$$\frac{dh}{dt} = \frac{du}{dt} + \frac{C_1}{\rho} \frac{dp}{dt} + C_1 \; P \; \frac{dv}{dt} \tag{3-40}$$

Equations (3-37) through equation (3-40) together with the mass balance equation and the energy balance equation can be used to solve the boundary length derivatives. After eliminating dh/dt, du/dt, dp/dt, dv/dt, and dρ/dt, the following result is obtained:

$$\frac{dL_f}{dt} = [PRU1 \cdot \rho_i \cdot (W_i - W_{i+1}) - Q_{si} - W_{i-1} \; h_{i-1} + W_i \; h_i$$

$$+u_i \; (W_i - W_{i+1}) + (PRU1 \cdot \rho_i \cdot PRMB - PRUB) \cdot \frac{d}{dt} L_b + \rho_i \cdot \overline{A}_i$$

$$\cdot \; \Delta\ell_i \cdot PRU2 \cdot \frac{dX_i}{dt}]/[PRUF - PRU1 \cdot \rho_i \cdot PRMF] \tag{3-41}$$

where

$$PRU1 = -v^2 \; (PHX - C_1 \; R)/PVX \tag{3-42-1}$$

$$PRU2 = - \; (\frac{PHX - C_1 R}{PVX})[\frac{PVX \cdot (C_1 S - h_{fg})}{PHX - C_1 R} + v_{fg}] \tag{3-42-2}$$

$$PRMB = SXG1 \cdot (\rho_{i+1} \; A_{i+1} -\rho_i \; A_i) + SXG3 \cdot \rho_i \cdot (A_{i-1} - A_i) \tag{3-42-3}$$

$$PRMF = SXG2 \cdot (\rho_{i+1} \cdot A_{i+1} - \rho_i \; A_i) + SXG4 \cdot \rho_i \cdot (A_{i-1} - A_i)$$

$$\tag{3-42-4}$$

$$PRUB = (\rho_i \; A_i \; h_i - \rho_{i+1} \; A_{i+1} \; u_i) \cdot SXG1 - (\rho_{i-1} \; A_{i-1} \; h_{i-1}$$

$$- \; \rho_i \; A_i \; u_i) \cdot SXG3 + C_1 \cdot (PA1 \cdot SXG3 - PA2 \cdot SXG1) \tag{3-42-5}$$

$$PRUF = (\rho_i \ A_i \ h_i - \rho_{i+1} \ A_{i+1} \ u_i) \cdot SXG2 - (\rho_{i-1} \ A_{i-1} \ h_{i-1}$$

$$- \rho_i \ A_i \ u_i) \cdot SXG4 + C_1 \cdot (PA1 \cdot SXG4 - PA2 \cdot SXG2) \quad (3\text{-}42\text{-}6)$$

$$PVX \ = \frac{dv_f}{dP} + X \ \frac{dv_{fg}}{dP} \quad\quad\quad (3\text{-}42\text{-}7)$$

$$PHX \ = \frac{dh_f}{dP} + X \ \frac{dh_{fg}}{dP} \quad\quad\quad (3\text{-}42\text{-}8)$$

$$R \quad = v + P \cdot PVX \quad\quad\quad (3\text{-}42\text{-}9)$$

$$S \quad = P \cdot v_{fg} \quad\quad\quad (3\text{-}42\text{-}10)$$

For the boundary of a region, which is determined by the constant steam quality (i.e., X = 1 or X = 0), equation (3-41) is reduced to the following:

$$\frac{d}{dt} L_f = [PRU1 \cdot \rho_i \cdot (W_i - W_{i+1}) - Q_{si} - W_{i-1} \ h_{i-1} + W_i \ h_i$$

$$+ u_i \ (W_i - W_{i+1}) + (PRU1 \cdot \rho_i \cdot PRMB - PRUB) \cdot \frac{d}{dt} L_b]/$$

$$(PRUF - PRU1 \cdot \rho_i \cdot PRMF) \quad\quad\quad (3\text{-}43)$$

For the boundary determined by $X = X_{DNB}$, dX_{DNB}/dt is found as

$$\frac{dX_{DNB}}{dt} = (DX_{Tm}) \cdot \frac{dT_m}{dt} + (DX_{pc}) \frac{dP_c}{dt} + (DX_w) \frac{dW}{dt} + (DX_{Lf}) \frac{d}{dt} L_f$$

$$+ (DX_{Lb}) \cdot \frac{dL_b}{dt} \quad\quad\quad (3\text{-}44)$$

where

$$DX_{Tm} = 0.719 \cdot X_{DNB}/(T_m - T_s) \quad\quad\quad (3\text{-}45\text{-}1)$$

$$DX_{pc} = 0.0025 \cdot C_9 \cdot X_{DNB} - 0.719 \cdot X_{DNB} \frac{dT_s}{dP_c}/(T_m - T_s) \quad (3\text{-}45\text{-}2)$$

$$DX_w \ = -0.212 \cdot X_{DNB}/W \quad\quad\quad (3\text{-}45\text{-}3)$$

$$DX_{Lf} = 0.719 \cdot X_{DNB} (DD1 + 1/(L_f - L_b)) + 0.212 \cdot X_{DNB} \cdot DA1$$

$$(3\text{-}45\text{-}4)$$

$$DX_{Lb} = 0.719 \cdot X_{DNB} \cdot (DD2 - 1/(L_f - L_b)) + 0.212 \cdot X_{DNB}$$
$$\cdot DA2 \qquad (3\text{-}45\text{-}5)$$

For a subregion containing nonuniform tube cross section,

$$DD1 = (\frac{DID2 - DID1}{\Delta \ell_i})(\frac{I_p - WF}{NDI})/\overline{D}_i \qquad (3\text{-}45\text{-}6)$$

$$DD2 = (\frac{DID2 - DID1}{\Delta \ell_i})/\overline{D}_i - DD1 \qquad (3\text{-}45\text{-}7)$$

$$DA1 = (\frac{XA2 - XA1}{\Delta \ell_i})(\frac{I_p - WF}{NDI})/\overline{A}_i \qquad (3\text{-}45\text{-}8)$$

$$DA2 = (\frac{XA2 - XA1}{\Delta \ell_i})/\overline{A}_i - DA1 \qquad (3\text{-}45\text{-}9)$$

and for a constant tube cross-section subregion,

$$DD1 = 0, \quad DD2 = 0, \quad DA1 = 0, \quad DA2 = 0 \qquad (3\text{-}45\text{-}10)$$

WF is the tube length fraction occupied by the cross section XA2; the remainder, 1 - WF, is occupied by XA1.

By employing the tube energy equation, steam/water momentum equation and the thermodynamic property relationship,

$$\frac{dP_c}{dt} = DPU \cdot \frac{du}{dt} + DPR \cdot \frac{d\rho}{dt} \quad , \qquad (3\text{-}46)$$

those time derivatives, dT_m/dt, dW/dt, and dP_c/dt can be eliminated from equation (3-44).

Equation (3-46) resulted from solving equation (3-37) through equation (3-40) with

$$DPU = v_{fg}/[v_{fg} (PHX - C_1R) + (C_1S - h_{fg}) \cdot PVX] \qquad (3\text{-}47\text{-}1)$$

$$DPR = -[(C_1S - h_{fg})/\rho^2]/[v_{fg} (PHX - C_1R) + (C_1S - h_{fg})$$
$$\cdot PVX] \qquad (3\text{-}47\text{-}2)$$

After substituting the new form of dX_{DNB}/dt into equation (3-41), the following result is obtained:

$$\frac{dL_f}{dt} = (\gamma_2/\gamma_1) \frac{d}{dt} L_b + \gamma_3/\gamma_1 \qquad (3\text{-}48)$$

where

$$\gamma_1 = (1 - PRU2 \cdot DX_{pc} \cdot DPU)[(RAH2 - RAU2) \cdot SXG2 - (RAH1 - RAU1)$$
$$\cdot SXG4 + CPA1 \cdot SXG4 - CPA2 \cdot SXG2] - PRU2 \cdot \rho_i \cdot \overline{A}_i \cdot \Delta\ell_i$$
$$\cdot DX_{Tm} (RAUM3 - RAUM1) \cdot SXG4/(\rho_{mi} (\overline{A}\Delta\ell)_{mi} \cdot C_{mi}) - PRU2$$
$$\cdot \rho_i \cdot \overline{A}_i \cdot DX_w (-W_{i-1} \cdot SXG4 + W_i \cdot SXG2 - W_i/NDI) - (PRU1$$
$$\cdot \rho_i + PRU2 \cdot \rho_i \cdot DX_{pc} \cdot DPR)[SXG2 \cdot (RA2 - RA1) + SXG4$$
$$\cdot (RA3 - RA1)] - PRU2 \cdot \rho_i \cdot \overline{A}_i \cdot \Delta\ell_i \cdot DX_{Lf} \qquad (3\text{-}49\text{-}1)$$

$$\gamma_2 = - (1 - PRU2 \cdot DX_{pc} \cdot DPU)[(RAH2 - RAU2) \cdot SXG1 - (RAH1 - RAU1)$$
$$\cdot SXG3 + CPA1 \cdot SXG3 - CPA2 \cdot SXG1] + PRU2 \cdot \rho_i \cdot \overline{A}_i \cdot \Delta\ell_i$$
$$\cdot DX_{Tm} \cdot (RAUM3 - RAUM1) \cdot SXG3/(\rho_{mi} \cdot (\overline{A}\Delta\ell)_{mi} \cdot C_{mi}) + PRU2$$
$$\cdot \rho_i \cdot \overline{A}_i \cdot DX_w (-W_{i-1} \cdot SXG3 + W_i \cdot SXG1 + W_i/NDI) + (PRU1$$
$$\cdot \rho_i + PRU2 \cdot \rho_i \cdot DX_{pc} \cdot DPR) \cdot [SXG1 \cdot (RA2 - RA1) + SXG3$$
$$\cdot (RA3 - RA1)] + PRU2 \cdot \rho_i \cdot \overline{A}_i \cdot \Delta\ell_i \cdot DX_{Lb} \qquad (3\text{-}49\text{-}2)$$

and

$$\gamma_3 = -(1 - PRU2 \cdot DX_{pc} \cdot DPU)[Q_{si} + W_{i-1} \, h_{i-1} - W_i \, h_i - u_i \, (W_i$$

$$- W_{i+1})] + PRU2 \cdot \rho_i \, \overline{A}_i \cdot \Delta\ell_i \, DX_{Tm} \, (Q_{gi} - Q_{si})/(\rho_{mi} \, (\overline{A}\Delta\ell)_{mi}$$

$$\cdot C_{mi}) + PRU2 \cdot \rho_i \cdot \overline{A}_i \cdot DX_w \left[\frac{W_{i-1}^2}{\rho_{i-1} \, A_{i-1}} - \frac{W_i^2}{\rho_i \, A_i} \right.$$

$$\left. +C_2 \, (P_{i-1} \, A_{i-1} - P_i \, A_i) + PCT - C_{6i} \, \frac{f_i}{8} \, \pi \, \overline{D}_i \cdot \Delta\ell_i \, \frac{W_i^2}{\rho_i \, \overline{A}_i^2} \right]$$

$$+ (PRU1 \cdot \rho_i + PRU2 \cdot \rho_i \, DX_{pc} \cdot DPR)(W_i - W_{i+1}) \qquad (3-49-3)$$

where

$$PCT = C_2 \, (A_i - A_{i-1})(\ell_{i+1} - \ell^*) \, P_{i-1} \, E_p/\Delta\ell_i + C_2 \, (A_i - A_{i-1})(\ell^*$$

$$- \ell_i) \, P_i \cdot E_p/\Delta\ell_i \qquad \text{if } A_i < A_{i-1}$$

$$= 0 \qquad \text{if } A_i = A_{i-1}$$

$$= C_2 \, (A_i - A_{i-1}) \, P_{i-1} \qquad \text{if } A_i > A_{i-1} \qquad (3-49-4)$$

Let L_1, L_2, L_3, and L_4 represent the locations for the onset of nucleate boiling, $X = 0$, $X = X_{DNB}$ and $X = 1$, which are the tube lengths measured from the water entrance of the steam generator, then for $X = 0$,

$$\frac{dL_f}{dt} = \frac{dL_2}{dt} \quad , \quad \frac{dL_b}{dt} = \frac{dL_1}{dt}$$

in equation (3-43) and i = index for subregion with $X = 0$; for $X = X_{DNB}$,

$$\frac{dL_f}{dt} = \frac{dL_3}{dt} \quad , \quad \frac{dL_b}{dt} = \frac{dL_2}{dt}$$

in equation (3-43) with i = index for subregion with $X = X_{DNB}$; for $X = 1$,

$$\frac{dL_f}{dt} = \frac{dL_4}{dt} \quad , \quad \frac{dL_b}{dt} = \frac{dL_3}{dt}$$

in equation (3-43) and i = index for a subregion with $X = 1$.

    b. The time derivative of the boundary at the onset of nucleate boiling.

The water in the region of the onset of nucleate boiling is treated as incompressible fluid. Therefore the following two equations are applicable:

$$\frac{d\rho_i}{dt} = \frac{d\rho_i}{du_i}\frac{du_i}{dt} + \frac{d\rho_i}{dp_i}\frac{dp_i}{dt} \simeq \frac{d\rho_i}{du_i}\frac{du_i}{dt} \tag{3-50}$$

$$W_i = W_{i+1} \tag{3-51}$$

The mass equation and the energy equation are solved simultaneously with the above two equations for the length derivative. The resultant equation is:

$$\frac{d}{dt}L_1 = [Q_{s1} + W_{i-1}\,h_{i-1} - W_i\,h_i]/[\rho_i\,(SXG2 \cdot RA21 + SXG4 \cdot RA31)/$$

$$(\frac{d\rho_i}{du_i}) - (RAH2 - RAU2) \cdot SXG2 + (RAH1 - RAU1) \cdot SXG4 - CPA1$$

$$\cdot SXG4 + CPA2 \cdot SXG2] \tag{3-52}$$

where

$$RA21 = RA2 - RA1 \tag{3-52-1}$$

$$RA31 = RA3 - RA1 \tag{3-52-2}$$

This condition, $T_{ss} = T_{sat}$ (P) is incorporated into the term, Q_{si}, where

$$Q_{si} = C_{7i} \, EK_{m \to s,i} \, (T_{mi} - T_{si}) \qquad (3-53)$$

and

$$T_{si} = T_{ssi} - [EK_{m \to ss,i}/(h_s \cdot A_{ss})] \cdot (T_m - T_{ssi}) \qquad (3-54)$$

Equation (3-54) is obtained from an energy balance relationship such as equation (4-15).

CHAPTER 4

DETERMINATION OF THE EQUIVALENT CONDUCTANCES,

TUBE AVERAGE TEMPERATURE AND TUBE

SURFACE TEMPERATURES

The nonlinear steam generator dynamic model requires detailed evaluations of the conductances and tube temperatures for both steady state and transient states. The conductance (defined as the heat transfer per unit temperature difference between two subregions per unit time) is a function of the state variables. The tube surface temperatures are necessary for determination of the onset of nucleate boiling and the heat transfer coefficients which are contained in the conductances. A method for determining the conductances, tube average temperatures and tube surface temperatures is given below.

For uniform properties along tube coordinate in a section, the heat transfer from helium to the tube and that from the tube to the steam/water can be expressed as follows:

$$Q_g = EK_{g \to m} (T_g - T_m) \tag{4-1}$$

$$= EK_{gs \to m} (T_{gs} - T_m) \tag{4-2}$$

$$= h_p A_{sg} (T_g - T_{gs}) \tag{4-3}$$

$$Q_s = EK_{m \to s} (T_m - T_s) \tag{4-4}$$

$$= EK_{m \to ss} (T_m - T_{ss}) \tag{4-5}$$

45

For regions except the subcooled nucleate boiling, Q_s can also be written as

$$Q_s = h_s A_{ss} (T_{ss} - T_s) \tag{4-6}$$

and for the subcooled nucleate boiling region,

$$Q_s = h_{NCB} A_{ss} (T_{ss} - T_{sat}) + h_c A_{ss} (T_{ss} - T_s) \tag{4-7}$$

The conductance equations for equation (4-1) through equation (4-5) are given below[26]:

$$EK_{g \to m} = \frac{2\pi r_0 \Delta\ell k h_p}{k + h_p r_0 \left[0.5 + \frac{\ln (r_0/r_{in})}{1 - (r_0/r_{in})^2}\right]} \tag{4-8}$$

$$EK_{gs \to m} = \frac{2\pi k \, \Delta\ell}{0.5 + \frac{\ln (r_0/r_{in})}{1 - (r_0/r_{in})^2}} \tag{4-9}$$

$$EK_{m \to s} = \frac{2\pi r_{in} \, \Delta\ell \, k \, h_s}{k + h_s r_{in} \left[\frac{\ln (r_{in}/r_0)}{(\frac{r_{in}}{r_0})^2 - 1} - 0.5\right]} \tag{4-10}$$

and

$$EK_{m \to ss} = \frac{2\pi k \, \Delta\ell}{\frac{\ln (r_{in}/r_0)}{(\frac{r_{in}}{r_0})^2 - 1} - 0.5} \tag{4-11}$$

For steady state, the tube average temperature is obtained by setting $Q_g = Q_s$.

From here,

$$T_m = (EK_{g \to m} \cdot T_g + EK_{m \to s} \cdot T_s)/(EK_{g \to m} + EK_{m \to s}) \qquad (4\text{-}12)$$

The tube surface temperature on the primary fluid side is obtained from the equation shown below:

$$h_p A_{sg} (T_g - T_{gs}) = EK_{gs \to m} (T_{gs} - T_m) \qquad (4\text{-}13)$$

i.e. for steady state,

$$T_{gs} = \frac{h_p A_{sg} T_g + EK_{gs \to m} T_m}{h_p A_{sg} + EK_{gs \to m}} \qquad (4\text{-}14)$$

The tube surface temperature on the secondary fluid side is obtained by solving either

$$h_s A_{ss} (T_{ss} - T_s) = EK_{m \to ss} (T_m - T_{ss}) \qquad (4\text{-}15)$$

for regions except the subcooled nucleate boiling region or

$$EK_{m \to ss} (T_m - T_{ss}) = h_{NCB} A_{ss} (T_{ss} - T_{sat}) + h_c A_{ss} (T_{ss} - T_s) \qquad (4\text{-}16)$$

for the sbucooled nucleate boiling region. The result is (for the steady state):

$$T_{ss} = \frac{h_s A_{ss} T_{ss} + EK_{m \to ss} T_m}{h_s A_{ss} + EK_{m \to ss}} \qquad (4\text{-}17)$$

for regions except the subcooled nucleate boiling region or

$$T_{ss} = \frac{EK_{m \to ss} \, T_m + h_c \, A_{ss} \, T_s + h_{NCB} \cdot A_{ss} \cdot T_{sat}}{h_c \, A_{ss} + h_{NCB} \cdot A_{ss} + EK_{m \to ss}} \qquad (4\text{-}18)$$

for the subcooled nucleate boiling region.

For the transient state, the tube temperature is calculated from the energy equation. The tube surface temperatures are obtained using similar procedures as used in the steady state since surface temperatures represent the temperatures of locations with zero volume. The following is a proof to show that equation (4-14), (4-17) and equation (4-18) employed in the steady state can also be used in the transient state.

Consider a tube section containing two subsections in the radial direction, namely subsection 1 and subsection 2, as shown in Figure 4.1. Each subsection has a width, an average radius and temperature denoted by ε_1, $\bar{r}_1$, $<T>_1$, and ε_2, $\bar{r}_2$, $<T>_2$ respectively. Let $\Delta \ell$ be the length of the tube section, then the energy equations for these two subsections appear as (for simplicity, a fixed boundary is employed)

$$\rho_{m1} \, 2\pi \bar{r}_1 \, \varepsilon_1 \, \Delta \ell \, C_m \, \frac{d<T>_1}{dt} = EK_{g \to 1} \, (T_g - <T>_1)$$
$$- EK_{1 \to 2} \, (<T>_1 - <T>_2) \qquad (4\text{-}19)$$

$$\rho_{m2} \, 2\pi \bar{r}_2 \, \varepsilon_2 \, \Delta \ell \, C_m \, \frac{d<T>_2}{dt} = EK_{1 \to 2} \, (<T>_1 - <T>_2)$$
$$- EK_{2 \to S} \, (<T>_2 - T_s) \qquad (4\text{-}20)$$
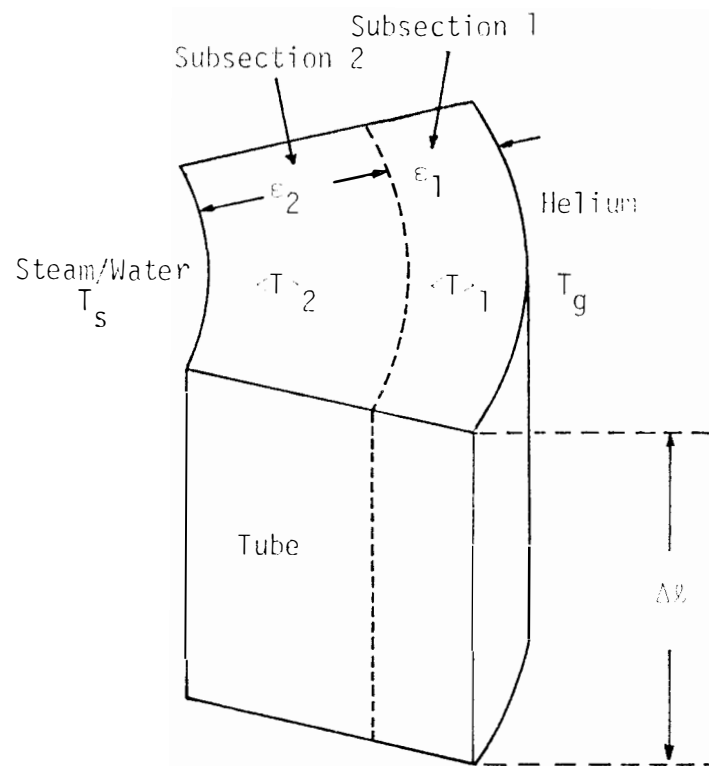
Figure 4.1. A Tube Section Containing Two Subsections in the Radial Direction.

where ρ_m is tube density and each EK is the conductance for heat transfer between two regions denoted by subindices.

If the tube surface is considered as a limiting case of a subsection with an infinitesimal width, then by taking the limit, $\varepsilon_1 \to 0$, the following equations are achieved:

$$\lim_{\varepsilon_1 \to 0} <T>_1 = T_{gs} \tag{4-21}$$

$$\lim_{\varepsilon_1 \to 0} <T>_2 = T_m \tag{4-22}$$

$$\lim_{\varepsilon_1 \to 0} EK_{g \to 1} = EK_{g \to gs} = h_p A_{gs} \tag{4-23}$$

$$\lim_{\varepsilon_1 \to 0} EK_{1 \to 2} = EK_{gs \to m} \tag{4-24}$$

$$\lim_{\varepsilon_1 \to 0} EK_{2 \to S} = EK_{m \to s} \tag{4-25}$$

Equations (4-19) and (4-20) become:

$$h_p A_{gs} (T_g - T_{gs}) - EK_{gs \to m} (T_{gs} - T_m) = 0 \tag{4-26}$$

$$\rho_m A_m \Delta \ell C_m \frac{dT_m}{dt} = EK_{gs \to m} (T_{gs} - T_m) - EK_{m \to s} (T_m - T_s) \tag{4-27}$$

From equation (4-26), one can obtain

$$T_{gs} = \frac{h_p A_{gs} T_g + EK_{gs \to m} T_m}{h_p A_{gs} + EK_{gs \to m}}$$

which is equation (4-14).

It means that equation (4-14) is valid in the transient state.
Equation (4-27) is a energy balance equation for the tube metal.

Similarly, by taking the limit, $\varepsilon_2 \to 0$, one can show that equations (4-17) and (4-18) are also valid in the transient state.

CHAPTER 5

CORRELATIONS AND PROPERTIES OF THE WORKING

FLUIDS AND TUBE METALS

In this chapter, the correlations, the physical and thermodynamic properties of the working fluids and the physical properties of the tube metals used in the Fort St. Vrain steam generator model are presented.

5.1 Effects of the Coil Geometry

When fluid flows through a curved tube, the fluid particle with higher velocity experiences a higher acceleration force along the coil radial direction and moves toward the outer wall in the tube. The centrifugal force which is opposite to the radial acceleration force at the outer wall is larger than at the inner wall. A secondary flow is formed, which is superimposed on the main flow. The frictional energy loss near the tube wall is larger than for a corresponding flow in a straight tube. Also, a given amount of heat can be transferred more easily in a coiled tube than in a straight tube of the same length. Therefore the friction factor and the heat transfer coefficient for the coiled tube are higher than for the straight tube. Moreover, coils allow more heat transfer area to be packaged in a given space of the shell than for a straight tube.

The heat transfer and friction coefficients for coiled geometry for laminar and turbulent flow were summarized by Srinivasan et al.[27] In this model, the ratio of the coil to the straight tube frictional factor is taken from Ito's.[28]

With turbulent flow,

$$\frac{f_c}{f_s} = [Re \ (\frac{r_o}{R_c})^2]^{1/20} \tag{5-1}$$

Equation (5-1) predicts the results for large coils.

For heat transfer, Seban and McLaughlin[29] recommend that equation (5-1) can also be used for the ratio of the heat transfer coefficient for the coil to that for the straight tube.

The effects of the coil on two phase correlations are reported only sparsely. Based on a study by Crain, Bell and Owhadi,[30,31] equation (5-1) is adopted for two phase forced convection boiling inside a helical coil.

The heat transfer and pressure drop for cross flow through banks of multistart helical tubes with uniform inclinations and uniform longitudinal pitches have been developed by Gilli.[32] However, with the design of the tube pattern in the Fort St. Vrain steam generator, (i.e., with equal lengths of helically wound tubes) it is considered to be more practical to use empirical correlations[33] which are based on a modification of Grimison's relation.

5.2 Summary of the Correlations

Unless indicated otherwise, the following are correlations for straight tubes:

1. For the single phase friction factor for H_2O, the Colebrook equation[34] is employed.

$$\frac{1}{\sqrt{f}} = -2.0 \log (\frac{\varepsilon/D}{3.7} + \frac{2.51}{Re\sqrt{f}} \tag{5-2}$$

2. The two phase friction factor for H_2O

$$f_{T.P.} = [2 \log (\frac{\varepsilon/D}{3.7} + \frac{2.51}{Re_{T.P.} \sqrt{f}_{T.P.}})]^{-2} \tag{5-3}$$

where the two phase Reynolds number is:

$$Re_{T.P.} = Re_f (1 + X \frac{\mu_{fg}}{\mu_g}) \tag{5-4}$$

3. The friction factor for helium flow through the tube bank in helical coil geometry is obtained using the Grimison frictional factors[35] for in-line tube bank data (see Figure 5.1).

4. For the single phase steam heat transfer coefficient, the Dittus-Boelter equation[36] is used

$$h_t = 0.023 \frac{k}{d_i} Re^{0.8} P_r^{0.4} \tag{5.5}$$

5. The heat transfer coefficient for two phase water after departure from the nucleate boiling is obtained from the Z. L. Miropolśkiy correlation[37]:

$$h_t = 0.023 \left\{ \frac{GD}{\mu_g} [X + (\frac{v_f}{v_g})(1 - X)] \right\}^{0.8} (\frac{C_p \mu}{k})_g^{0.8}$$

$$\cdot \frac{k_g}{D} [1 - 0.1 (\frac{v_g}{v_f} - 1)^{0.4} (1 - x)^{0.4}] \tag{5-6}$$
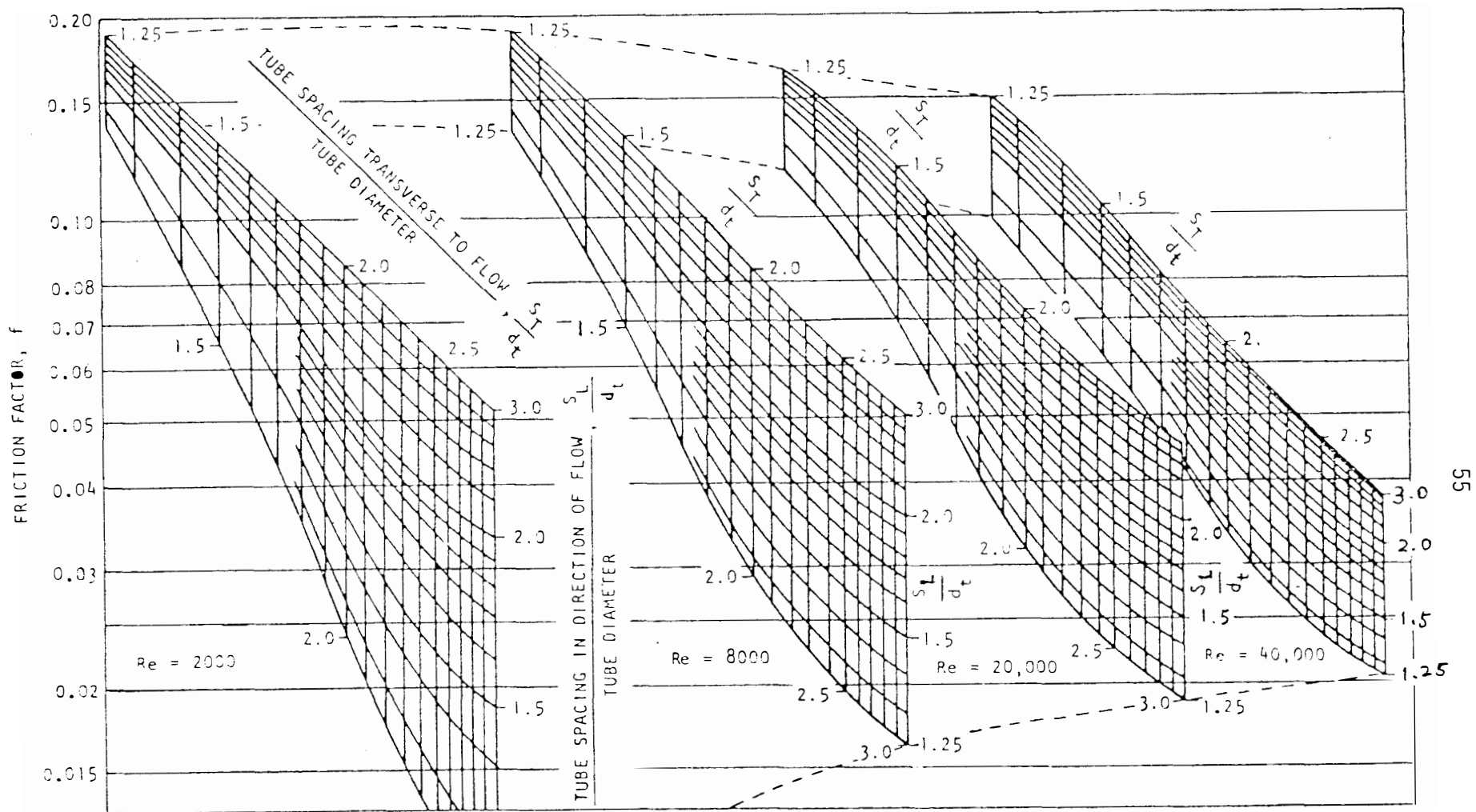
Figure 5.1.   Grimison Friction Factors for In-Line Tube Banks.

6. The heat transfer coefficients in the two phase nucleate boiling and subcooled boiling regions are as follows. The flow-type heat transfer coefficients developed by Chen[38] are used

$$h_c = 0.023 \left[\frac{G(1 - X)d_i}{\mu_f} \right]^{0.8} \left[\frac{C_p \mu}{k} \right]_f^{0.4} \left(\frac{k_f}{d_i} \right) \cdot F \qquad (5\text{-}7)$$

$$h_{NCB} = 0.00122 \left[\frac{k_f^{0.79} C_{pf}^{0.45} \rho_f^{0.49}}{\sigma^{0.5} \mu_f^{0.29} h_{fg}^{0.24} \rho_g^{0.24}} \right]$$

$$\cdot \Delta T_{sat}^{0.24} \Delta p_{sat}^{0.75} S_R \qquad (5\text{-}8)$$

where

$$F = \left[\frac{Re_{T.P.}}{Re_f} \right]^{0.8} = F_1 (1/X_{tt}) \qquad (5\text{-}9)$$

$$S_R = \text{suppression factor} = F_2 (Re_{T.P.})$$

$$X_{tt} \approx \left(\frac{1 - X}{X} \right)^{0.9} \left(\frac{\rho_g}{\rho_f} \right)^{0.5} \left(\frac{\mu_f}{\mu_g} \right)^{0.1} \qquad (5\text{-}10)$$

For saturated boiling, the heat transferred is calculated as

$$Q_s = (h_c + h_{NCB}) A_{ss} (T_{ss} - T_{sat}) \qquad (5\text{-}11)$$

For subcooled boiling, the heat transferred is expressed as

$$Q_s = h_{NCB} A_{ss} (T_{ss} - T_{sat}) + h_c A_{ss} (T_{ss} - T_s) \qquad (5\text{-}12)$$

7. The heat transfer coefficient for single phase water flow is obtained from the Dittus-Boelter correlation.

8. The heat transfer correlation for the helium flow across the tube bank is obtained from the modified Grimison in-line tube bank heat transfer relation.[39] The Nusselt number is expressed as

$$N_u = B(Re)^n \ (P_r/0.69)^{0.33} \qquad\qquad (5\text{-}13)$$

where B and n are constants for a given coil geometry, which may be determined from Table 5.1.

9. The condition for departure from nucleate boiling for water in the helical coil is[40]:

$$X_{DNB} = 1.565 \times 10^{-3} \ Q^{0.719} \ G^{-0.212} \ \exp \ (1.724 \times 10^{-4}P) \qquad (5\text{-}14)$$

where

Q = heat flux in BTU/(hr-ft^2)

G = mass flux in lbm/(ft^2-hr)

P = fluid pressure in psi

5.3 Physical and Thermodynamic Properties of the Working Fluids and Physical Properties of the Tube Metals

In the following, some important properties of helium, steam/water and the tube metals used for the dynamic modeling of the Fort St. Vrain steam generator are summarized.

1. The information on the helium properties presented below was summarized by Sanders,[41] which is based on a report, GA-1355[42]:

a. viscosity of helium

$$\mu = 6.7 \times 10^{-4} \ (T_g + 460.0)^{0.68}$$

TABLE 5.1

GRIMISON DATA FOR IN-LINE TUBE BANK HEAT TRANSFER RELATIONS[a,b]

X_L [c]	$X_T d = 1.00$		$X_T d = 1.25$		$X_T d = 1.5$		$X_T d = 2.0$		$X_T d = 3.0$		$X_T d = 4.0$		$X_T d \geq 5.0$	
	B	n	B	n	B	n	B	n	B	n	B	n	B	n
1.0	0.282	0.610	0.0868	0.700	0.0335	0.784	0.0250	0.800	0.0288	0.775	0.0386	0.742	0.0513	0.710
1.25	0.389	0.582	0.291	0.610	0.193	0.644	0.0857	0.718	0.0656	0.745	0.865	0.718	0.109	0.695
1.5	0.472	0.560	0.344	0.588	0.275	0.608	0.132	0.681	0.0896	0.720	0.117	0.694	0.127	0.685
2.0	0.452	0.540	0.391	0.570	0.297	0.598	0.195	0.642	0.162	0.661	0.157	0.665	0.150	0.670
2.5	0.351	0.565	0.357	0.576	0.332	0.567	0.284	0.604	0.219	0.630	0.183	0.650	0.162	0.662
3.0	0.243	0.616	0.297	0.598	0.342	0.584	0.355	0.580	0.267	0.609	0.200	0.640	0.174	0.654
4.0	0.132	0.680	0.237	0.621	0.322	0.589	0.355	0.580	0.289	0.601	0.212	0.633	0.193	0.640
6.0	0.108	0.700	0.204	0.636	0.306	0.495	0.362	0.578	0.289	0.601	0.221	0.628	0.217	0.630

[a] Extended and modified slightly to include subsequent investigations.

[b] $Nu = B(Re)^n (Pr/0.69)^{0.33}$.

[c] X_L = longitudinal pitch spacing (inch).

[d] X_T = transverse pitch spacing (inch).

where μ = viscosity (lbm/ft-hr)

T_g = helium temperature (°F)

atmospheric pressure $\leq P \leq$ 2000 psia

b. heat capacity of helium at constant pressure

C_p = 1.2425 Btu/lb-°F

which is independent of both temperature and pressure.

c. the gas constant in the ideal gas relationship

R = 10.73 (psia-ft)/(lbm-mole-°R)

d. thermal conductivity of helium

$$k = 0.0853219 + 10.1319 \times 10^{-5} \, T_g - 1.17909 \times 10^{-8} \, T_g^2$$

for P close to 670 psia

where k = thermal conductivity [Btu/hr-ft^2-(°F/ft)]

T_g = helium temperature (°F)

2. The physical and thermodynamic properties (i.e. thermal conductivity, viscosity, heat capacity and the relationships among pressure, temperature, density, enthalpy, etc.) of steam/water are based on the International Formulation Committee's equations from the International Conference on Properties of Water, Steam 1967[43] and the correlating formulae of Bruges and Gibson.[44]

The computer subroutines for the thermodynamic property equations are used, which return the property value when one supplies the appropriate inputs for each required function. In these subroutines,

some of the property functions such as $\partial V_g/\partial p$, $\partial V_f/\partial p$, $\partial h_g/\partial p$, $\partial h_f/\partial p$ for the steam/water in saturation and $T = T(u)$, $\rho = \rho(T)$ for the subcooled water are in polynomial forms which are obtained from the least square fitted method.

3. The physical properties of the tube metals[45]

    a.   the density of the tube metal

$$\rho_m = 501.12 \text{ lbm/ft}^3 \text{ for the upper coil (superheater II)}$$

$$\rho_m = 489.024 \text{ lbm/ft}^3 \text{ for the lower coil (economizer-}$$

        evaporator-superheater)

    b.   thermal conductivity

$$k = (((((3.4472 \times 10^{-14} \times T_m - 1.2983 \times 10^{-10}) \times T_m$$
$$+ 1.7832 \times 10^{-7}) \times T_m - 1.0941 \times 10^{-4}) \times T_m + 9.1764$$
$$\times 10^{-2}) \times T_m + 74.557)/12 \text{ Btu/hr-ft-}°F \qquad (5\text{-}18)$$

    for the upper coil

T_m is in °F.

$k = 16.9167$ Btu/hr-ft-°F for the lower coil

    c.   heat capacity

$$C_p = 0.12 \text{ Btu/lb-}°F \text{ for the upper coil}$$

$$C_p = 0.11 \text{ Btu/lb-}°F \text{ for the lower coil}$$

CHAPTER 6

CALCULATIONAL METHODS

In this chapter, methods for steady state and transient calculations using a digital computer (IBM 360) are described.

6.1 Steady State

The steady state distribution provides the following information in dynamic modeling:

1. initial conditions for transient calculations

2. information to verify the adequacy of the correlations employed in the model if it is compared with experimental data or design data

3. information for determining the number of lumps to be used in a few lump dynamic model.

The first step in the steady state analysis is to divide the steam generator into a finite number of sections of equal length along the tube. In each section, fluid properties are assumed constant.

In the beginning, the fluid properties at one end of the steam generator are assumed as known quantities. Then fluid properties of the next section are calculated according to the following equations:

for the steam/water side,

$$W = constant \qquad (6-1)$$

$$h_{i+1} = h_i - Q_i/W_i \qquad (6-2)$$

$$p_{i+1} = p_i + f_i \cdot \pi \cdot D_i \cdot |G_i| \, G_i \cdot \Delta \ell_i / (8 A_i \, \rho_i \, C_2)$$

$$+ |G_i|^2 \, (\frac{1}{\rho_i} - \frac{1}{\rho_{i+1}})/C_2 \qquad (6\text{-}3)$$

$$\rho_{i+1} = f_1 \, (p_{i+1}, h_{i+1}) \qquad (6\text{-}4)$$

$$T_{si+1} = f_2 \, (p_{i+1}, h_{i+1}) \qquad (6\text{-}5)$$

for the helium side,

$$W_g \qquad = \text{constant} \qquad (6\text{-}6)$$

$$h_{gi+1} = h_{gi} - Q_i/W_g \qquad (6\text{-}7)$$

$$P_{gi+1} = P_{gi} - f_{effi} \cdot G_{NRi} \, |G_{gi}| \, G_{gi}/(2 \cdot \rho_{gi} \cdot C_2)$$

$$+ |G_{gi}|^2 \, (\frac{1}{\rho_{gi}} - \frac{1}{\rho_{gi+1}})/C_2 + \rho_{gi} \cdot g \cdot A_{eff} \cdot C_3$$

$$\cdot \Delta \ell_i \quad /(C_2 \cdot A_{eff}) \qquad (6\text{-}8)$$

$$\rho_{gi+1} = P_{gi+1}/[R_u \cdot (T_{gi} + 460.0)] \qquad (6\text{-}9)$$

$$T_{gi+1} = h_{gi+1}/C_{pg} + T_{gb} \qquad (6\text{-}10)$$

and

$$Q_i \qquad = EK_{g \to s,i} \, (T_{gi} - T_{si}) \qquad (6\text{-}11)$$

In the above equations, equation (6-1) and (6-6) result from conservation of mass; equation (6-2) and (6-7) are energy balance equations; equation (6-3) and (6-8) come from momentum balances. Equation (6-4), (6-5), (6-9) and (6-10) are thermodynamic relationships and Q_i is a heat transfer term. Detailed definitions of notation are given in the Nomenclature.

The equivalent conductances for heat flow from helium to steam/water together with the tube average temperature and tube surface temperatures on both the helium and the steam/water sides are obtained by calling subprograms which calculate those quantities as a function of geometry and properties of the fluids and metal. Equations (4-8), (4-9), (4-10) and (4-11) are for conductance calculations. The temperature equations for the tube metal are given in equation (4-12), (4-14), (4-17) and (4-18).

The boundary between superheater I and superheater II is the joint of the upper coil tube and the lower coil tube. The boundaries for defining the saturated region and the location of departure from nucleate boiling are determined by comparing the calculated steam quality, X with X = 0, X = X_{DNB}, and X = 1. The departure from nucleate boiling correlation X_{DNB} is given in Chapter 5, equation (5-14). The steam quality is calculated from

$$X = (h - h_f)/h_{fg} \tag{6-12}$$

where

$$h_{fg} = h_g - h_f$$

The location of the onset of nucleate boiling can be found by comparing the saturation temperature, $T_{sat}(P)$, with the local tube wall temperature, T_{ss}. P is a local pressure.

After the state variables at the other end of the steam generator are calculated, the steam generator inlet conditions which are obtained are compared with the design values[46] (or the desired operational

levels if design values are not available), and a new set of state variables for the beginning section is determined from a convergence criterion for the next calculation step. The iterative procedure is continued until the comparison between inlet conditions and design values (or the desired operational levels) is satisfied. The steady state calculation can be verified by comparing the outlet conditions obtained from calculation with the design data (or the resultant outlet levels obtained by setting inlets equal to the desired operational conditions).

The flowchart in Figure 6.1 illustrates the procedure for the steady state calculation.

6.2 Transient State

The system equations which consist of equation (3-20) through equation (3-54) and the state equations for each subregion are solved with a time step less than or equal to 10^{-2} sec. For the purpose of efficiency while keeping good accuracy, two sections for each flow region, i.e., twelve sections in the primary fluid, tube metal and the secondary fluid side respectively are selected for demonstrating the model transient responses. But the computer program developed can handle other lumping assumptions (see Section 6.3).

The steam/water enthalpy, the helium temperature and pressure are evaluated in the direction of the respective fluid flow; the steam/water pressure is evaluated in the direction opposite to the steam/water flow. This is because of the input conditions of the steam generator. The steam outlet pressure is provided by the model downstream from the steam generator outlet on the secondary side while the water inlet enthalpy,
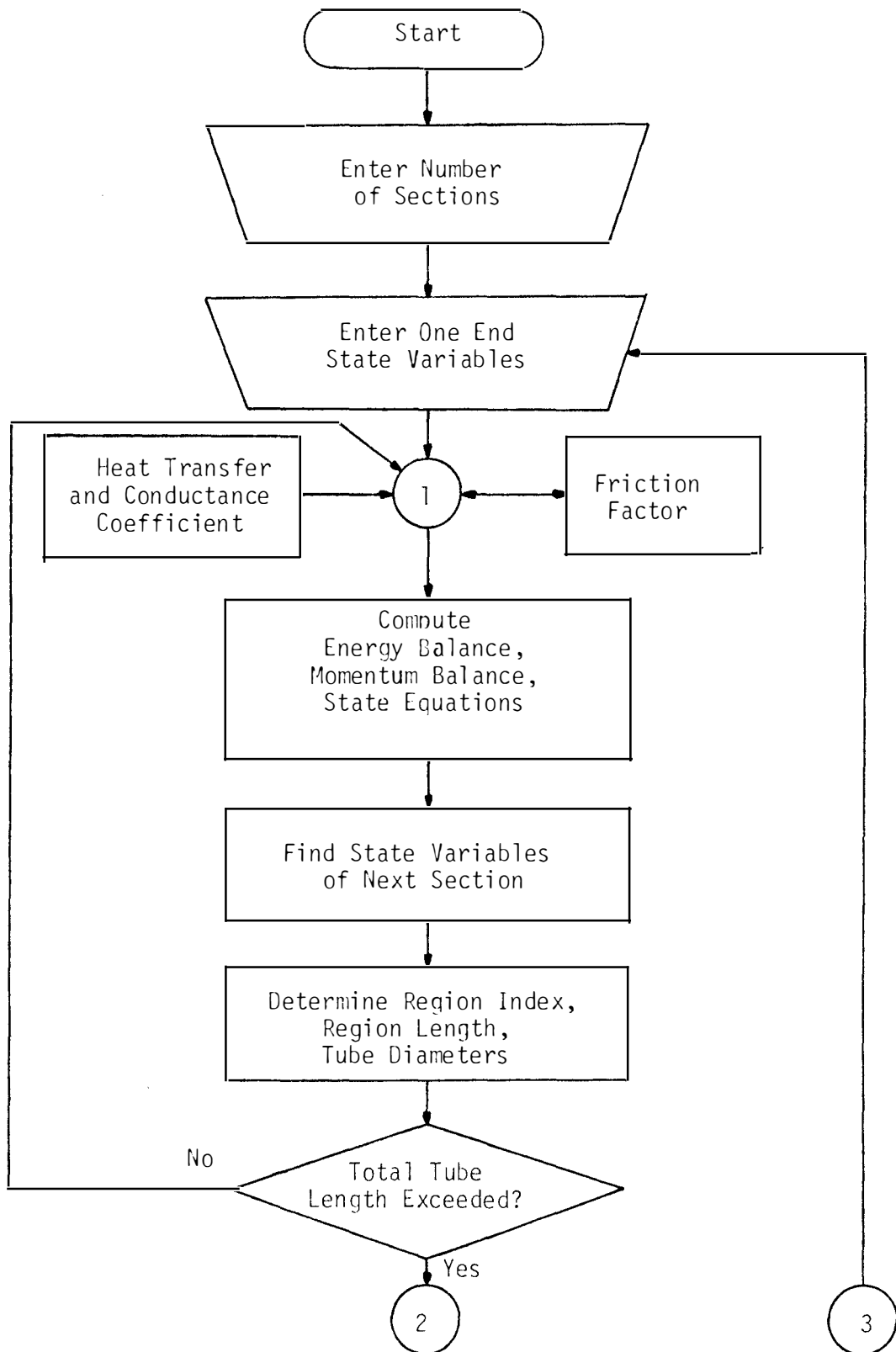
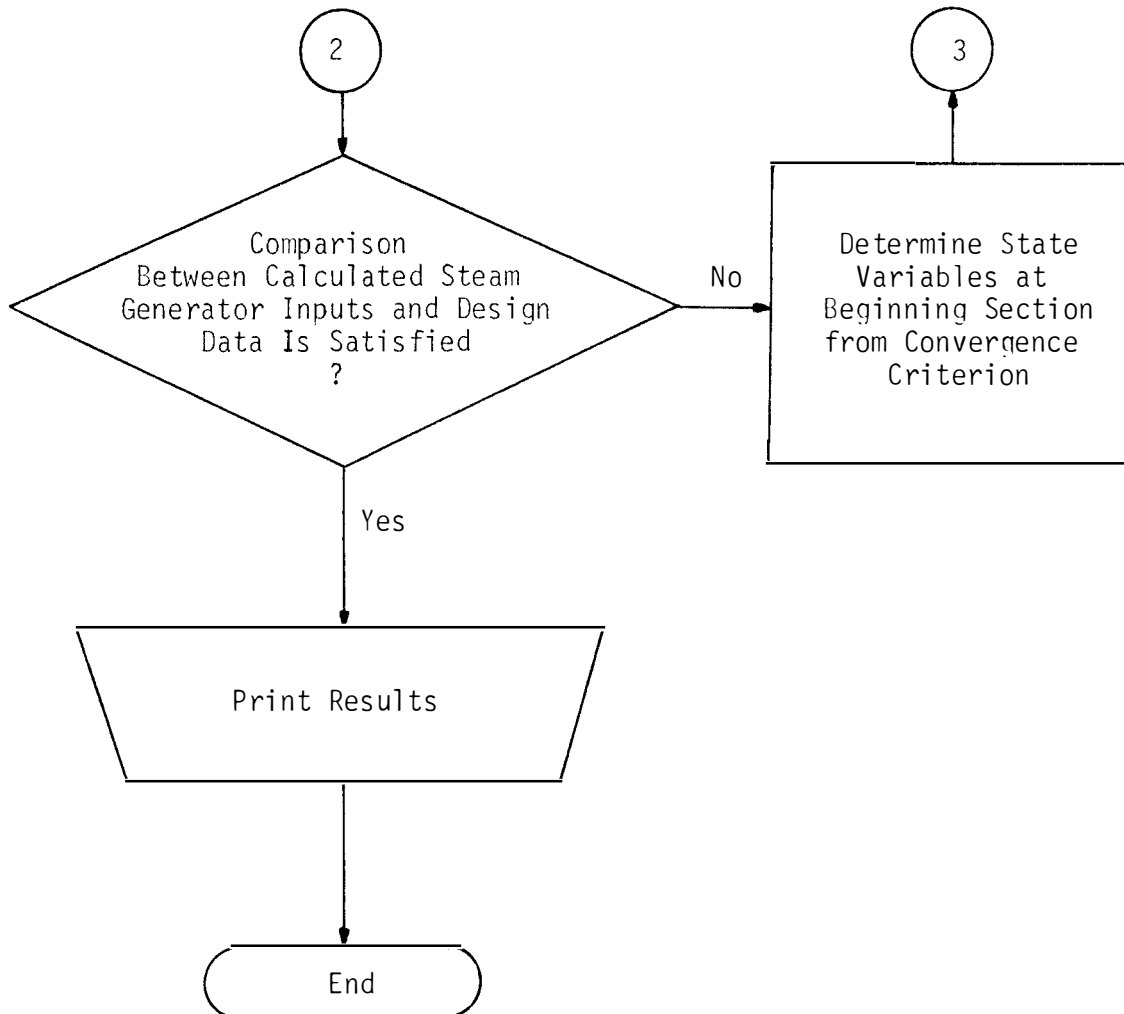Figure 6.1. A Simplified Flowchart of the Steady State Calculation.

Figure 6.1 (continued)

mass flow rate at the entrance and the helium pressure, temperature, and mass flow rate at the inlet are supplied by the models upstream from the steam generator inlets.

To evaluate time derivatives of state variables from differential equations, the heat transfer terms and friction factors must be predetermined. The heat transfer involves an evaluation of the heat conductance coefficient, which is described in Chapter 4, page 45. Time derivatives of state variables such as helium temperature, tube temperature, steam/water internal energy and four moving boundaries (boundaries for $T_{sat}(p) = T_{wall}$, $X = 0$, $X = X_{DNB}$ and $X = 1$) are then used to determine these state variables of the next time step for each section by employing an integration method, the Euler method. Since only a finite number of digits is significant in the state variables, the time derivatives of state variables are set to zero when they are smaller than 10^{-2}. Therefore a noise signal induced by the limitation on insignificant digits in the state variables at the initial time can be avoided.

The helium pressure and the steam/water pressure are determined from their momentum equations.

The mass flow rate and its time derivative are directly related to the mass flow rate perturbation by equations (3-2) and (3-3), which is based on the analysis described in Section 3.3, page 18.

At each time step, fluid thermodynamic properties including pressure, specific internal energy, specific enthalpy, density (or specific volume), temperature and steam quality must be evaluated since these properties

are required in the dynamic equations at each time step. In general, two thermodynamic properties determined from the dynamic equations and/or the predefined conditions such as regime boundary conditions are sufficient to determine another thermodynamic property. However, in the subcooled water region, the thermodynamic properties required are weak functions of pressure and only a single variable relationship is used for approximation.

Thermodynamic calculations for these secondary side (steam/water side) sections with their downstream boundaries defined by regime boundary conditions are different from other section calculations. These sections for an example, are section 3, 5, 7 and section 9 on the steam/water side as shown in Figure 6.2. Section 5, 7 and section 9 of the saturated region have their steam qualities determined from their boundary conditions and pressure from their momentum equations respectively. Therefore other properties of these three sections are explicitly or implicitly determined in terms of pressure and steam quality. The energy equations of these three sections combined with mass equations are used for boundary determinations for steam qualities at $X = 0$, $X = X_{DNB}$ and $X = 1$.

For section 3 of the subcooled region, water temperature is calculated from the heat transfer equation, i.e., equation (3-54), in which the tube surface temperature, T_{ssi}, is determined by the boundary condition, $T_{ssi} = T_{sat}(P)$, where P is its pressure determined by the momentum equation. Other thermodynamic properties of this section are a function of temperature. The energy equation combined with the mass
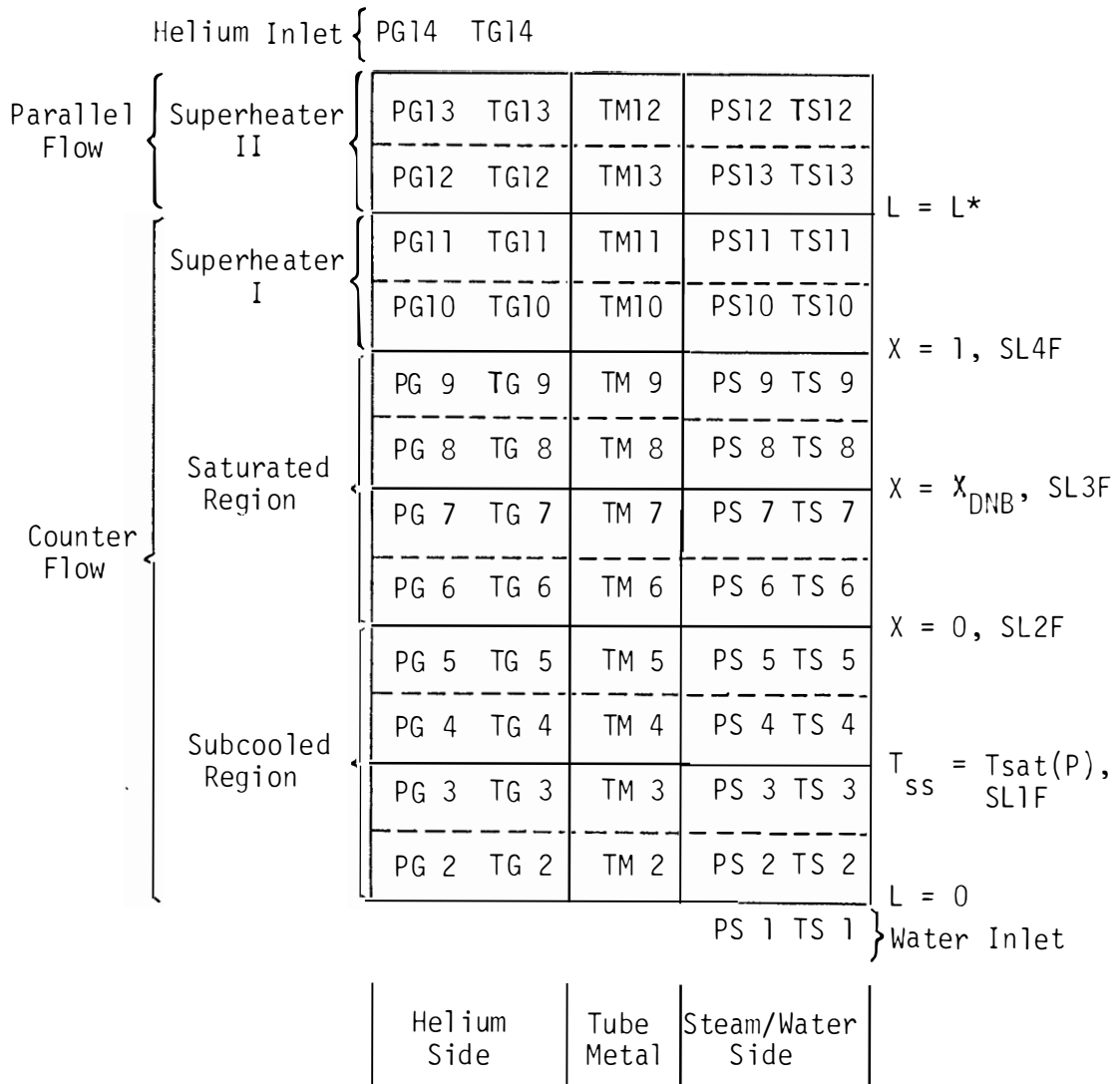
Figure 6.2. A Model Diagram and Its State Variables for the Lumping Case with Two Sections in Each Flow Region.

PGi   = helium pressure at section i

TGi   = helium temperature at section i

TMi   = tube temperature at section i

PSi   = steam/water pressure at section i

TSi   = steam/water temperature at section i

SLlF, SL2F, SL3F, SL4F = boundary lengths

L   = tube length

L*   = a fixed boundary

X   = steam quality

X_{DNB} = steam quality at which departure from nucleate boiling occurs

T_{ss} = tube wall temperature

Tsat (P) = saturated temperature at pressure P

Figure 6.2 (continued)

equation is used for determining the boundary length of the onset of nucleate boiling.

In other fluid sections (excluding the sections mentioned above), the pressure is also determined from the momentum equation but the temperature (for helium) or the internal energy (for steam/water) is evaluated from the energy equation combined with the mass equation. Other properties are therefore functions of pressure and temperature or internal energy in explicit or implicit forms.

The physical properties of the fluids, such as viscosity and thermal conductivity, which are necessary for evaluating the heat transfer coefficients and conductances are also calculated as functions of pressure and temperature.

For each tube metal section, the average temperature is determined from the energy balance equation and the surface temperatures are calculated from equation (4-14), (4-17) and equation (4-18). The tube density is given in Section 5.3.

Because of the existence of algebraic loops among equations including thermodynamic relationships, physical property equations and conductance equations, iterative procedures are always necessary.

In summary, the dynamic equations together with the model assumptions are used to solve for a set of state variables which determine the state of a section at each time step. The set of state variables contains two thermodynamic properties, one mass flow rate and the section's boundaries. Other state variables induced by state relations are supplementary for calculations.

As shown in Table 2.1, page 9, the Fort St. Vrain steam generator consists of several different tube materials and different tube wall thicknesses. It is necessary (depending on a section's boundaries) to find adequate tube properties and dimensions for each section at each time step. This can be achieved easily by comparing the upper boundary and the lower boundary of a section with the specific locations where tube characteristics change. However, if a region contains two tube characteristics, then the average value for that section is used. An example of the fluid flow area is given below:

$$\overline{A}_i = [A_i(\ell_{i+1} - \ell^*) + A_{i-1}(\ell^* - \ell_i)]/(\ell_{i+1} - \ell_i)$$

The calculational sequence in the time domain is illustrated in Figure 6.3.

The steam generator model is a part of the nuclear power plant system dynamic model. Those outputs and inputs of the steam generator to and from systems in its vicinity are shown in Figure 6.4.

6.3 The Computer Codes

The digital computer program in FORTRAN IV language was developed for both the steady state and the transient state. A name, KOLU(S), was assigned to the steady state code and another name, KOLU(T) was given to the transient state code for identification. Both the steady state and the transient state codes consist of a main program and a common set of subprograms. The main program is essential for calculating the state variables from the balance equations and reading and defining the input information. The set of subprograms provides a number of individual unit
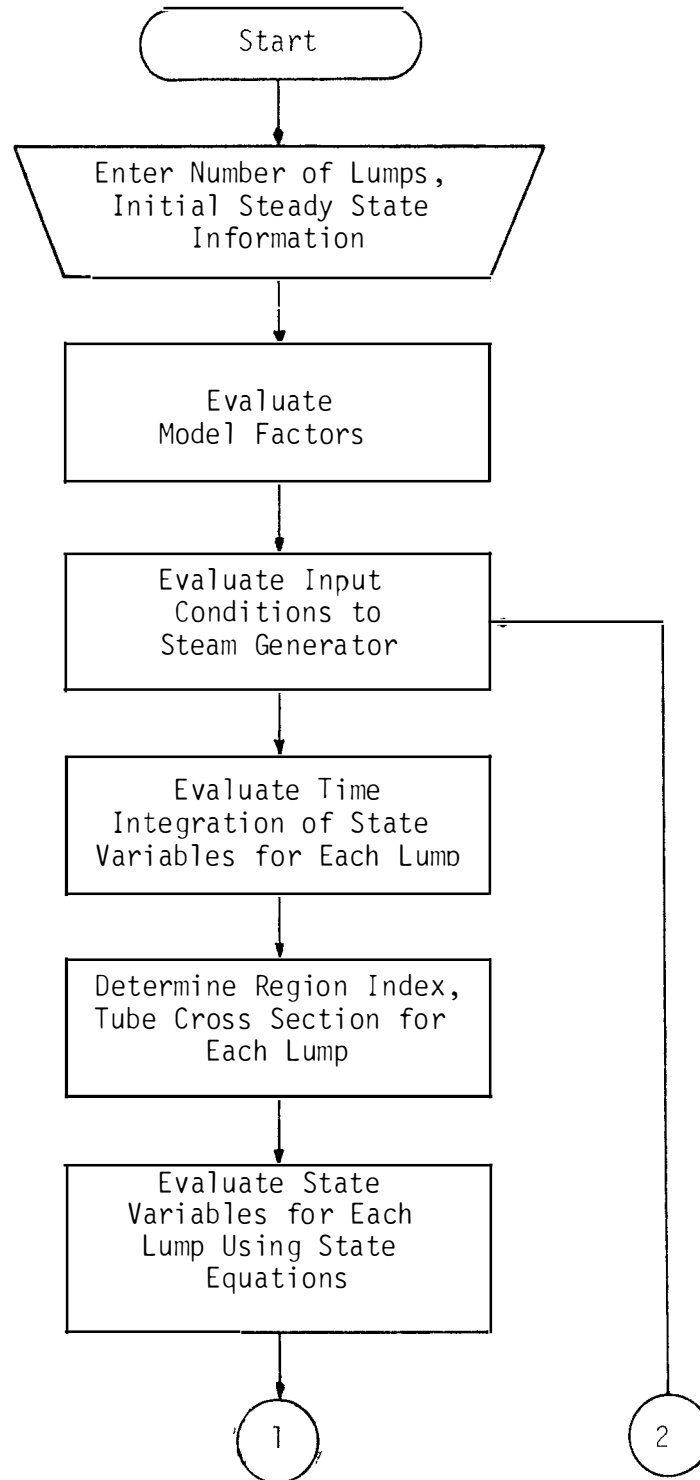
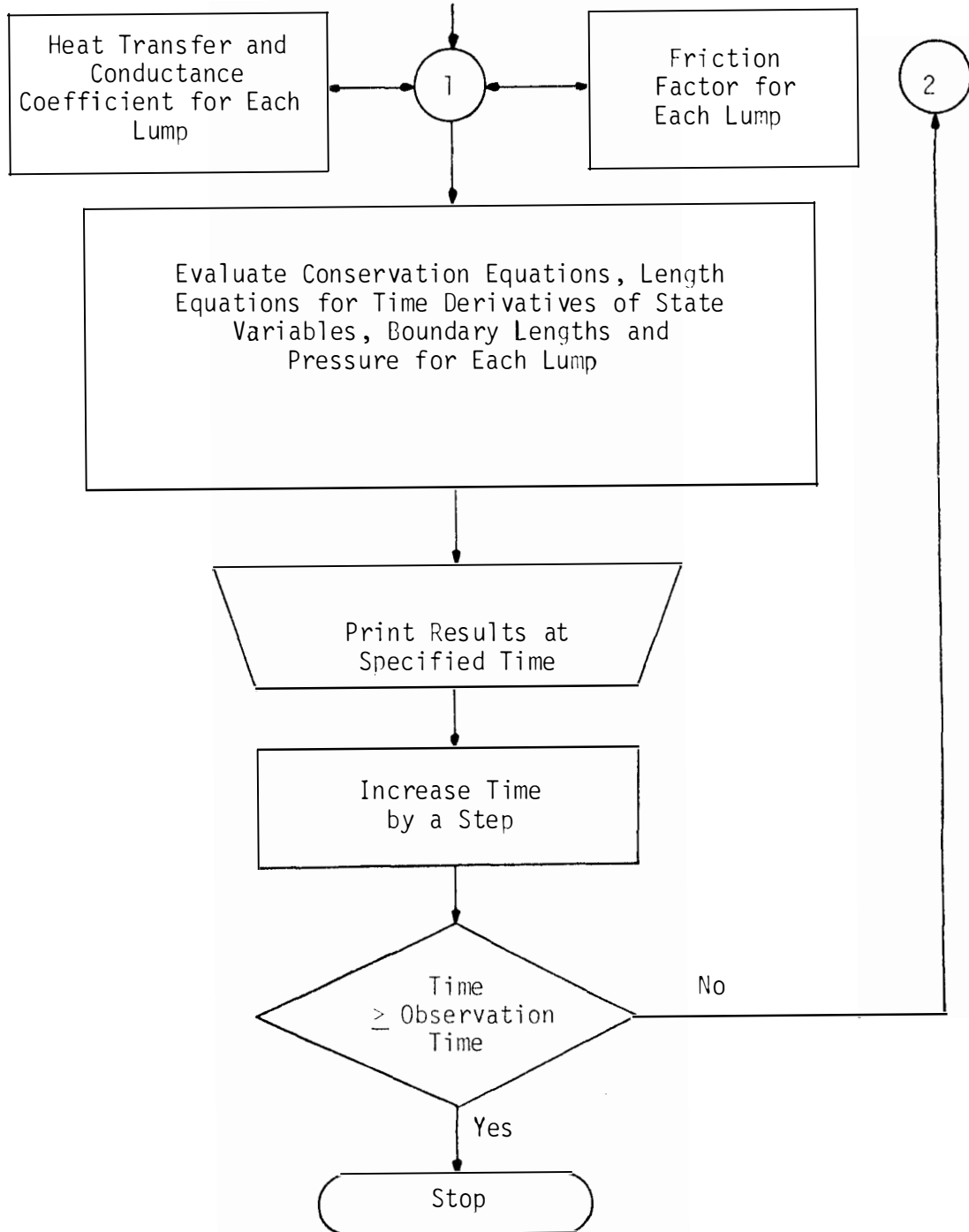Figure 6.3. A Simplified Flowchart of the Transient Calculation.

Figure 6.3 (continued)
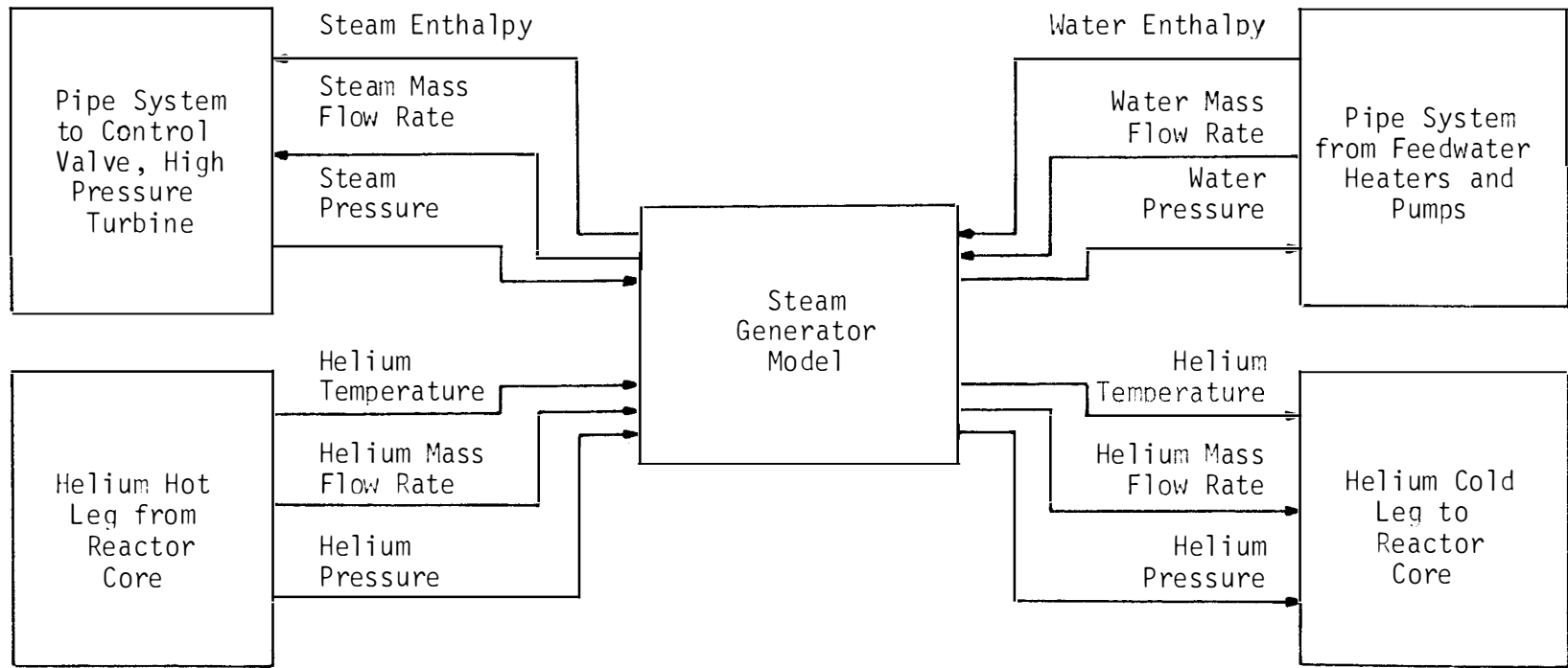
Figure 6.4.   The Steam Generator Model and Other Models in Its Vicinity.

75

subroutines or functions for the physical and the thermodynamic properties of steam/water, the correlations for friction factors and heat transfer for each of the flow regimes. This type of program structure makes it easy to replace the property functions and the correlations with alternate formulations if this is desirable.

Both the steady state and the transient state codes can handle the case of different number of nodes by simply replacing one statement in the codes. This provides a convenient way to select a simple or multilump model, depending on the purpose of the study.

However, since six flow regions are employed in the model, the minimum number of sections used on the secondary fluid side is limited to six. The maximum number of sections can be used in both codes is not limited, but no case with a very large number of sections has been tested so far.

CHAPTER 7

MODEL TESTING AND DISCUSSION

The model was used to perform simulations in order to verify the
model formulation, to determine the required number of sections used in
the transient model and to check the numerical methods and selected
correlations. The following steps were taken:

1. The steady state is calculated using 300 sections to obtain
distributions of the selected state variables and characteristics of
interest. Comparison of the outlet results with reported design data is
made.

2. Step changes to the input conditions of the steam generator
(i.e. to the water inlet enthalpy, mass flow rate, steam outlet pressure,
helium inlet temperature, helium inlet mass flow rate and pressure) are
performed for transient calculations. The transient outputs at the
final observation time are compared with the results obtained from
steady state calculations with 300 sections using the same conditions
that exist after the step changes.

3. Two lumping cases are studied for the transient calculations.
Case 1 employs two sections for each flow region and Case 2 employs two
sections for the subcooled convective region and one section for the
remaining flow regions. A comparison of the results for Case 1 and
Case 2 is given.

4. Calculations with time steps of 10^{-1} sec and 10^{-3} sec are
performed for the transient model in addition to a time step of 10^{-2} sec.

77

Numerical comparisons are presented for three selected perturbation cases.

5. The steam generator responses to variation of the feedwater mass flow rate and variation of helium inlet temperature are studied by running the steady state code with 300 sections. These results are used to assess the importance of nonlinear effects.

Finally, comparison of the transient responses for three models is given in Section 7.6.

7.1 Comparison of a Steady State Calculation with Design Data

A set of typical results from the steady state calculation are shown in Figure 7.1. In this figure, the tube length is used as one of the coordinates. For the tube length greater than 149.99 ft, the secondary flow changes direction from upward to downward. The state variable distributions shown in Figure 7.1 include primary fluid temperature and pressure, tube average and surface temperatures and secondary fluid pressure and temperature. The characteristics of the heat transfer in different regimes are reflected in the tube wall temperature and average temperature distributions. For example, the heat transfer coefficient in the two phase dryout region results in a high tube temperature in that region. Also, the effects of changes of the tube wall thickness on temperature and pressure distributions are shown. These effects cause rapid changes in the state variable distributions which can be found at the locations with tube length equal to 125.70 ft and 149.99 ft.
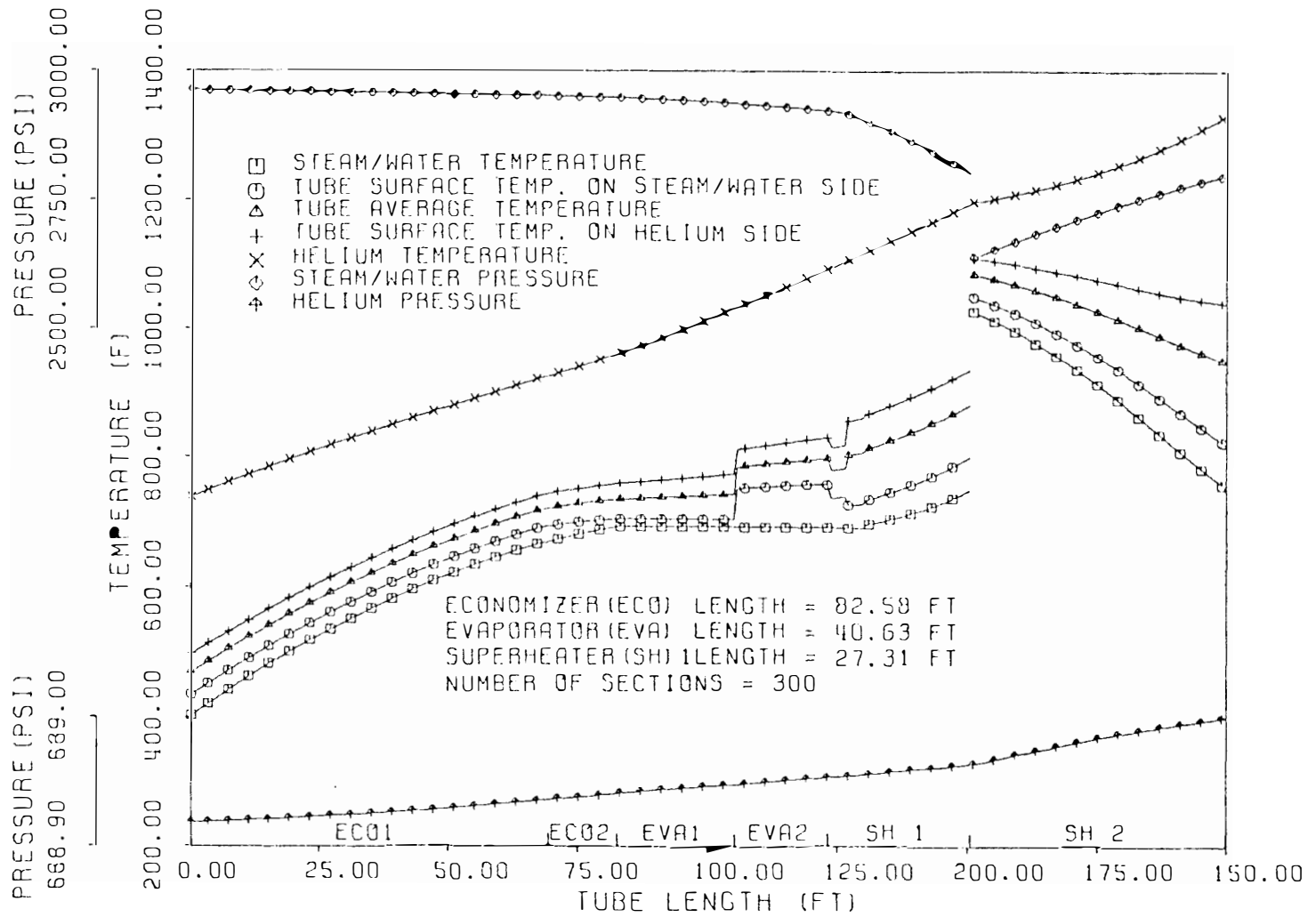
Figure 7.1. A Typical Steady State Calculation for Fort St. Vrain 330 MW(e) Steam Generator.

As indicated in Chapter 6, page 61, the steady state program matches one end condition with design data and calculates to the other end. It is possible to compare these calculated results with design values. Furthermore, the resultant section lengths, i.e. the lengths of economizer, evaporator and superheaters obtained from steady state calculations can be used to compare with the reported design values for the lengths of each section. The design information is obtained from reference 16 and reference 17. Numerical comparison between the steady state calculation and design data is given in Table 7.1.1.

Numerical results heavily rely on physical parameters and correlations used. Those parameters are listed in Table 2.1, page 9, and the correlations are given in Chapter 5. In general, the comparison of the steady state calculation with design data as shown in Table 7.1.1 is good.

7.2 Transient Responses

The transient model is a few section model which consists of the six flow regions described in Section 3.1, Capter 3, page 15. In order to study the adequacy of the number of sections selected, two lumping cases are analyzed for the transient calculations. The state variables of interest associated with lumping Case 1 are shown in Figure 6.2, page 69. For lumping Case 2, the section numbers corresponding to those in Case 1 are shown in Figure 7.2.

The transient calculations start with an initial steady state which is given in Table 7.2.1. This table is obtained by running the steady state code calculation with 300 sections and taking data from the steady

TABLE 7.1.1

COMPARISON BETWEEN DESIGN DATA AND STEADY STATE
CALCULATION (NUMBER OF SECTIONS = 300)

Items for Comparison		Design Values	Calculated Results
Water inlet temperature (F)	steam	415.[a]	415.
Steam outlet pressure (psi)	generator	2640.[a]	2640.
Helium inlet temperature (F)	input	1331.[a]	1331.
Helium inlet pressure (psi)	conditions	690.[a]	690.
Steam outlet temperature (F)		1030.[a]	1032.95
Water inlet pressure (psi)		2980.[a]	2968.90
Superheater II steam inlet temperature (F)		750.[a]	758.53
Superheater II steam inlet pressure (psi)		2790.[a]	2799.04
Helium outlet temperature (F)		741.[a]	742.89
Helium outlet pressure (psi)		686.[a]	688.92
Superheater II helium outlet temperature (F)		1192.[a]	·1199.16
Superheater I length (ft)		24.29[b]	28.638
Evaporator I length (ft)		25.51[b]	17.982
Evaporator II length (ft)		23.38[b]	22.644
Economizer length (ft)		76.81[b]	81.252

[a]Values obtained from reference 16.

[b]Values obtained from reference 17.
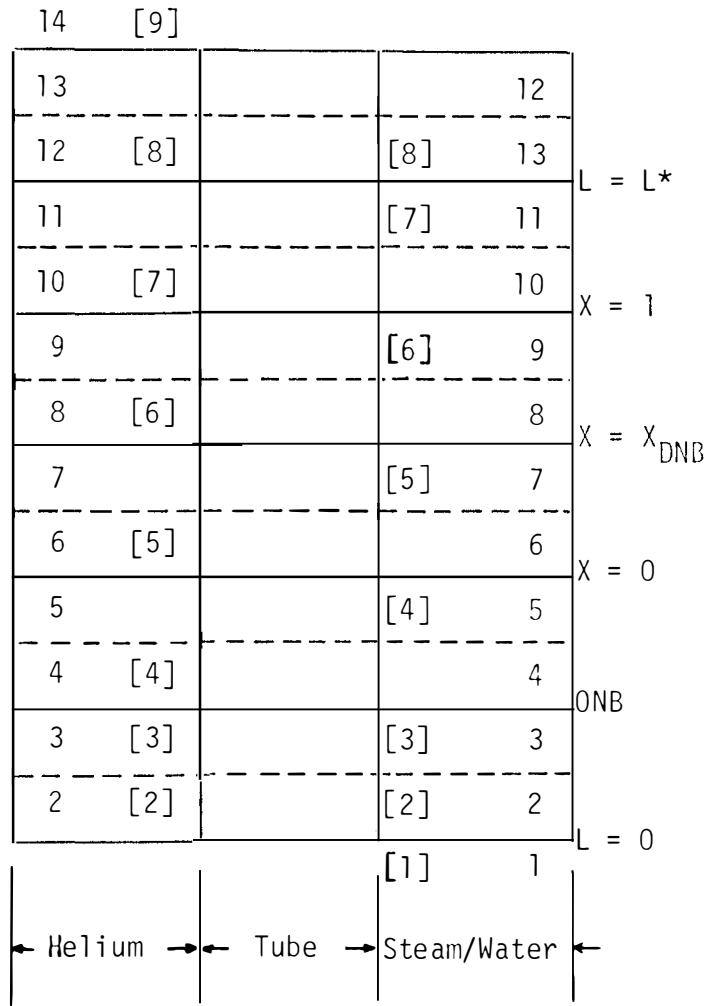
[ ]: A lumping case with two sections in the subcooled convective region and one section in each of the remaining flow regions. Otherwise, a lumping case with two sections in each flow region.

Figure 7.2. The Correspondence of the Section Number between Two Lumping Cases.

TABLE 7.2.1

INITIAL STEADY STATE VALUES FOR TWO LUMPING CASES[a]

Flow Regime and Section	Boundary Length (Ft)	Helium		Tube Temperature (F)	Steam/Water	
		Pressure (PSI)	Temperature (F)		Pressure (PSI)	Temperature (F)
Helium inlet section						
14 [9]		689.000 [689.000]	1333.109 [1333.109]			
Superheater II						
13	199.800 (fixed)	688.985	1244.537	1101.364 [1084.904]	2640.000 [2640.000]	1026.942 [1026.942]
12 [8]		688.964 [688.964]	1196.634 [1196.634]	1007.559	2728.720	908.770
Superheater I						
11	150.516 (fixed)	688.959	1148.521	883.973 [864.478]	2799.136 [2799.136]	749.660 [749.660]
10 [7]		688.955 [688.955]	1096.336 [1096.337]	831.733	2869.688	709.160

TABLE 7.2.1 (continued)

Flow Regime and Section	Boundary Length (Ft)	Helium Pressure (PSI)	Helium Temperature (F)	Tube Temperature (F)	Steam/Water Pressure (PSI)	Steam/Water Temperature (F)
Evaporator II						
9	123.210 [123.210]	688.952	1065.831	789.489 [781.037]	2922.149 [2922.149]	691.366 [691.366]
[6]						
8		688.949 [688.949]	1034.586 [1034.586]	784.221	2929.151	691.726
Evaporator I						
7	105.228 [105.228]	688.945	998.329	737.078 [732.084]	2935.984 [2935.984]	692.077 [692.077]
[5]						
6		688.941 [688.941]	963.939 [963.939]	733.625	2941.995	692.385
Economizer II						
5	82.584 [82.584]	688.939	946.270	732.108 [729.344]	2946.837 [2946.837]	692.632 [692.632]
[4]						
4		688.937 [688.937]	927.443 [927.443]	726.726	2948.537	683.637

TABLE 7.2.1 (continued)

Flow Regime and Section		Boundary Length (Ft)	Helium		Tube Temperature (F)	Steam/Water	
			Pressure (PSI)	Temperature (F)		Pressure (PSI)	Temperature (F)
Economizer I							
3	[3]	69.264 [69.264]	688.926 [688.926]	841.821 [841.821]	724.790 [724.790]	2950.418 [2950.418]	669.807 [669.807]
2	[2]		688.919 [688.919]	740.277 [740.277]	600.950 [600.950]	2957.580 [2957.580]	567.387 [567.387]
Water inlet section							
1	[1]					2963.558 [2963.558]	403.000 [403.000]

a[ ]: for lumping case with two sections in the subcooled convective region and one section in each of the remaining flow regions (lumping Case 2). Otherwise, for lumping case with two sections in each of the flow regions (lumping Case 1).

state distributions for the state variables in the model diagram according to the model structure described in Section 3.7, Chapter 3, page 29. In Table 7.2.1, the initial steady states for two lumping cases are given.

The input conditions of the steam generator for generating the numerical values in Table 7.2.1 and the resultant output state variables are given below:

Input information:

helium inlet pressure (PG 14): 689.0 psi

helium inlet temperature (TG 14): 1333.1 °F

helium mass flow rate: 78.936111 lbm/sec/module

steam outlet pressure (PS13): 2640.0 psi

water inlet temperature (TS1): 403.0 °F

water mass flow rate: 0.988220 lbm/sec/tube

Output information (from the steady state code calculation):

helium outlet pressure (PG2): 688.9 psi

helium outlet temperature (TG2): 740.3 °F

steam outlet temperature (TS13): 1026.9 °F

water inlet pressure (PS1): 2963.6 psi

boundary length at onset of nucleate boiling (SL1F): 69.264 ft

boundary length at X = 0 (SL2F): 82.584 ft

boundary length at X = X_{DNB} (SL3F): 105.228 ft

boundary length at X = 1 (SL4F): 123.210 ft

In the following sections (i.e. from Section 7.2.1 to Section 7.2.6), transient responses that resulted from Case 1 are used for interpretation of the physical phenomena for the steam generator system. It is found

that the asymptotic results in Case 1 are fairly consistent with the values from the steady state calculation. Those responses in Case 2 together with effects of reducing the number of sections in the transient model are discussed in Section 7.3.

For the convenience of explaining the tables and figures given below, the following notations are used.

Let SV be a state variable which may be the steam/water pressure, PS, the steam/water temperature, TS, the helium temperature, TG, the helium pressure, PG and the tube temperature, TM. Let SV_{in} be the state variable, SV, at the fluid entrance of the steam generator and let SV_o be the state variable SV at the fluid exit of the steam generator. From the above definition, it is noted that, for the lumping Case 1,

$$PS_{in} = PS1 \quad ; \quad TS_o = TS13 \quad ; \quad PG_o = PG2 \quad ; \text{ and } TG_o = TG2$$

Furthermore, let

ΔSV_k = change in SV_k in the transient state at the final observation
   time, where k = in or o.

A positive ΔSV_k indicates an increase in SV_k.

Also, let

Δe_{SV_k} = difference in SV_k between the transient state at the final
   observation time and the steady state after perturbation.

A positive Δe_{SV_k} implies that the transient value is greater than the steady state value.

Therefore, in the above notation, ΔSV_k gives an idea about the changes in responses of the steam generator output conditions and Δe_{SV_k}

reveals the deviations of the transient responses at the final observation time from those predicted by the steady state code.

Moreover, let

Economizer I = subcooled convective regions

Economizer II = subcooled nucleate boiling regions

Evaporator I = saturated nucleate boiling regions

Evaporator II = departure from nucleate boiling regions

Superheater I = superheated regions with tube length < 149.99 ft

Superheater II = superheated regions with tube length $\geq$ 149.99 ft

7.2.1 Responses to a Step Change in Water Inlet Enthalpy

Transient responses for 9°F step increase in water inlet temperature (or 2.5% step increase in water inlet enthalpy) are shown in Figure 7.2.1. As a result of increasing inlet water energy, the temperature of each section on the steam/water side increases, which is shown in the curves of TS3, TS5, TS7, TS9, TS11 and TS13. Due to thermal expansion, the steam/water pressure for each section is increased. This is shown in PS1, PS3, PS5, PS7, PS9 and PS11. PS13 is one of the input conditions. It is held constant for this case. Because the increase in the total pressure of each section is relatively small, the increased energy has a dominant effect on promoting water evaporation. Therefore the locations of the regime boundaries, i.e. the onset of nucleate boiling, saturated water with zero steam quality, departure from nucleate boiling and the steam with unit steam quality move downward toward the water entrance as shown in the curves of SL1F, SL2F, SL3F and SL4F. The increased steam/water temperature can prevent heat transfer from the tube to the
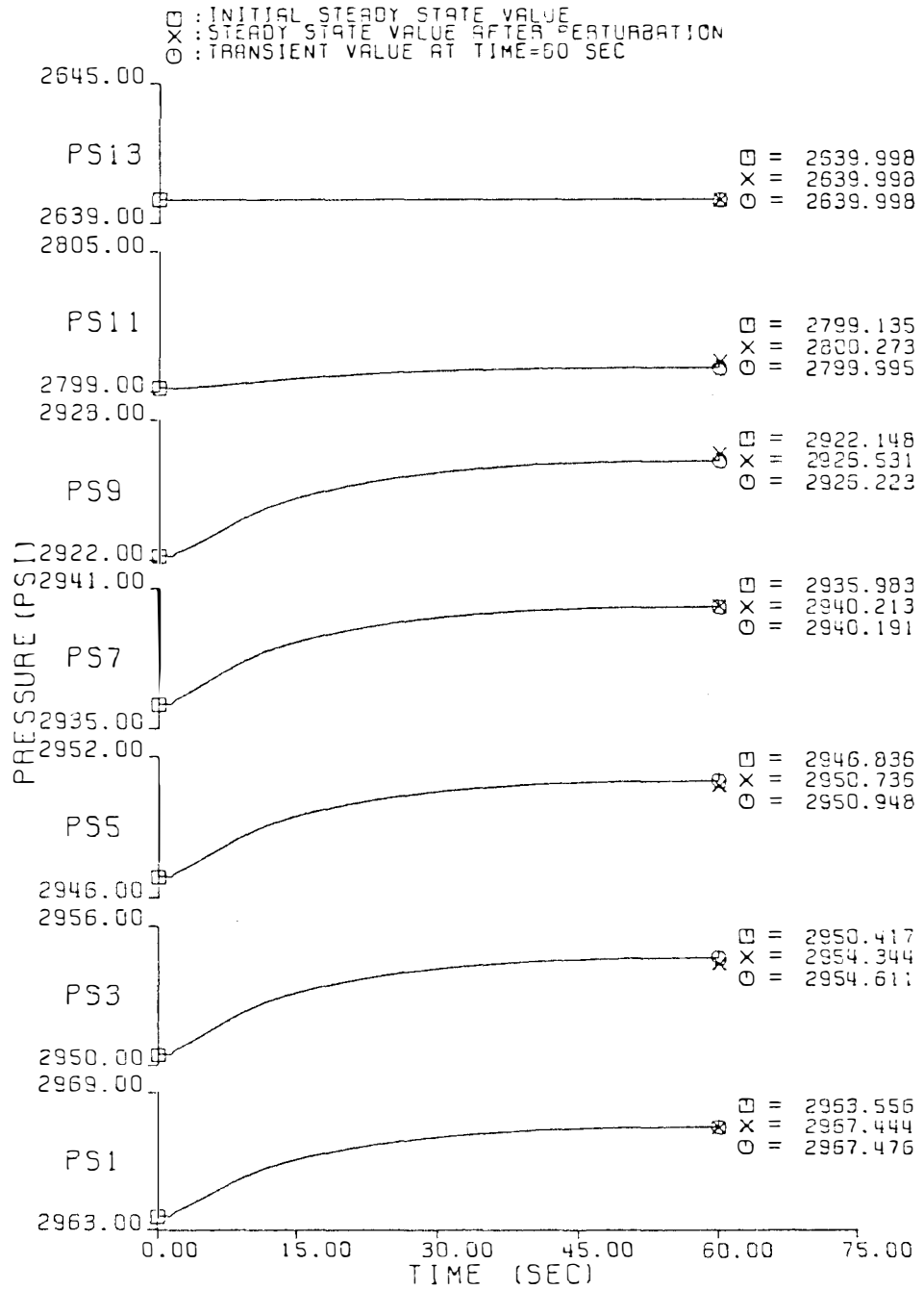
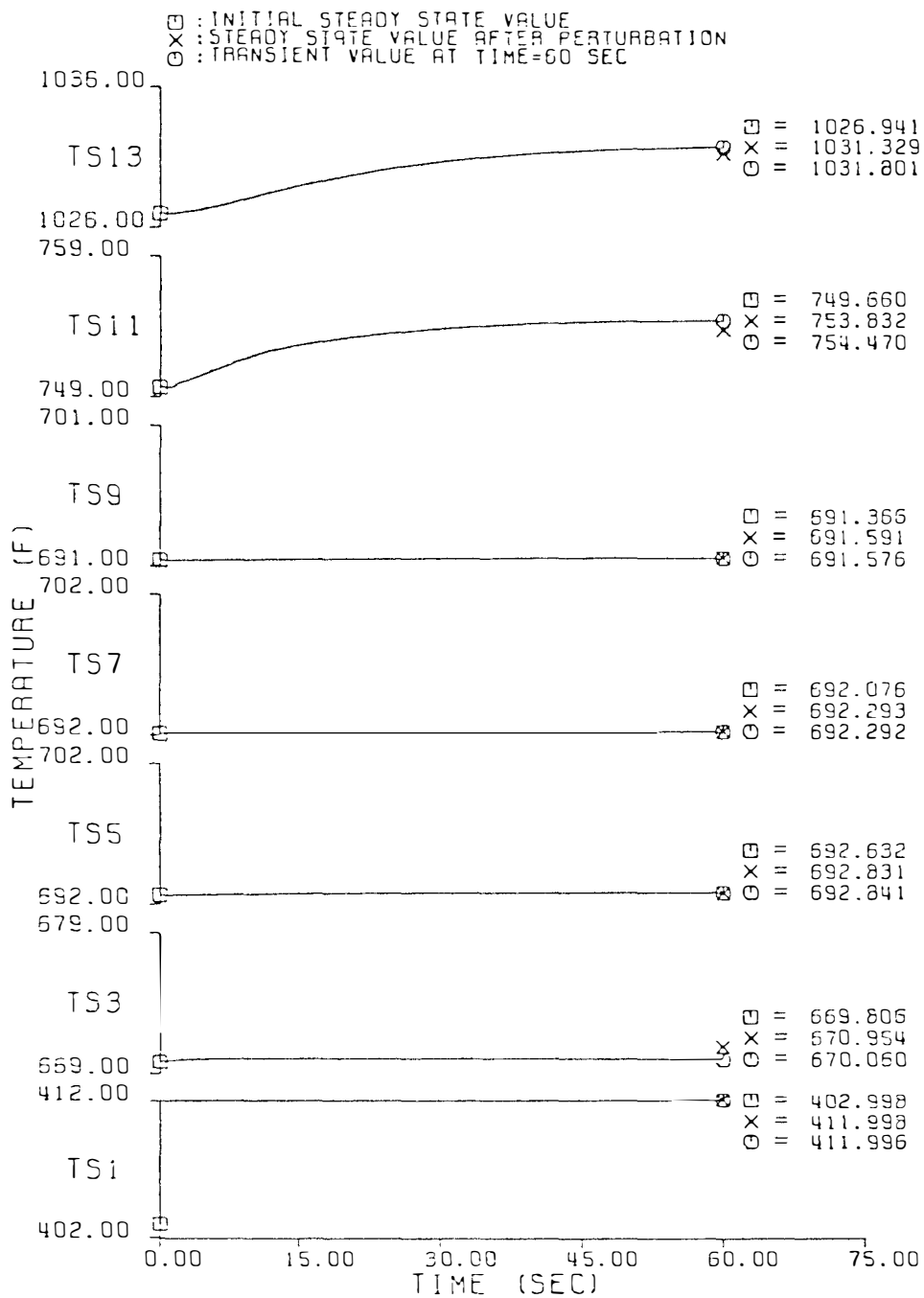Figure 7.2.1. Transient Responses to 9°F Step Increase in Feedwater Temperature.
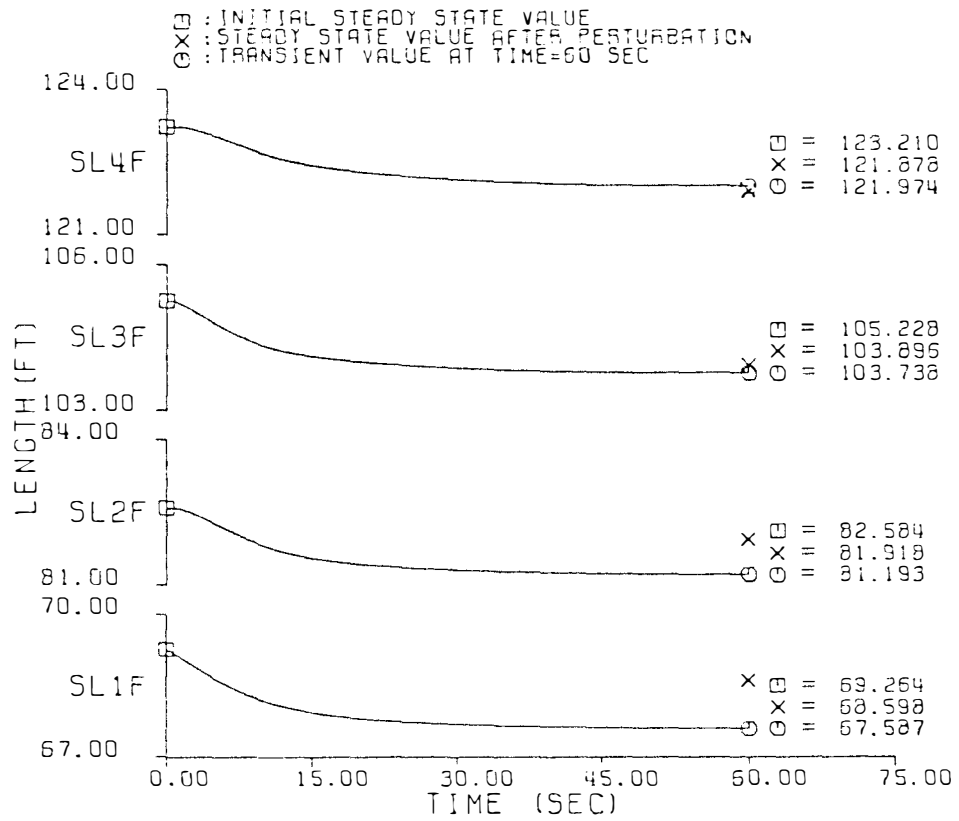
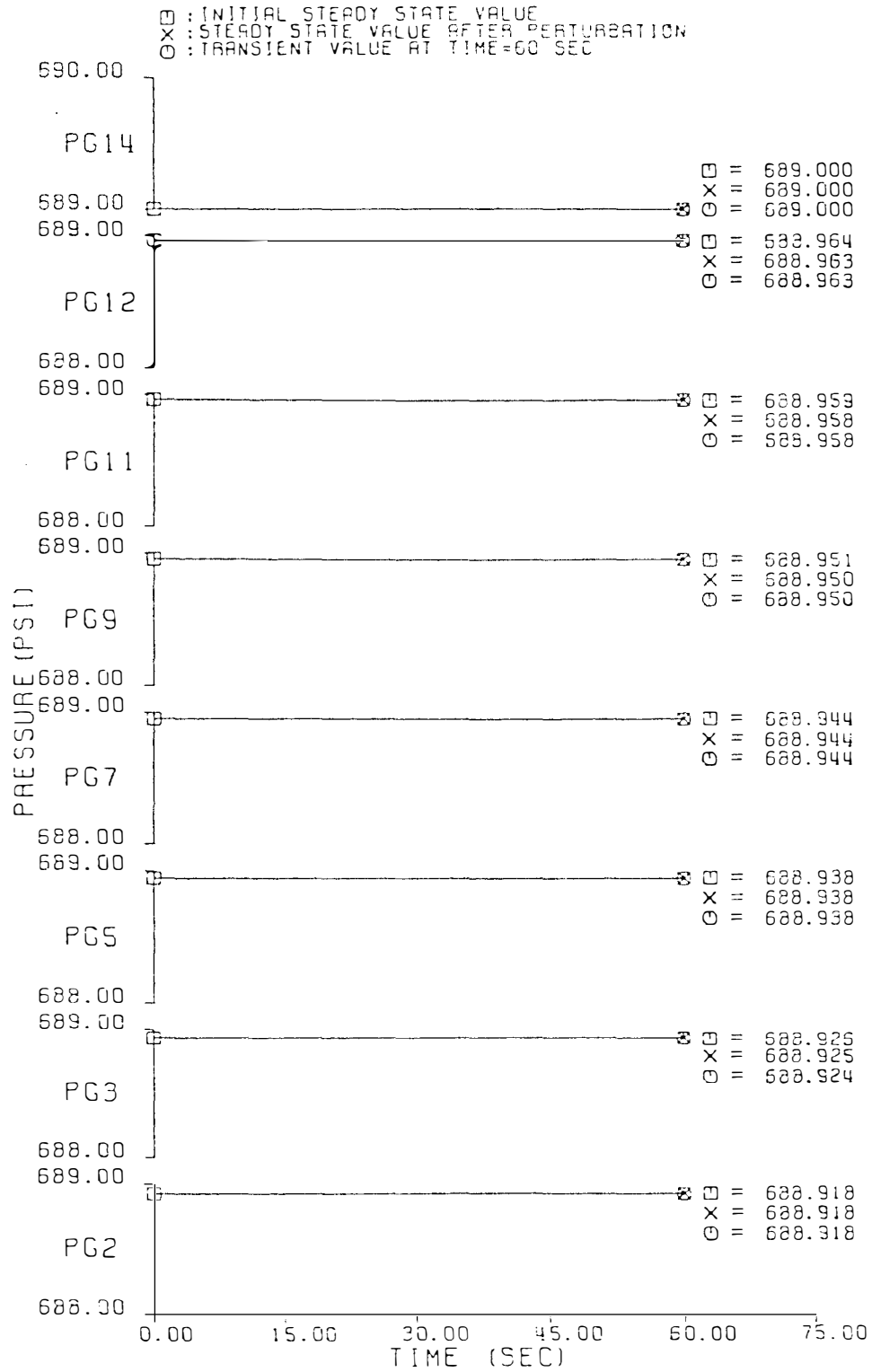Figure 7.2.1 (continued)

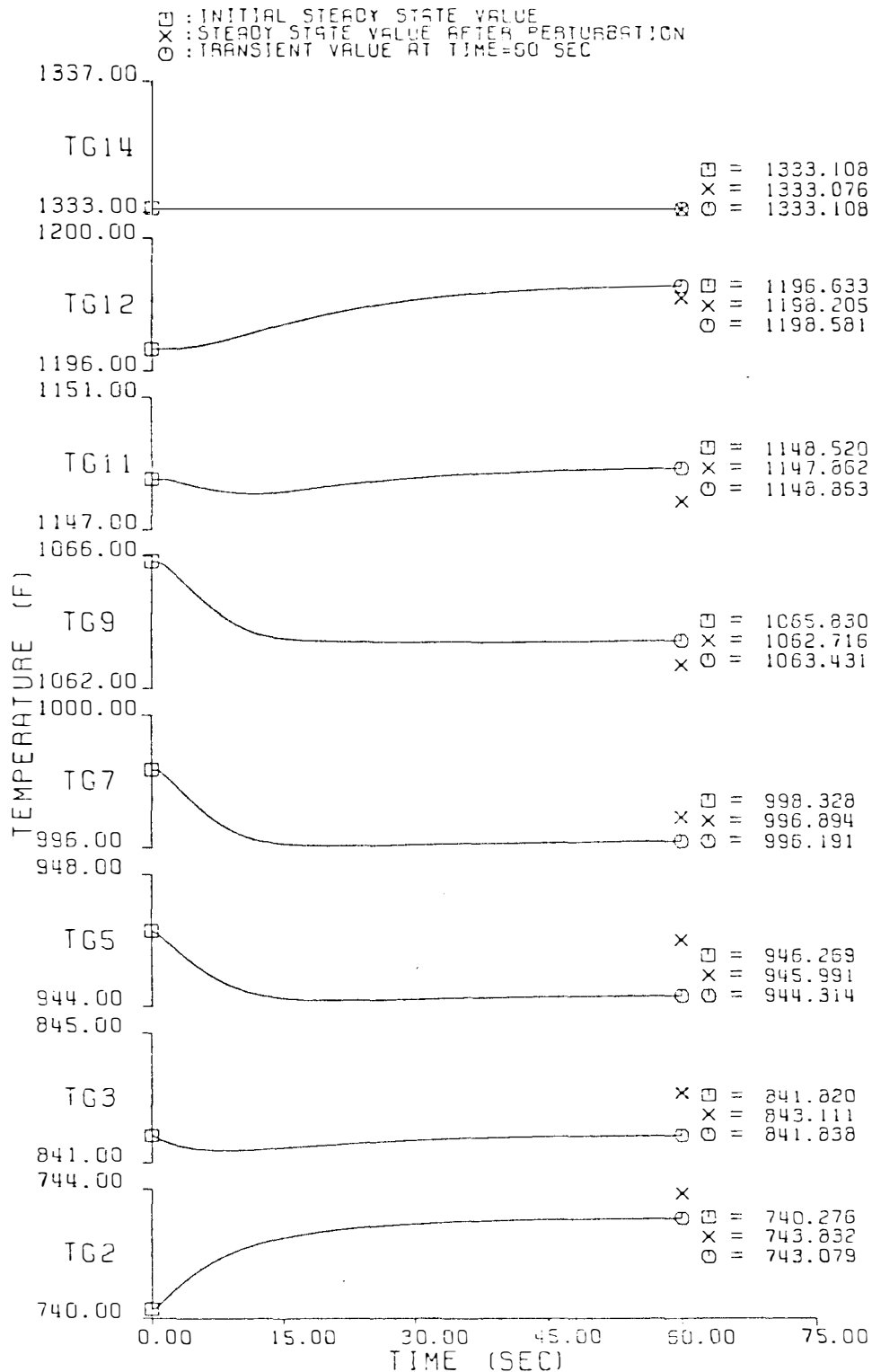Figure 7.2.1 (continued)

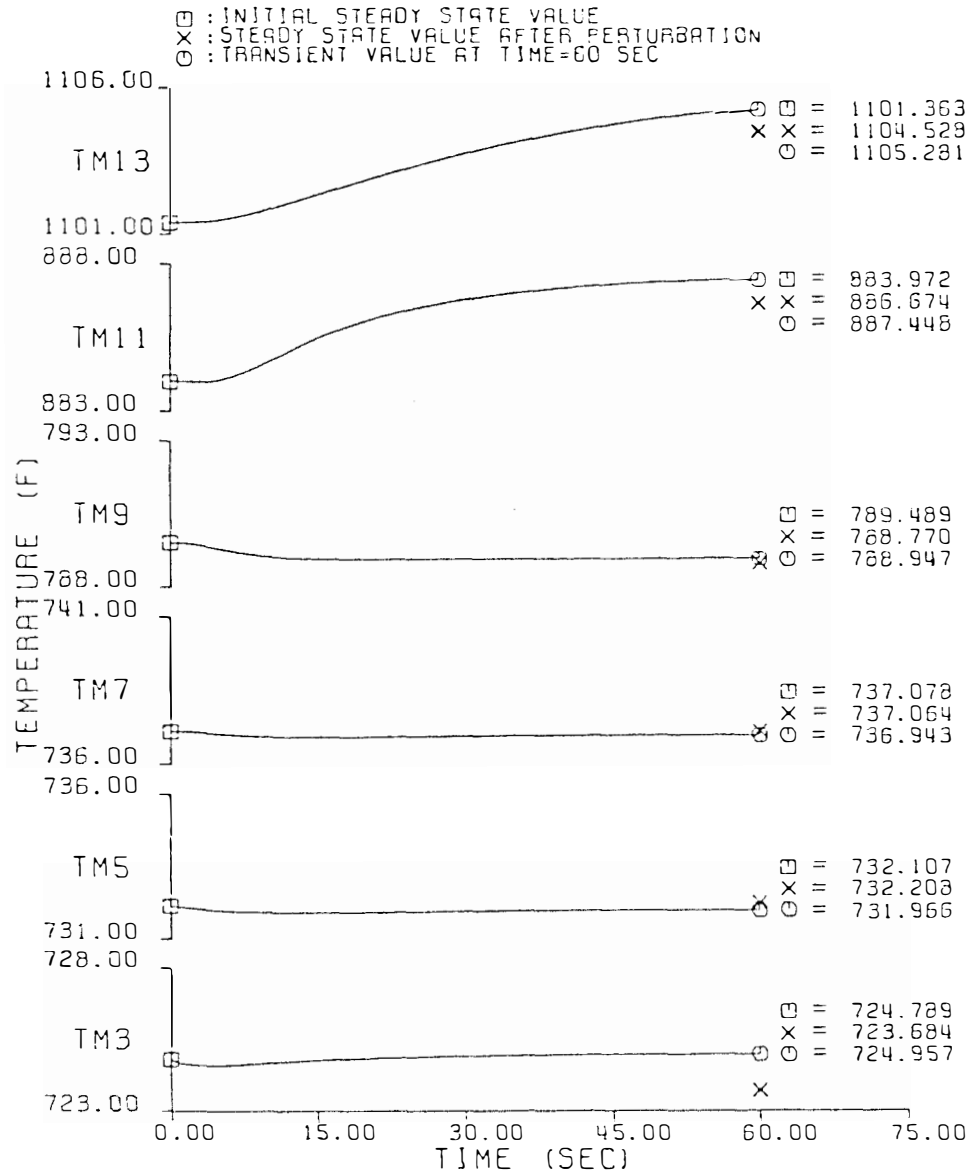Figure 7.2.1 (continued)

Figure 7.2.1 (continued)

Figure 7.2.1 (continued)

steam/water and from the helium to the tube metal, since the temperature difference between two media is the dominant factor for determining heat flow. This effect together with the boundary movement determines the tube average temperature and the helium temperature in each section. For sections in the fixed boundary region, their temperatures are closely related to the heat accumulated, hence TM11 and TM13 rise. But TM3, TM5, TM7 and TM9 in the moving boundary regions depend also on boundary locations. For a 9°F step increase in feedwater temperature, changes in helium temperatures may also depend on the heat transferred and the boundary moving as shown in TG2 through TG12 in Figure 7.2.1. The helium pressures, PG2 through PG12 are not affected significantly due to the relatively small variations in helium temperatures.

A detailed numerical comparison between the transient responses at 60 sec and the steady state values after a 9°F step increase in the inlet water temperature is shown in Table 7.2.2. In general, the comparison is in good agreement. The changes in the steam generator transient outputs and their deviations from those predicted by the steady state code are also shown. It is seen that the essential responses to a step change in inlet water enthalpy are in steam outlet temperature, water inlet pressure and then the helium temperature.

7.2.2 Responses to a Step Change in
        the Feedwater Mass Flow Rate

Responses to a 0.05 lbm/sec per tube step decrease in the feedwater mass flow rate are shown in Figure 7.2.2. One of the effects of decreasing the secondary fluid mass flow rate is the decrease in heat

TABLE 7.2.2

COMPARISON OF TRANSIENT RESPONSES AT 60 SEC AND STEADY STATE VALUES
AFTER 9°F STEP INCREASE IN FEEDWATER TEMPERATURE[a]

Flow Regime and Section	Boundary Length (Ft)	Helium		Tube Temperature (F)	Steam/Water	
		Pressure (PSI)	Temperature (F)		Pressure (PSI)	Temperature (F)
Helium inlet section						
14 [9]		689.000[b]	1333.109[b]			
		689.000	1333.109			
		[689.000]	[1333.109]			
Superheater II						
13		688.985[b]	1245.415[b]	1104.529[b]	2640.000[b]	1031.330[b]
		688.985	1246.005	1105.281	2640.000	1031.801
					[2640.000]	[1031.540]
[8]						
12		688.964[b]	1198.206[b]	1011.693[b]	2729.195[b]	914.256[b]
		688.964	1198.583	1011.520	2729.133	914.339
		[688.964]	[1198.625]			
Superheater I						
11		688.959[b]	1147.863[b]	886.674[b]	2800.274[b]	753.833[b]
		688.958	1148.864	887.449	2799.996	754.471
					[2799.767]	[754.438]
[7]						
10		688.954[b]	1094.265[b]	830.029[b]	2875.097[b]	710.286[b]
		688.954	1094.153	830.756	2874.911	711.078
		[688.954]	[1094.364]			

TABLE 7.2.2 (continued)

Flow Regime and Section	Boundary Length (Ft)	Helium Pressure (PSI)	Helium Temperature (F)	Tube Temperature (F)	Steam/Water Pressure (PSI)	Steam/Water Temperature (F)
Evaporator II						
9	121.878[b] 121.974 [121.780]	688.951[b] 688.951	1062.717[b] 1063.432	788.771[b] 788.947	2926.532[b] 2926.224 [2924.650]	691.592[b] 691.576 [691.495]
[6]						
8		688.948[b] 688.948 [688.947]	1031.756[b] 1032.003 [1031.217]	783.594[b] 783.600	2933.456[b] 2933.290	691.947[b] 691.939
Evaporator I						
7	103.896[b] 103.738 [103.198]	688.944[b] 688.944	996.894[b] 996.191	737.065[b] 736.943	2940.214[b] 2940.193 [2938.900]	692.294[b] 692.292 [692.226]
[5]						
6		688.941[b] 688.940 [688.940]	962.655[b] 962.204 [962.472]	733.591[b] 733.536	2945.999[b] 2946.145	692.589[b] 692.597

TABLE 7.2.2 (continued)

Flow Regime and Section		Boundary Length (Ft)	Helium Pressure (PSI)	Helium Temperature (F)	Tube Temperature (F)	Steam/Water Pressure (PSI)	Steam/Water Temperature (F)
Economizer II							
5		81.918[b]	688.939[b]	945.991[b]	732.209[b]	2950.737[b]	692.831[b]
		81.193	688.938	944.314	731.966	2950.949	692.842
		[81.027]				[2949.416]	[692.764]
	[4]						
4			688.936[b]	927.226[b]	727.060[b]	2952.450[b]	684.493[b]
			688.936	925.279	726.562	2952.687	683.876
			[688.936]	[925.494]			
Economizer I							
3	[3]	68.598[b]	688.925[b]	843.112[b]	723.684[b]	2954.345[b]	670.954[b]
		67.587	688.925	841.838	724.958	2954.611	670.060
		[67.407]	[688.925]	[842.089]		[2953.080]	[669.927]
2	[2]		688.917[b]	743.832[b]	605.078[b]	2961.482[b]	571.626[b]
			688.918	743.079	604.284	2961.612	570.833
			[688.918]	[743.380]		[2960.056]	[570.766]

TABLE 7.2.2 (continued)

Flow Regime and Section	Boundary Length (Ft)	Helium Pressure (PSI)	Helium Temperature (F)	Tube Temperature (F)	Steam/Water Pressure (PSI)	Steam/Water Temperature (F)
Water inlet section						
1 [1]					2967.445^b 2967.477^b [2965.905]	411.998^b 411.996^b [411.996]

[a] [ ]: Transient responses for the lumping case with two sections in the subcooled convective region and one section in each of the remaining flow regions.

[b] Values obtained from the steady state calculations using 300 sections with the input conditions after perturbation. Values without any mark are the transient responses for the lumping case with two sections in each of the flow regions.

$\Delta PG_o = -0.001 \, [-0.001]$ $\Delta e_{PG_o} = 0.001 \, [\, 0.001]$

$\Delta TG_o = 2.802 \, [\, 3.103]$ $\Delta e_{TG_o} = -0.753 \, [-0.452]$

$\Delta PS_{in} = 3.919 \, [\, 2.347]$ $\Delta e_{PS_{in}} = 0.032 \, [-1.54]$

$\Delta TS_o = 4.859 \, [\, 4.598]$ $\Delta e_{TS_o} = 0.471 \, [\, 0.21]$
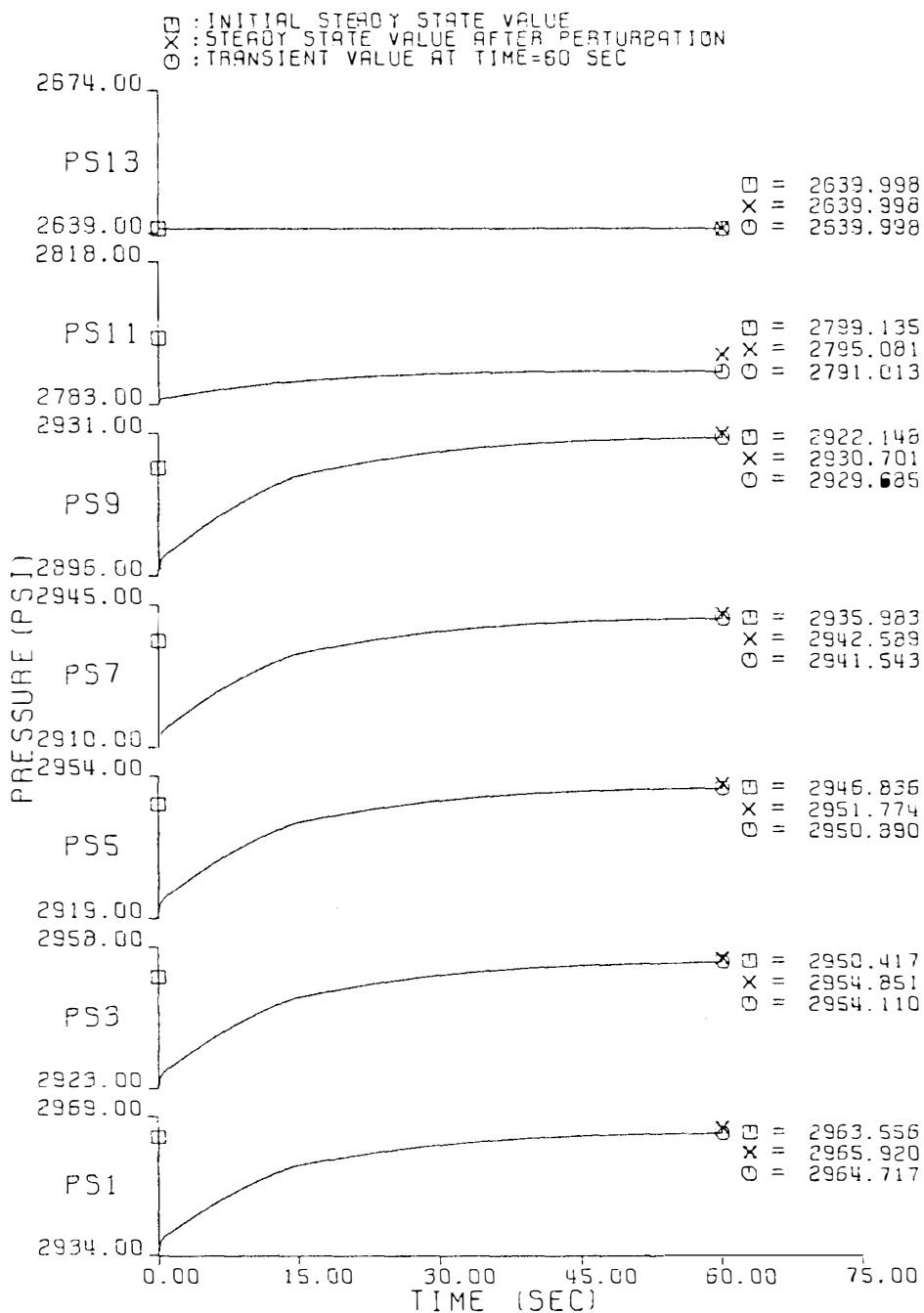
Figure 7.2.2.   Transient Responses to 0.05 Lbm/Sec per Tube Step
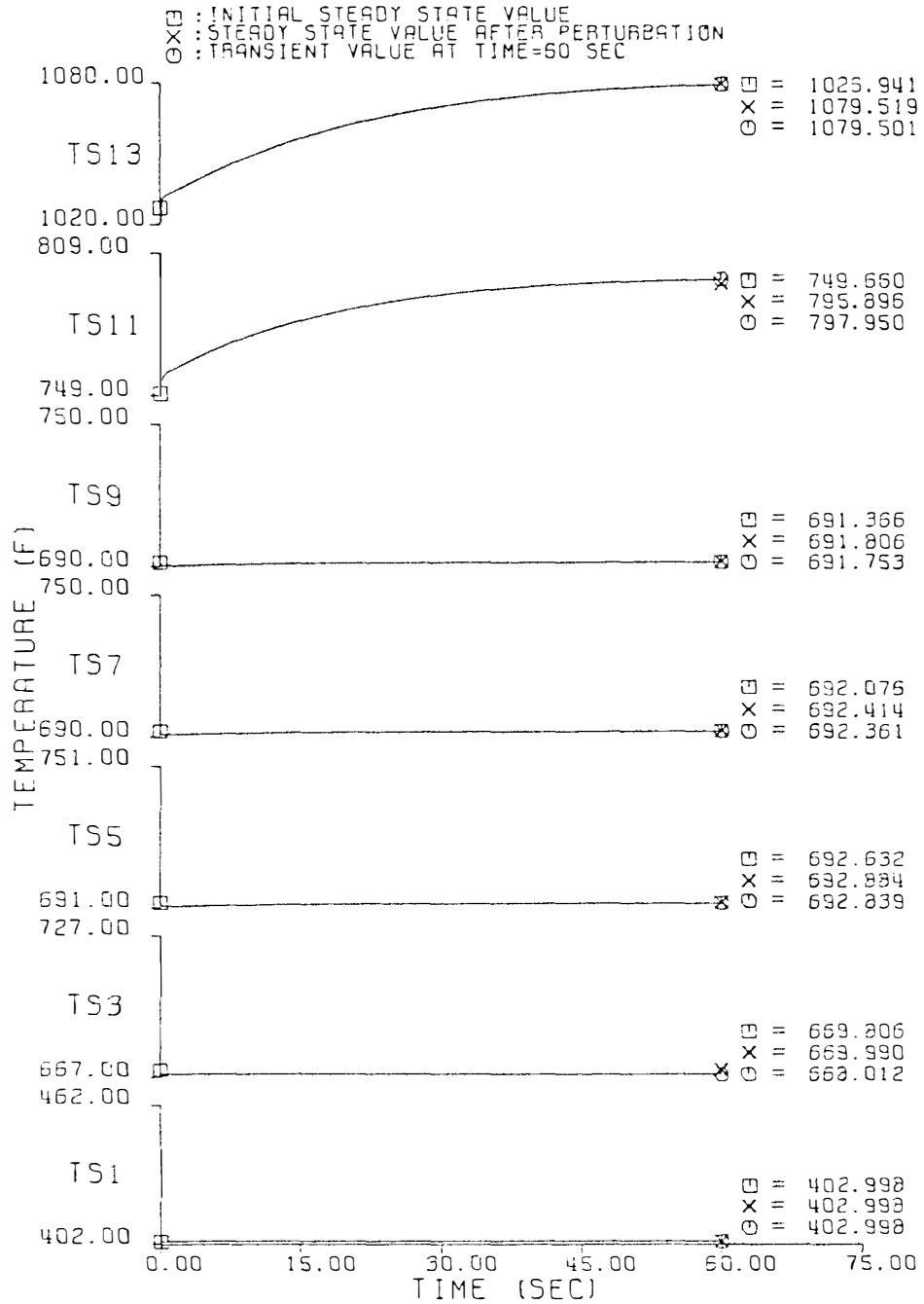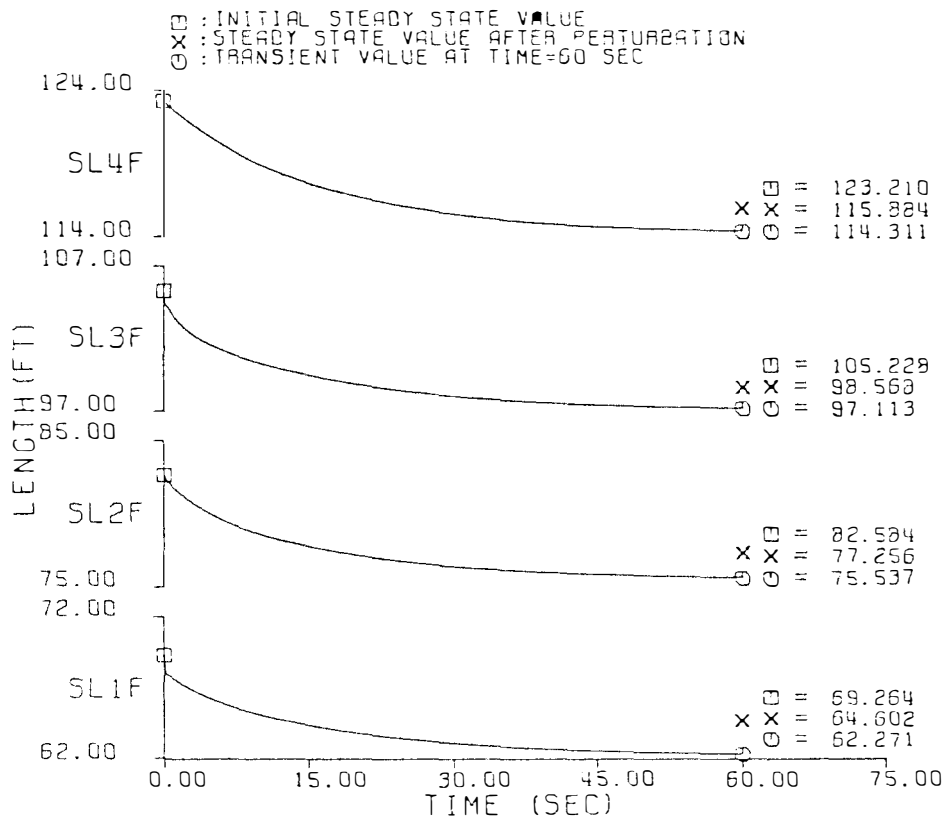   Decrease in Feedwater Mass Flow Rate.

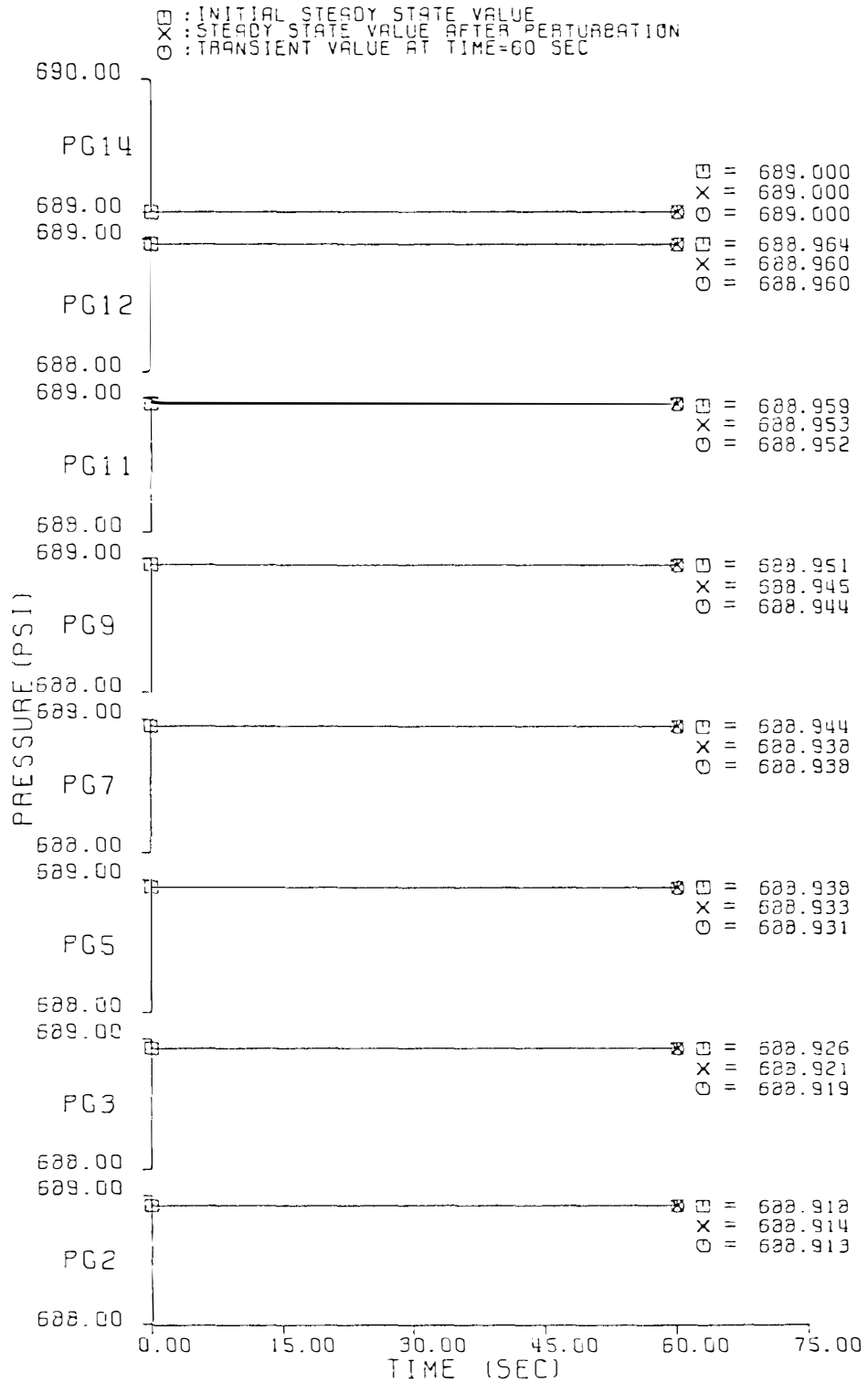Figure 7.2.2 (continued)

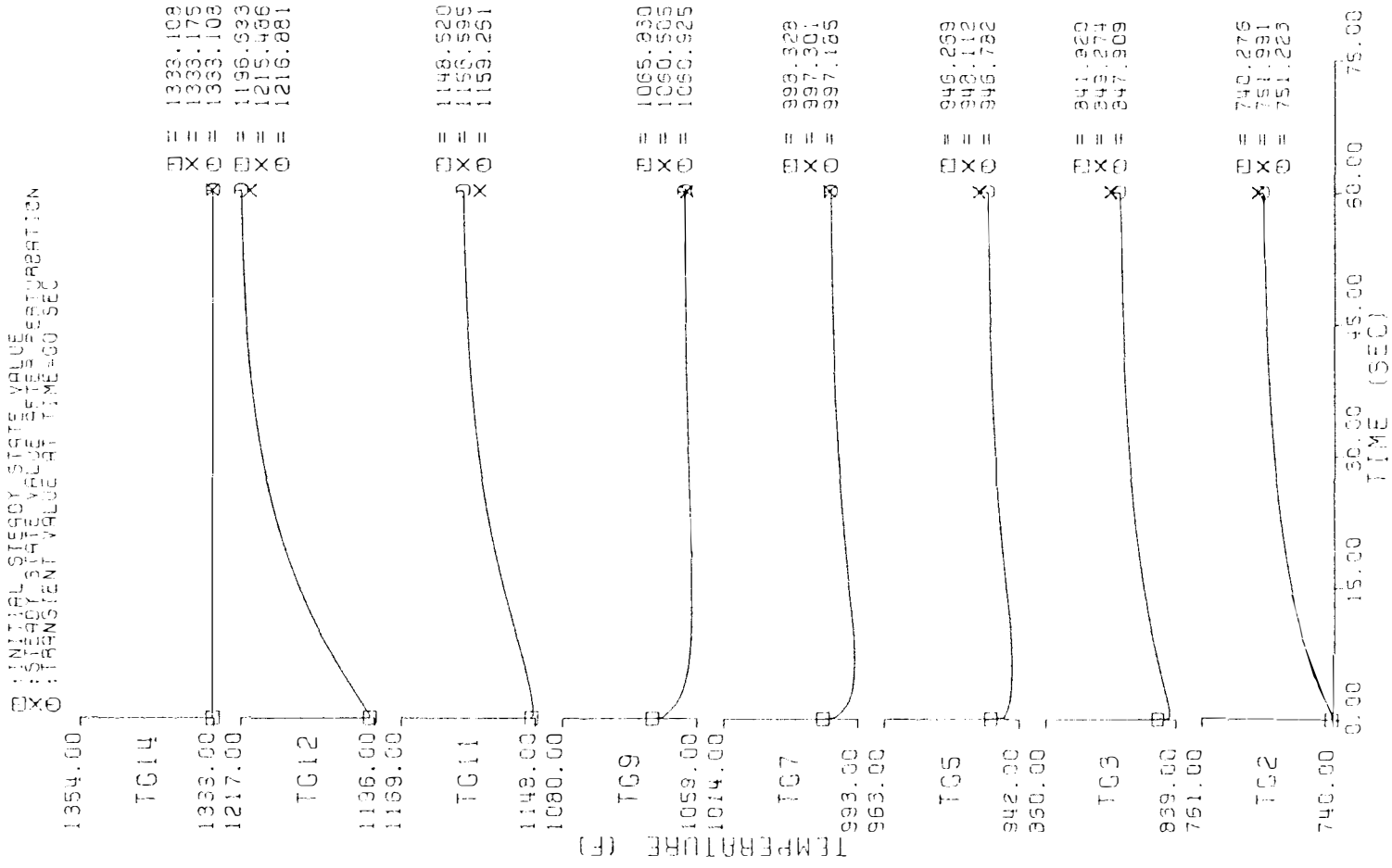Figure 7.2.2 (continued)

Figure 7.2.2 (continued)
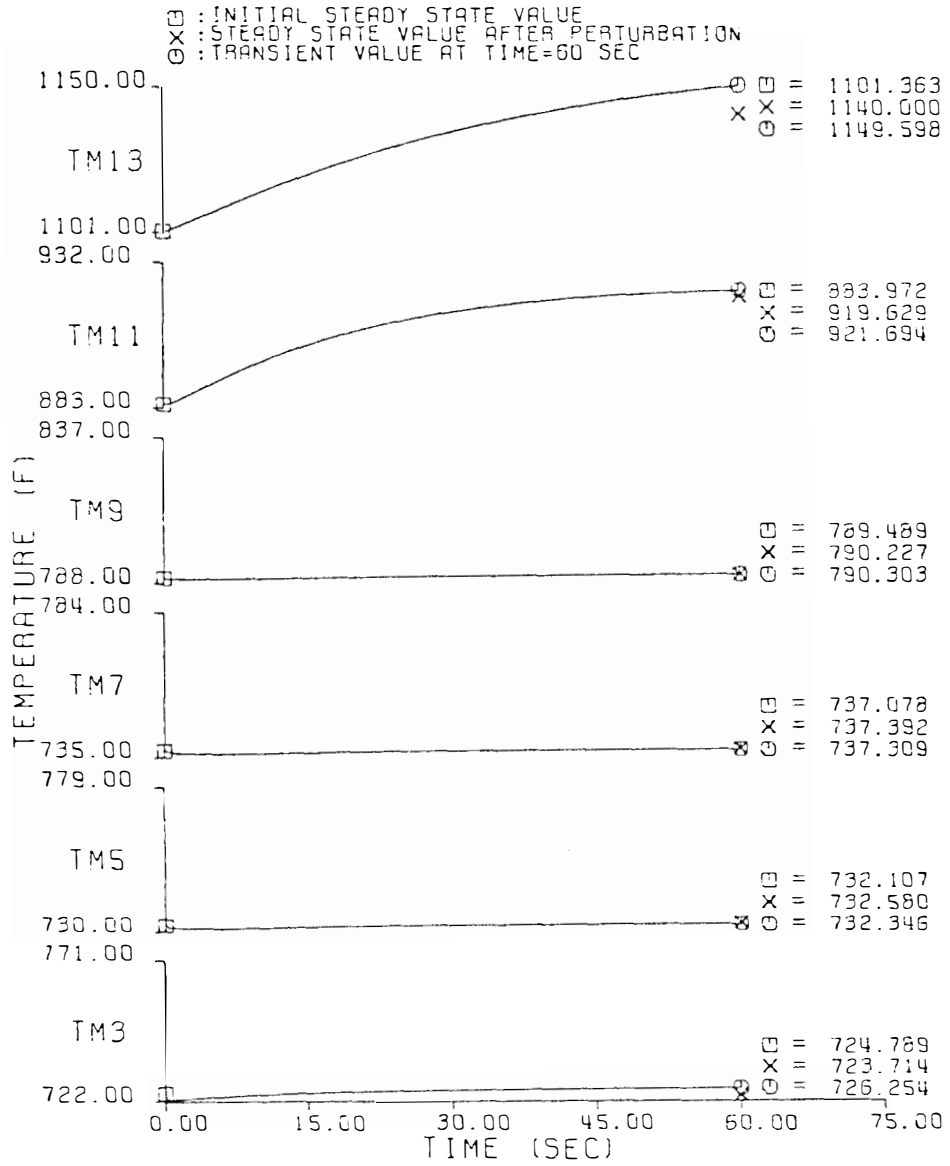
104

Figure 7.2.2 (continued)

Figure 7.2.2 (continued)

removal per unit time from the steam generator. Therefore the steam/water temperature rises in each section, as shown in TS5, TS7, TS9, TS11 and TS13. TS3 is almost stationary, which may be due to the importance of the boundary movement toward the colder entrance in this section. The decrease in the heat removal rate enhances water evaporation, which causes the regime boundaries, SL1F, SL2F, SL3F and SL4F to move toward the water entrance. Compared with the internal energy increase, the boundary move has relatively little effect on each section's temperature. On the other hand, the decrease in the mass flow rate decreases the pressure drop across a section, therefore the pressure in each section at the beginning of the perturbation drops rapidly and then recovers slowly due to the thermal expansion in the steam/water. This is shown in PS1 through PS11. (PS13 is an input quantity.) The increase in the steam/water temperature prevents heat from being transferred from the tube metal to the secondary fluid. Therefore the tube temperature increases as shown in TM3 through TM13. Since the transfer of heat is decreased, the energy of the primary fluid is accumulated. However the temperature of a section depends on the internal energy, the movement of the boundaries and the nonlinear properties in a section. Therefore some of the helium section temperatures rise (such as TG2, TG3, TG5, TG11 and TG12) and some of the helium temperatures (TG7 and TG9) fall. The rise and fall of each helium section temperature is consistent with the steady state calculation. The helium pressure has little variation. This indicates that the thermal expansion of helium corresponding to a 0.05 lbm/sec per tube step change in the feedwater mass flow rate is insignificant.

A numerical comparison between the transient responses at 60 sec and the steady state values after a 0.05 lbm/sec per tube step decrease in the feedwater mass flow rate is shown in Table 7.2.3. Generally the deviations of the transient values from those of the steady state are slightly higher than those in the case of feedwater inlet enthalpy perturbation. This implies that the flow distributions change somewhat for the amount of change in water mass flow rate. The flow distribution change can not be treated accurately in a few section model. However, in the output responses of the steam generator, the consistency between the transient and the steady state values is good as shown in Table 7.2.3.

7.2.3 Responses to a Step Change
       in the Steam Outlet Pressure

A 58 psi (4 bars) step decrease in the steam outlet pressure leads to the response shown in Figure 7.2.3. The drop in the steam outlet pressure causes the drop of the steam/water pressure in the tube, which is shown in PS1 through PS11. Due to the decrease in pressure, the corresponding temperature of each section decreases, this is shown in TS3 through TS11. The deviation of the steam outlet temperature, TS13, of 1.8° may be due to the change of the state variable distributions which are not accurately counted in the transient model with a few sections. The variation of TS11 may be interpreted as the combined effect of the boundary movement and the pressure drop. It indicates that the boundary movement is relatively important on TS11. The response of each regime boundary depends on the boundary condition and the local thermodynamic properties. For example, SL1F, the boundary of the onset

TABLE 7.2.3

COMPARISON OF TRANSIENT RESPONSES AT 60 SEC AND STEADY STATE VALUES
AFTER 0.05 LBM/SEC PER TUBE STEP DECREASE IN THE
FEEDWATER MASS FLOW RATE[a]

Flow Regime and Section	Boundary Length (Ft)	Helium		Tube Temperature (F)	Steam/Water	
		Pressure (PSI)	Temperature (F)		Pressure (PSI)	Temperature (F)
Helium inlet section						
14 [9]		689.000[b] 689.000 [689.000]	1333.109[b] 1333.109 [1333.109]			
Superheater II						
13		688.983[b] 688.982	1255.045[b] 1262.700	1140.001[b] 1149.630	2640.000[b] 2640.000 [2640.000]	1079.520[b] 1079.510 [1071.370]
[8]						
12		688.961[b] 688.960 [688.960]	1215.486[b] 1216.881 [1216.300]	1055.608[b] 1036.965	2725.000[b] 2724.122	970.907[b] 956.389
Superheater I						
11		688.954[b] 688.953	1156.597[b] 1159.261	919.629[b] 921.697	2795.082[b] 2791.012 [2789.034]	795.896[b] 797.954 [792.662]
[7]						
10		688.948[b] 688.947 [688.945]	1089.434[b] 1089.482 [1092.645]	833.851[b] 834.454	2886.271[b] 2887.964	723.147[b] 725.398

TABLE 7.2.3 (continued)

Flow Regime and Section	Boundary Length (Ft)	Helium Pressure (PSI)	Helium Temperature (F)	Tube Temperature (F)	Steam/Water Pressure (PSI)	Steam/Water Temperature (F)
Evaporator II						
9	115.884[b] 114.311 [112.977]	688.945[b] 688.944	1060.506[b] 1060.926	790.227[b] 790.303	2930.703[b] 2929.686 [2920.592]	691.806[b] 691.754 [691.286]
[6]						
8		688.942[b] 688.941 [688.940]	1030.982[b] 1031.546 [1033.532]	785.286[b] 785.307	2936.700 2935.670	692.114[b] 692.061
Evaporator I						
7	98.568[b] 97.113 [95.592]	688.939[b] 688.938	997.301[b] 997.185	737.393[b] 737.309	2942.590[b] 2941.543 [2932.661]	692.415[b] 692.362 [691.907]
[5]						
6		688.936[b] 688.934 [688.933]	964.893[b] 964.403 [966.147]	734.142[b] 734.015	2947.644[b] 2946.715	692.673[b] 692.626
Economizer II						
5	77.256[b] 75.536 [74.172]	688.933[b] 688.932	948.112[b] 946.782	732.580[b] 732.347	2951.775[b] 2950.890 [2941.972]	692.884[b] 692.839 [692.383]
[4]						
4		688.931[b] 688.930 [688.928]	930.023[b] 928.004 [929.863]	727.476[b] 727.005	2953.228[b] 2952.421	683.917[b] 683.464

109

TABLE 7.2.3 (continued)

Flow Regime and Section	Boundary Length (Ft)	Helium Pressure (PSI)	Helium Temperature (F)	Tube Temperature (F)	Steam/Water Pressure (PSI)	Steam/Water Temperature (F)
Economizer I						
3 [3]	64.602^b 62.271 [61.081]	688.921^b 688.920 [688.919]	849.275^b 847.910 [849.991]	723.715^b 726.254	2954.852^b 2954.111 [2945.143]	669.990^b 668.012 [667.130]
2 [2]		688.914^b 688.914 [688.913]	751.991^b 751.223 [753.630]	604.866^b 603.926	2960.880^b 2959.868 [2950.767]	568.630^b 567.658 [567.175]
Water inlet section						
1 [1]					2965.921^b 2964.718 [2955.522]	403.000^b 403.000 [403.000]

^{a}[ ]: Transient responses for the lumping case with two sections in the subcooled convective region and one section in each of the remaining flow regions.

^{b}Value obtained from the steady state calculations using 300 sections with the input conditions after perturbation. Values without any mark are the transient responses for the lumping case with two sections in each of the flow regions.

$\Delta PG_o = -0.005 \, [-0.006]$ $\Delta e_{PG_o} \leq 0.001 \, [-0.001]$

$\Delta TG_o = 10.946 \, [13.353]$ $\Delta e_{TG_o} = -0.768 \, [1.639]$

$\Delta PS_{in} = 1.16 \, [-8.036]$ $\Delta e_{PS_{in}} = -1.203 \, [-10.399]$

$\Delta TS_o = 52.568 \, [44.428]$ $\Delta e_{TS_o} = -0.01 \, [-8.15]$
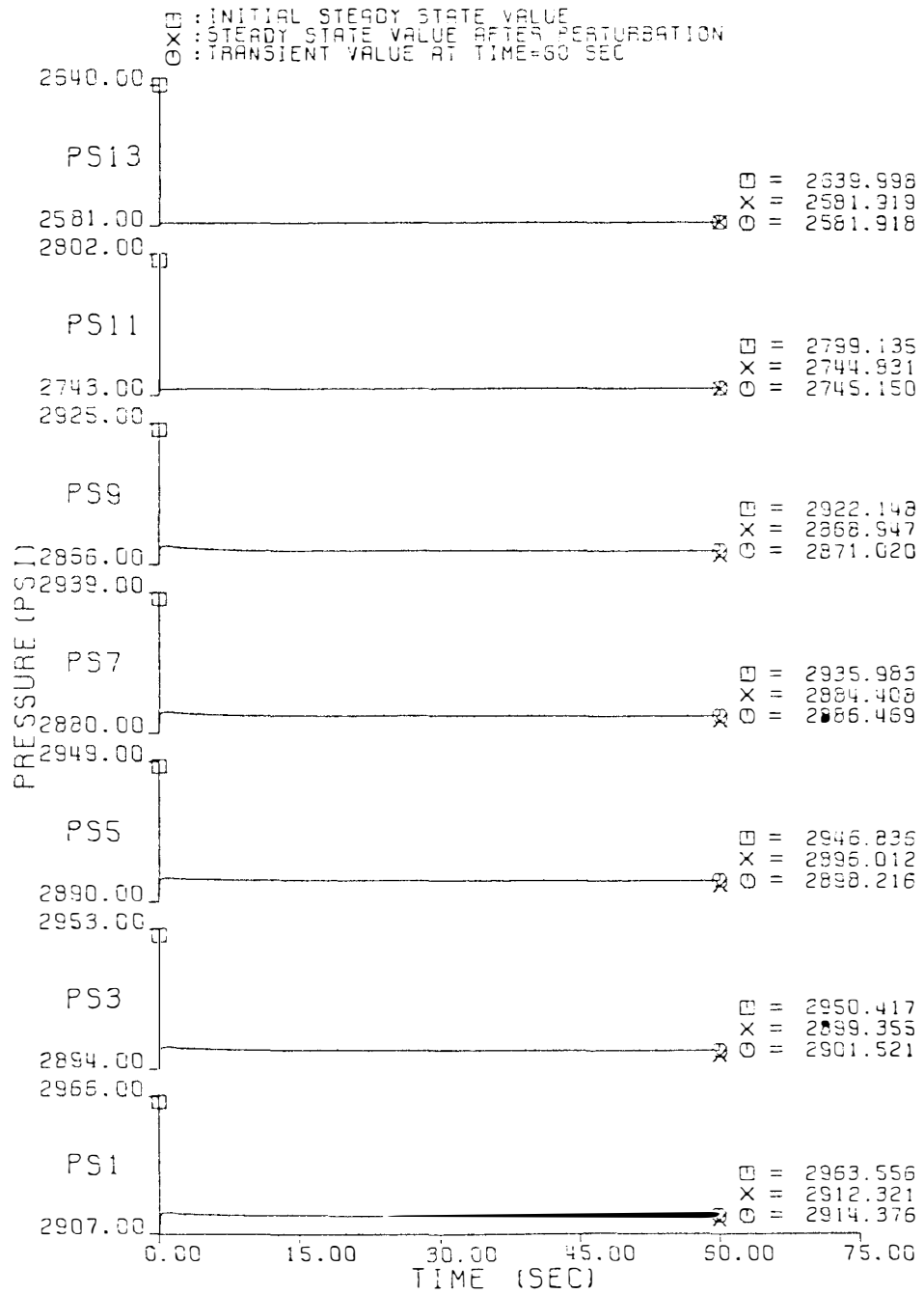
Figure 7.2.3. Transient Responses to 58 Psi Step Decrease in Steam
Outlet Pressure.

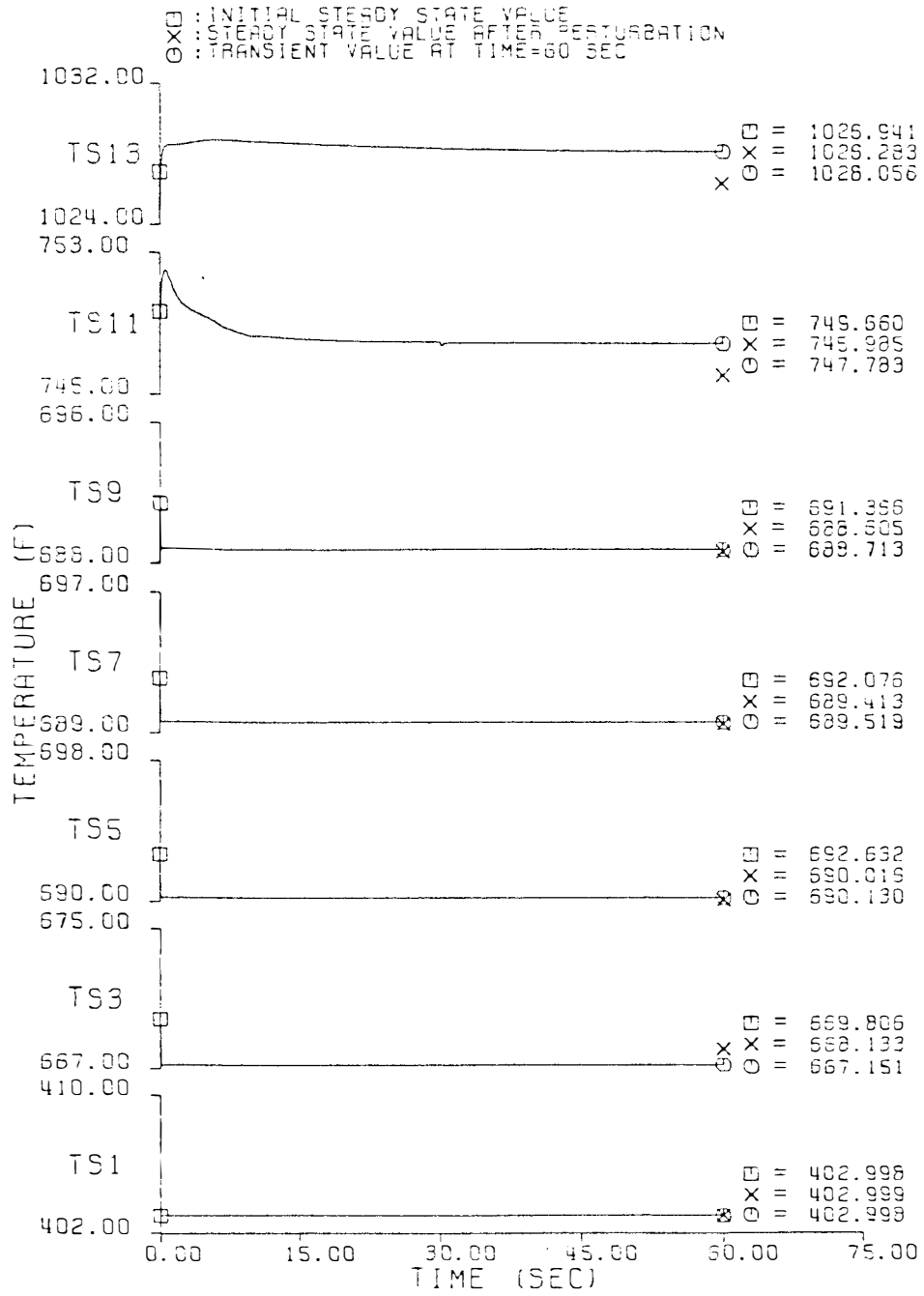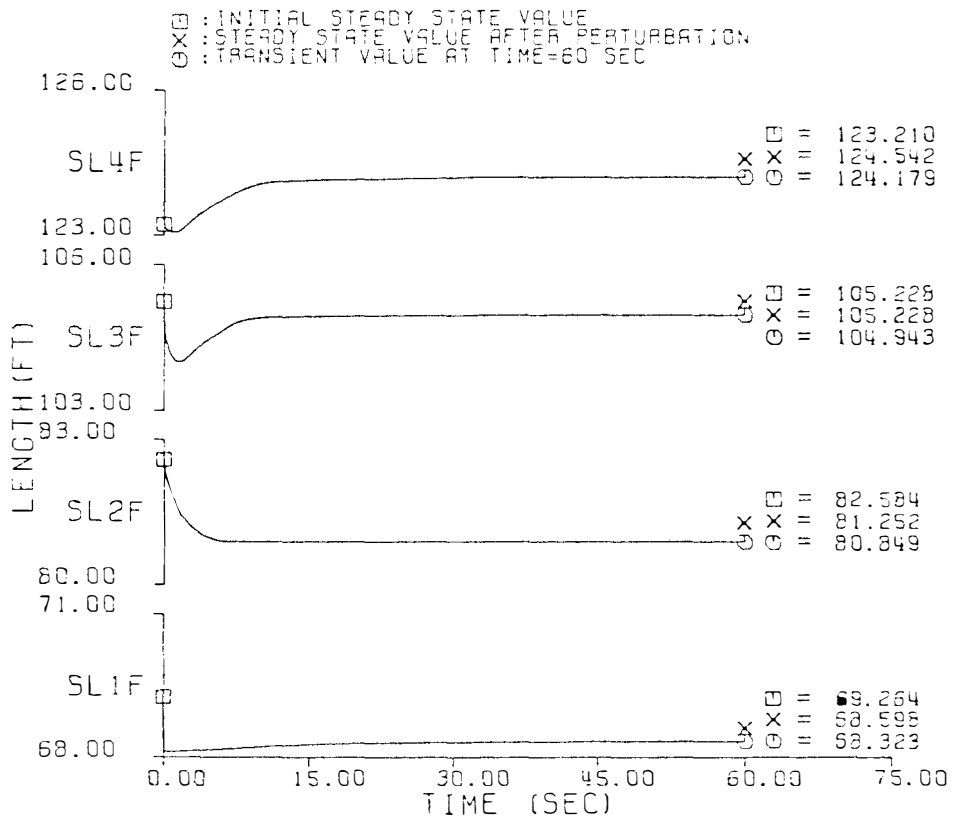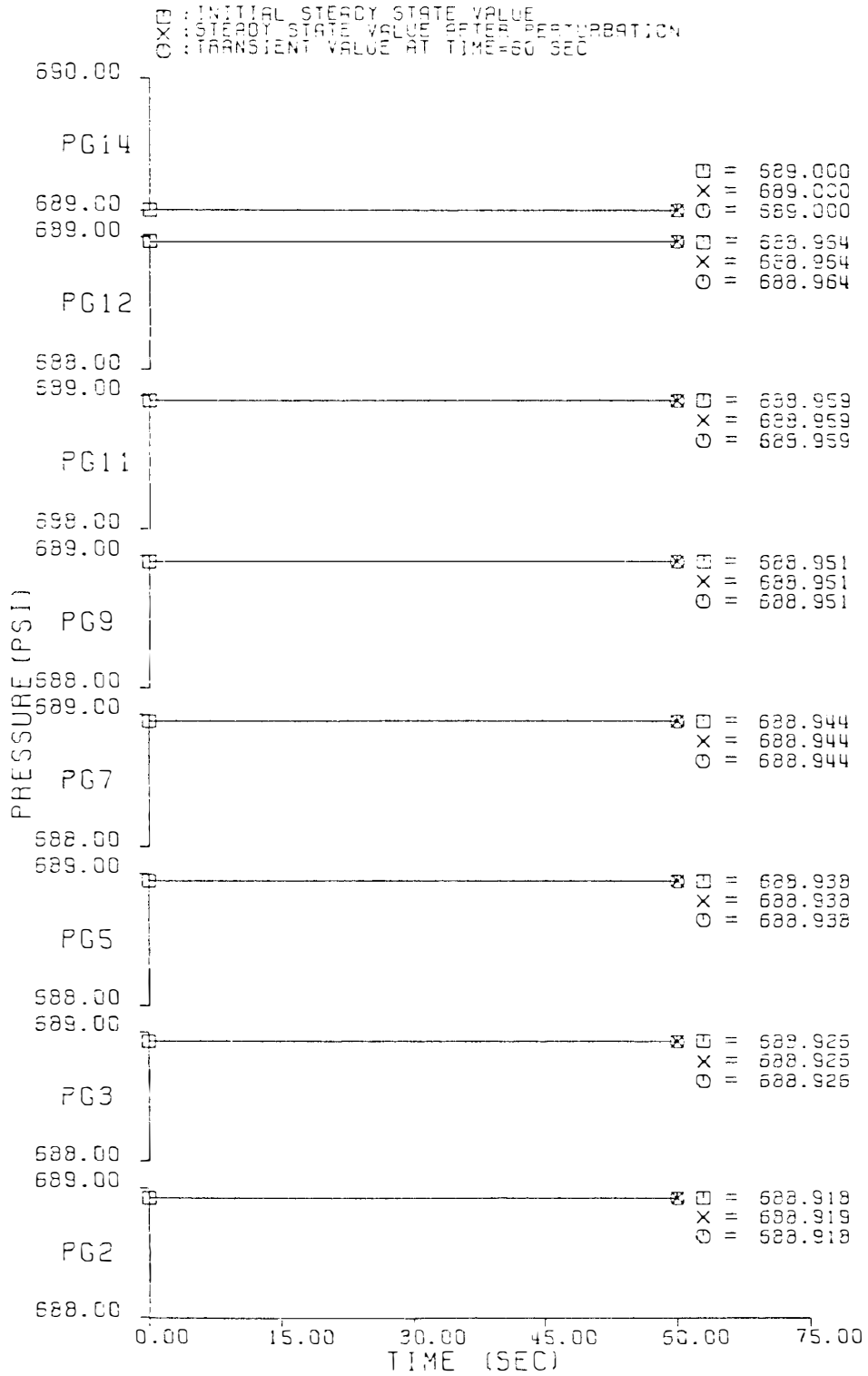Figure 7.2.3 (continued)
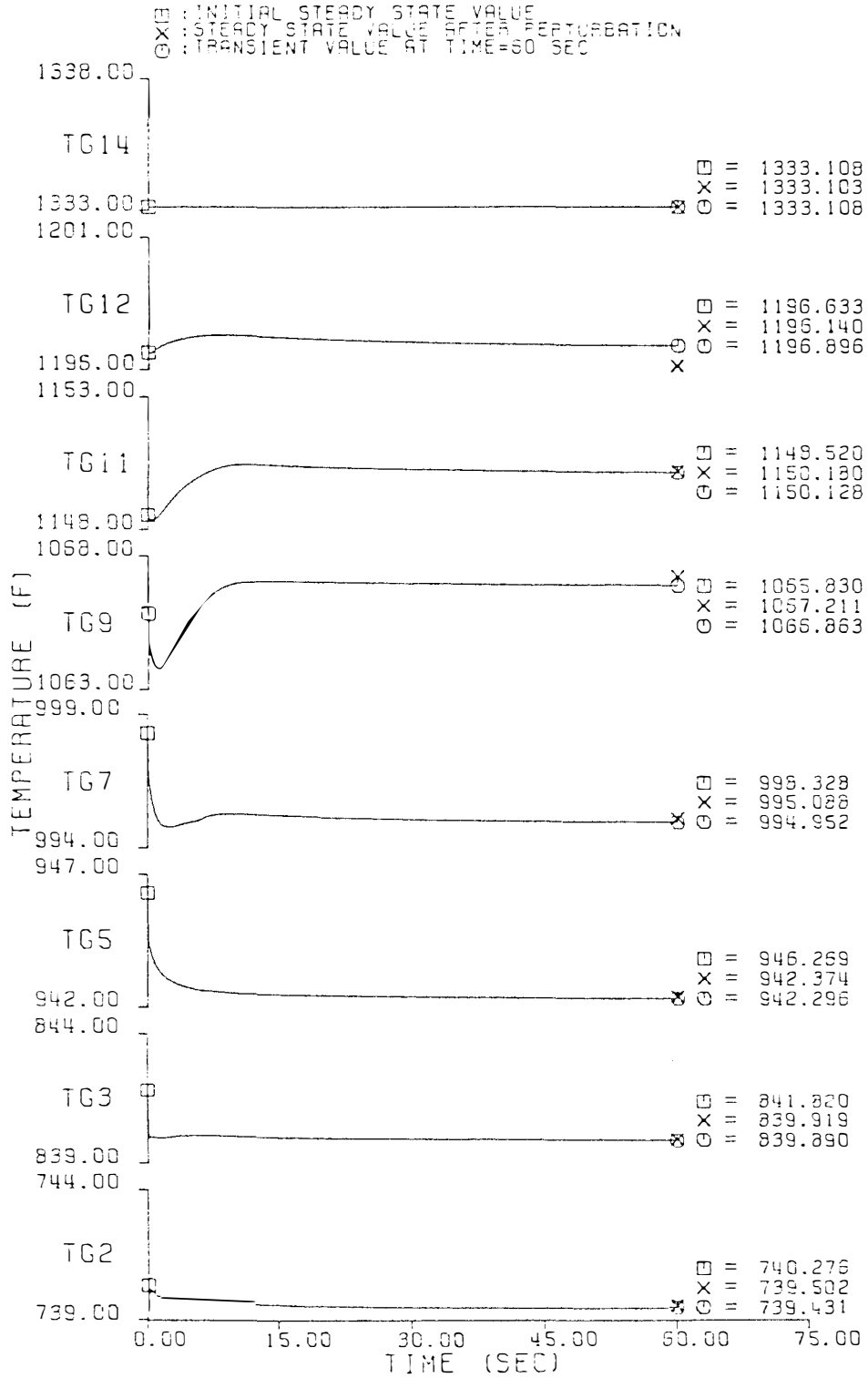
Figure 7.2.3 (continued)
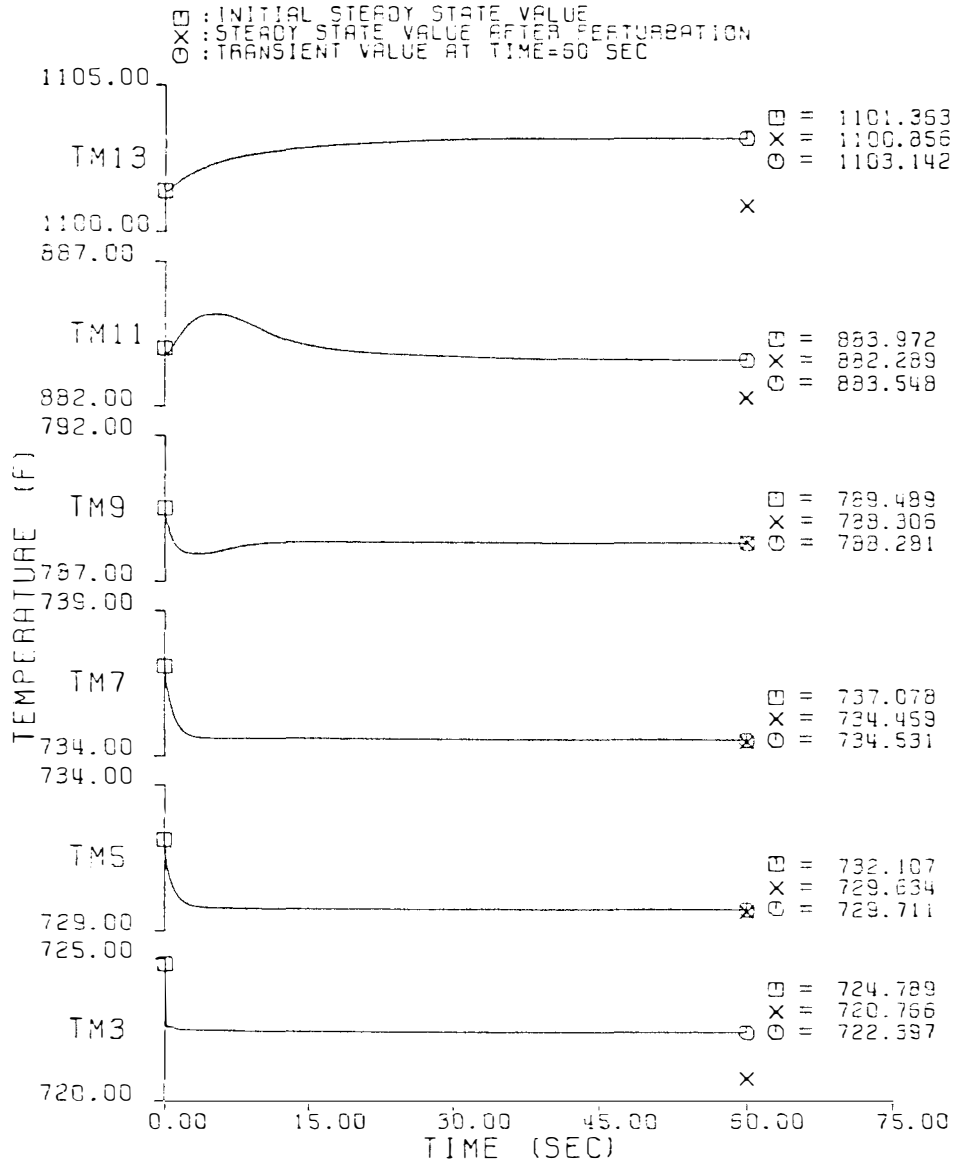
Figure 7.2.3 (continued)

Figure 7.2.3 (continued)

Figure 7.2.3 (continued)

of nucleate boiling determined by $T_{ss} = T_{sat}(P)$, drops rapidly initially due to the pressure loss, then recovers slightly due to the slight increase of the pressure at that location. The boundaries defined for the saturated region (SL2F, SL3F and SL4F) vary according to the pressure effect on the local property changes (such as the steam quality and the enthalpy). The steam quality for the departure from nucleate boiling is a function of pressure, heat flux and mass flux. The saturated liquid specific enthalpy, h_f, decreases as the pressure decreases while the saturated vapor specific enthalpy, h_g, increases as the pressure decreases. This is true for pressures greater than 444 psi. A specific enthalpy defined by $h = h_f + X (h_g - h_f)$ is defined by the combined effects of h_f, h_g and X with respect to a pressure change. The variations of SL2F, SL3F and SL4F reflect that the properties mentioned above are important factors in determining the responses of the saturated boundaries. The decrease in the steam/water temperature results in the decrease in the tube temperature, such as TM3 through TM11 because of the increase in heat transfer. TM13 is less accurate in comparison with steady value, which may be due to inaccuracy in TS13. However the deviation is within 2.3°F. Although the heat transferred from the helium to the tube is increased, both the boundary movement and the heat transferred can affect the helium temperature if the amount of heat transferred is small. Therefore TG2 through TG7 decrease while TG9 and TG11 increase. TG12 is almost stationary since it is close to the helium input, TG14 which is held constant for the case studied and insignificant heat is transferred to that section. Helium pressure has

no significant change for a 58 psi step decrease in the steam outlet
pressure as shown in PG2 through PG12 because the helium pressure is
insensitive to a small change in temperature.

A numerical comparison between the transient state at 60 sec and
the steady state after the perturbation is shown in Table 7.2.4. The
deviations of the transient values from the steady state values in
Table 7.2.4 are small since the essential response in the outputs of the
steam generator due to a 58 psi (4 bars) change in the steam outlet
pressure is in the water inlet pressure.

7.2.4   Responses to a Step Change in
        the Helium Inlet Temperature

Responses for 10°F step increase in the helium inlet temperature are
shown in Figure 7.2.4. Since the primary fluid, helium, carries more
heat into the steam generator, the temperature of each helium section
increases as shown in TG2 through TG12. TG14 is the input helium
temperature. The helium pressure, as shown in PG2 through PG12 changes
only slightly. Moving boundaries have relatively small effects on each
helium temperature. The increased temperature differences between
helium and tube metal sections cause more heat flow from the helium side
to the tube side, which results in the increase of each tube metal
temperature as shown in TM3 through TM13. The heat transfer from the
tube metal to the steam/water side is increased because of the increased
temperature difference between the tube metal section and the steam/water
section. Evaporation of water is enhanced and it is reflected in the
boundaries moving toward the water entrance as indicated in SL1F, SL2F,

TABLE 7.2.4

COMPARISON OF TRANSIENT RESPONSES AT 60 SEC AND STEADY STATE VALUES
AFTER 58 PSI STEP DECREASE IN STEAM OUTLET PRESSURE[a]

Flow Regime and Section	Boundary Length (Ft)	Helium		Tube Temperature (F)	Steam/Water	
		Pressure (PSI)	Temperature (F)		Pressure (PSI)	Temperature (F)
Helium inlet section						
14 [9]		689.000[b]	1333.109[b]			
		689.000	1333.109			
		[689.000]	[1333.109]			
Superheater II						
13		688.985[b]	1244.136[b]	1100.858[b]	2581.920[b]	1026.283[b]
		688.985	1245.206	1103.143	2581.920	1028.056
					[2581.920]	[1028.187]
[8]						
12		688.964[b]	1196.141[b]	1006.405[b]	2672.804[b]	907.098[b]
		688.964	1196.897	1006.203	2673.045	907.943
		[688.964]	[1197.212]			
Superheater I						
11		688.960[b]	1150.181[b]	882.290[b]	2744.832[b]	745.986[b]
		688.959	1150.129	883.549	2745.151	747.783
					[2745.307]	[748.223]
[7]						
10		688.955[b]	1100.575[b]	833.804[b]	2813.595[b]	706.554[b]
		688.955	1099.766	833.356	2815.124	707.092
		[688.955]	[1099.660]			

TABLE 7.2.4 (continued)

Flow Regime and Section	Boundary Length (Ft)	Helium		Tube Temperature (F)	Steam/Water	
		Pressure (PSI)	Temperature (F)		Pressure (PSI)	Temperature (F)

Evaporator II

	124.542[b]	688.952[b]	1067.212[b]	788.306[b]	2868.948[b]	688.606[b]
9	124.179	688.952	1066.864	788.282	2871.021	688.714
	[124.148]				[2871.998]	[688.765]
[6]						
		688.949[b]	1033.632[b]	782.611[b]	2876.856[b]	689.019[b]
8		688.948	1033.390	782.604	2878.884	689.125
		[688.948]	[1032.123]			

Evaporator I

	105.228[b]	688.945[b]	995.088[b]	734.460[b]	2884.409[b]	689.413[b]
7	104.943	688.945	994.952	734.531	2886.470	689.520
	[104.452]				[2887.881]	[689.593]
[5]						
		688.941[b]	958.789[b]	730.848[b]	2890.918[b]	689.751[b]
6		688.941	958.780	730.937	2893.031	689.861
		[688.941]	[959.261]			

Economizer II

	81.252[b]	688.939[b]	942.374[b]	729.634[b]	2896.013[b]	690.016[b]
5	80.849	688.939	942.296	729.712	2898.218	690.130
	[80.879]				[2899.354]	[690.189]
[4]						
		688.937[b]	924.504[b]	724.490[b]	2897.586[b]	681.685[b]
4		688.937	924.655	724.576	2899.779	681.713
		[688.937]	[924.834]			

TABLE 7.2.4 (continued)

Flow Regime and Section		Boundary Length (Ft)	Helium		Tube Temperature (F)	Steam/Water	
			Pressure (PSI)	Temperature (F)		Pressure (PSI)	Temperature (F)
Economizer I							
3	[3]	68.598[b] 68.323 [68.281]	688.926[b] 688.926 [688.926]	839.920[b] 839.891 [840.059]	720.766[b] 722.397	2899.356[b] 2901.523 [2902.666]	668.133[b] 667.152 [667.195]
2	[2]		688.919[b] 688.919 [688.919]	739.503[b] 739.432 [739.584]	599.610[b] 599.672	2906.408[b] 2908.493 [2909.634]	565.905[b] 565.995 [566.015]
Water inlet section							
1	[1]					2912.322[b] 2914.378 [2915.515]	403.000[b] 403.000 [403.000]

[a][ ]: Transient responses for the lumping case with two sections in the subcooled convective region and one section in each of the remaining flow regions.

[b]Values obtained from the steady state calculations using 300 sections with the input conditions after perturbation. Values without any mark are the transient responses for the lumping case with two sections in each of the flow regions.

$\Delta PG_o \leq 10^{-3}$ $[10^{-3}]$

$\Delta TG_o = -0.845$ $[-0.693]$

$\Delta PS_{in} = -49.18$ $[-48.043]$

$\Delta TS_o = 1.114$ $[1.245]$

$\Delta e_{PG_o} \leq 10^{-3}$ $[10^{-3}]$

$\Delta e_{TG_o} = -0.071$ $[0.081]$

$\Delta e_{PS_{in}} = 2.056$ $[3.193]$
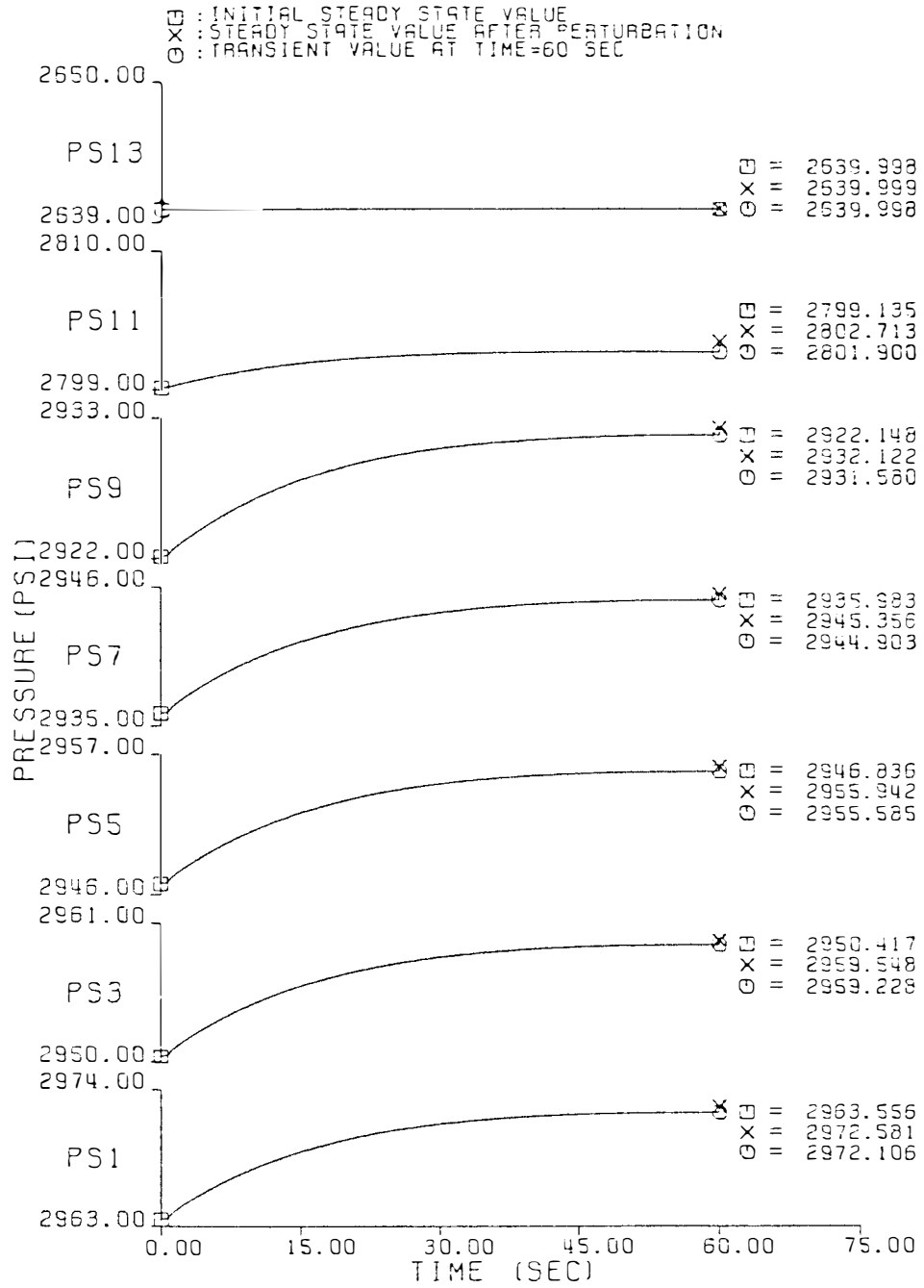
$\Delta e_{TS_o} = 1.773$ $[1.904]$

Figure 7.2.4. Transient Responses to 10°F Step Increase in Helium Inlet Temperature.

123

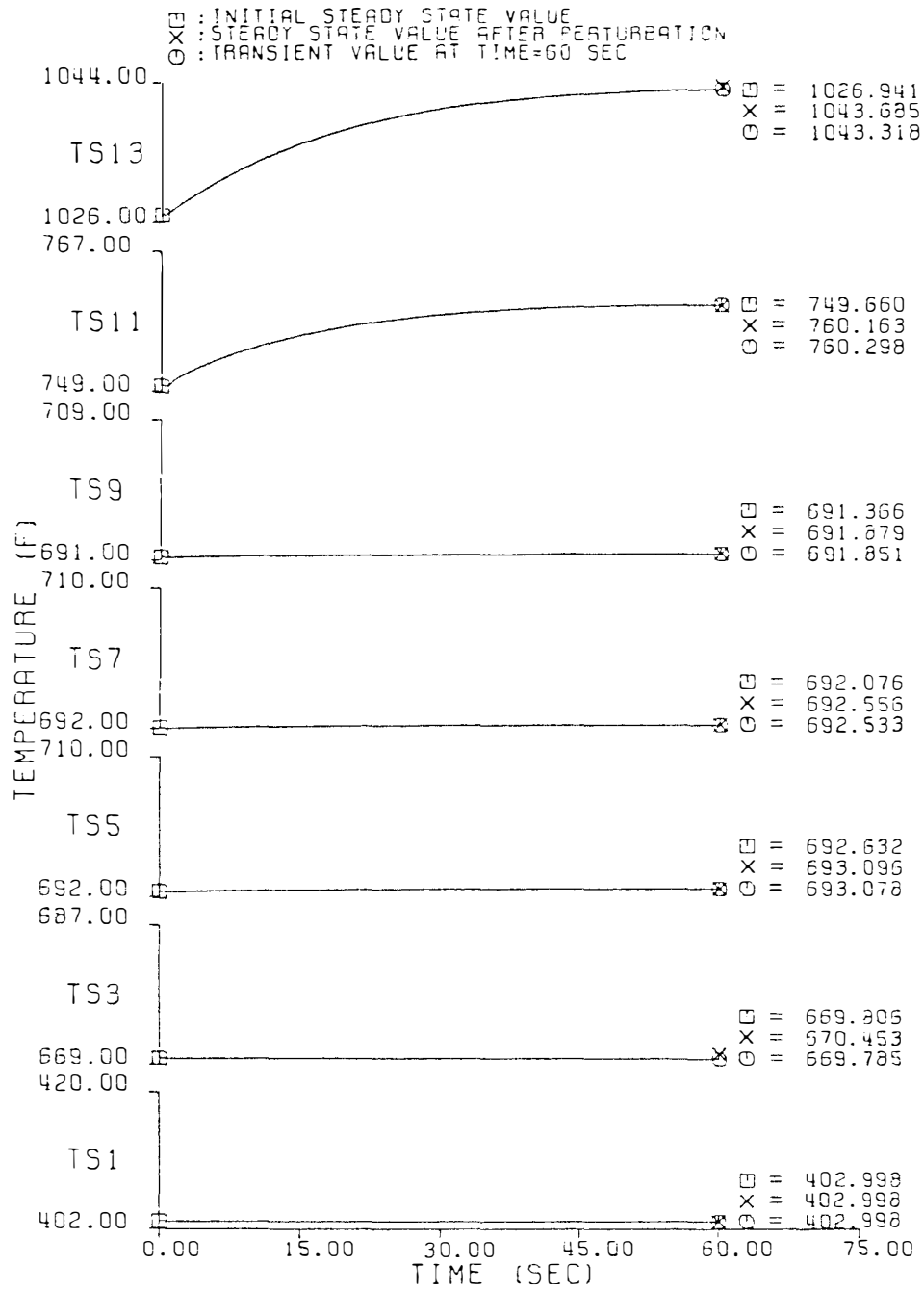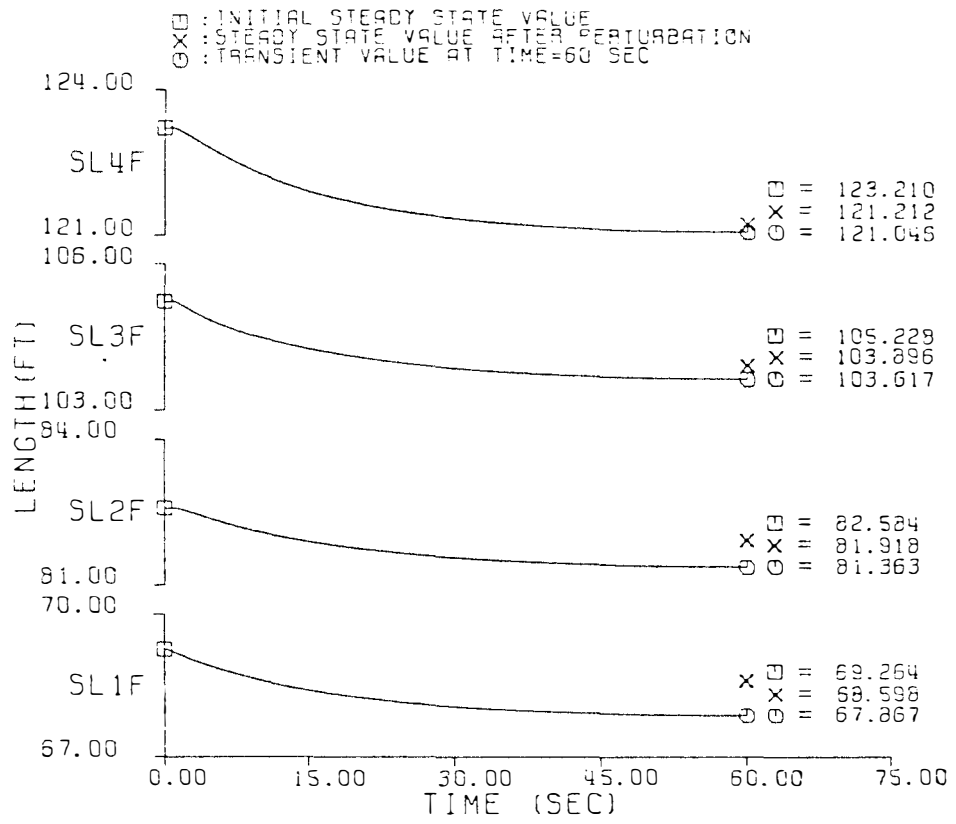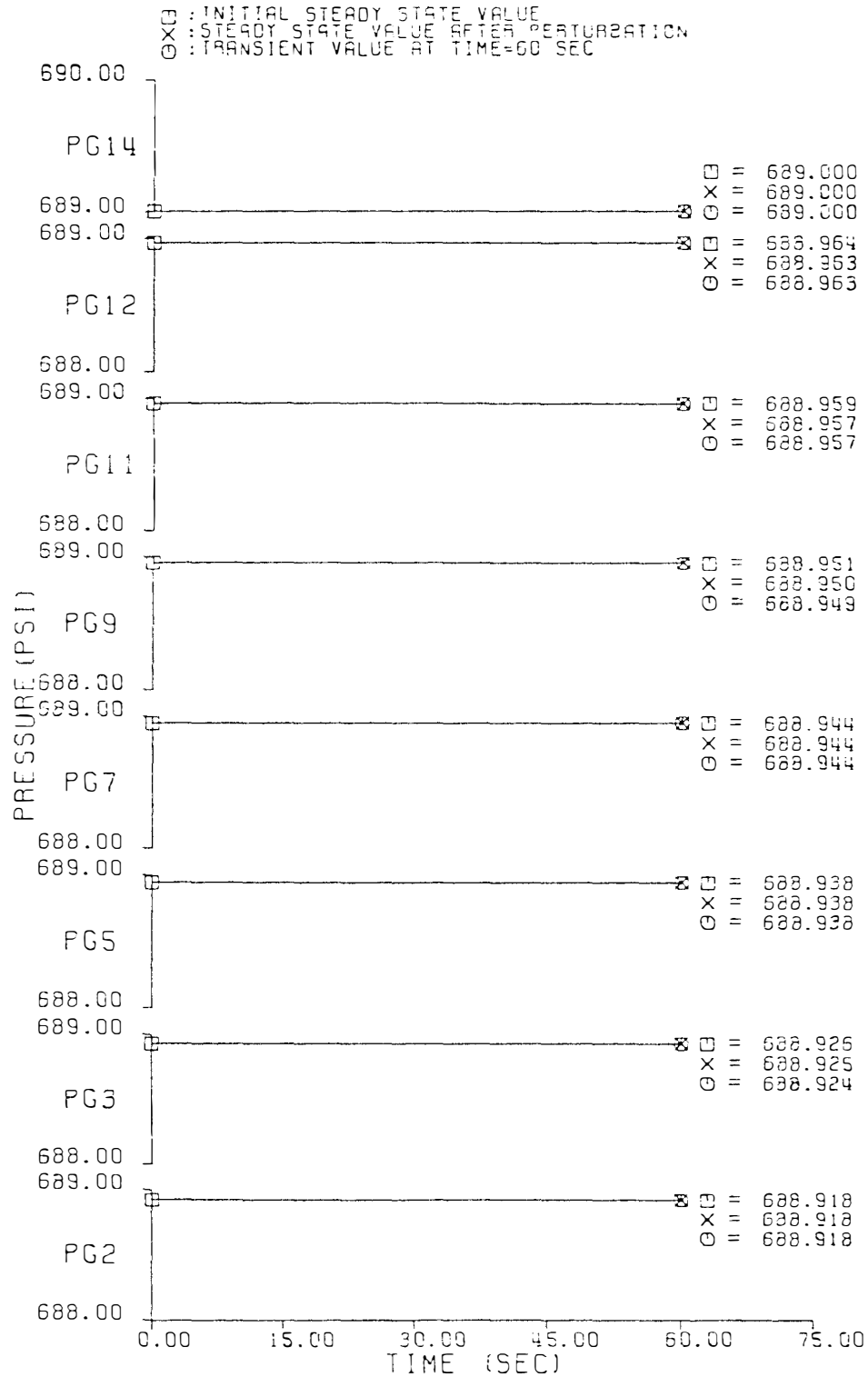Figure 7.2.4 (continued)

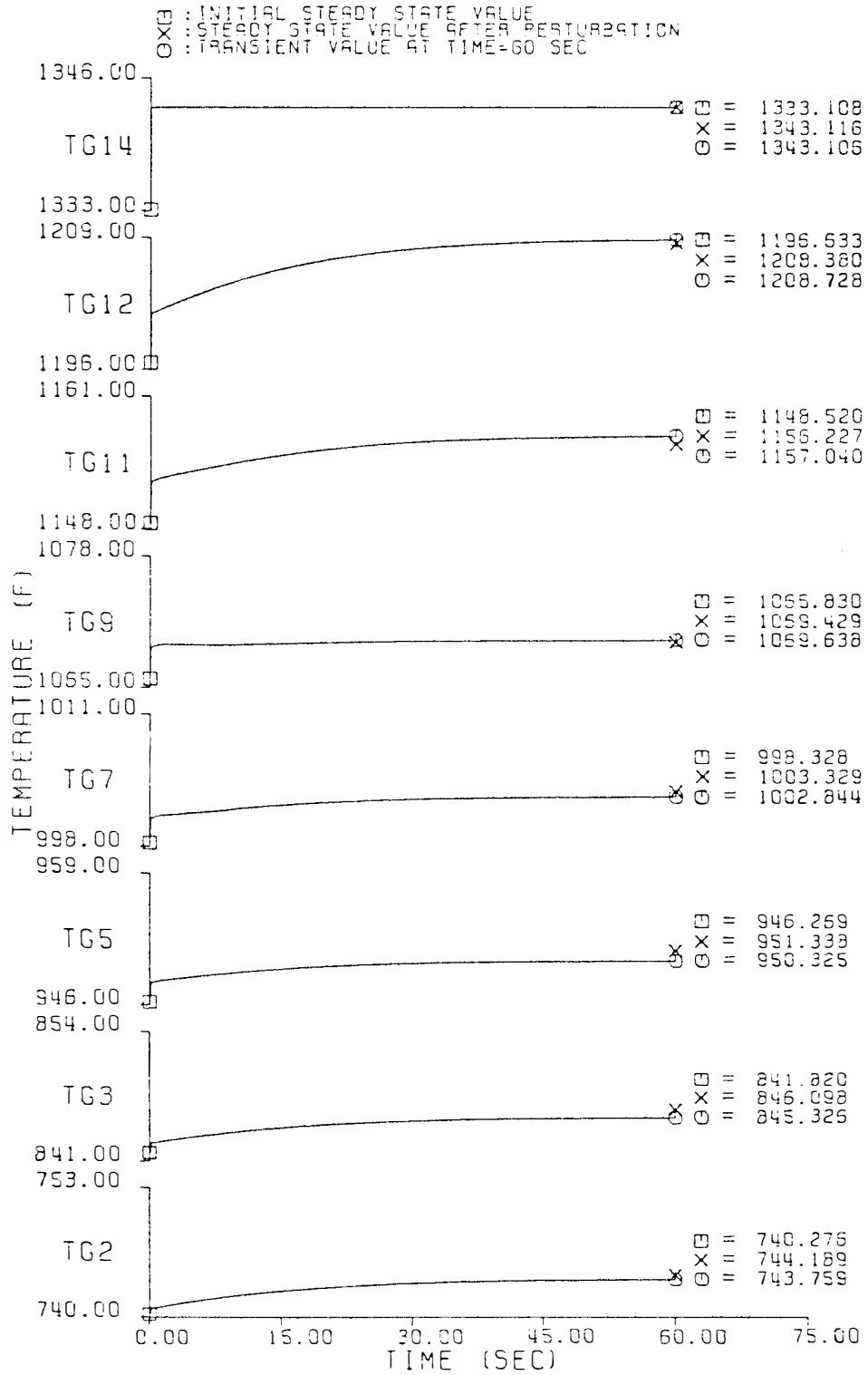Figure 7.2.4 (continued)

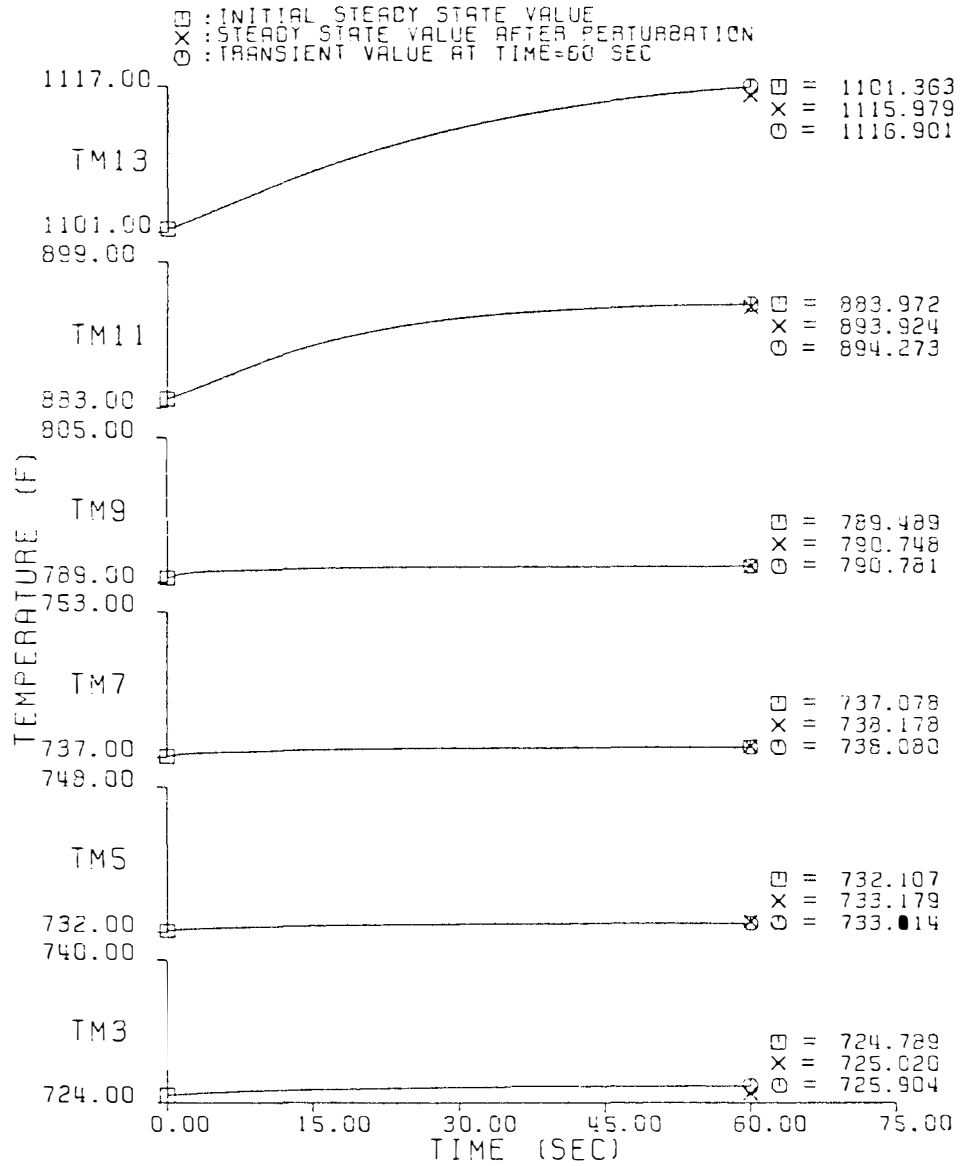Figure 7.2.4 (continued)

Figure 7.2.4 (continued)

Figure 7.2.4 (continued)

SL3F and SL4F. In the fixed boundary section, temperature rises due to the increased heat transfer to that section, such as the steam temperature TS11 and TS13. In the moving boundary section, the change of a section's temperature depends not only on the heat input but also on the shift of a section's boundaries such as TS3 through TS9. The steam/water pressures, PS1 through PS11 as shown in Figure 7.2.4 increase due to the thermal expansion of steam/water in the tube.

Table 7.2.5 presents a numerical comparison between the transient responses at 60 sec and the steady state values after perturbation. It is seen that the values are consistent. In the output responses of the steam generator, the changes in the helium outlet temperature, water inlet pressure and steam outlet temperature are significant and the deviations from the steady state values after perturbation are relatively small.

7.2.5 Responses to a Step Change in the Helium Mass Flow Rate

Responses for a 1 lbm/sec/module (or 1.27%) step increase in the helium inlet mass flow rate are shown in Figure 7.2.5. The increase in the helium mass flow rate causes an increase of the heat input rate to the steam generator. Therefore all the helium temperature responses, TG2 through TG12 increase rapidly initially then continue to change depending on the local conditions. At the final observation time, all helium temperature responses except TG9 are increased. The slight decrease in TG9 may be interpreted as the result of the increased heat transfer coefficient in competition with the slightly increased internal

TABLE 7.2.5

COMPARISON OF TRANSIENT RESPONSES AT 60 SEC AND STEADY STATE VALUES
AFTER 10°F STEP INCREASE IN HELIUM INLET TEMPERATURE[a]

Flow Regime and Section	Boundary Length (Ft)	Helium Pressure (PSI)	Helium Temperature (F)	Tube Temperature (F)	Steam/Water Pressure (PSI)	Steam/Water Temperature (F)
Helium inlet section						
14	[9]	689.000[b]	1343.107[b]			
		689.000	1343.107			
		[689.000]	[1343.107]			
Superheater II						
13		688.985[b]	1255.265[b]	1115.980[b]	2640.000[b]	1043.686[b]
		688.984	1256.506	1116.895	2640.000	1043.317
					[2640.000]	[1042.050]
	[8]					
12		688.963[b]	1208.380[b]	1022.841[b]	2730.408[b]	925.925[b]
		688.963	1208.729	1020.636	2730.179	923.961
		[688.963]	[1208.671]			
Superheater I						
11		688.958[b]	1156.228[b]	893.925[b]	2802.713[b]	760.164[b]
		688.958	1157.041	894.273	2801.901	760.298
					[2801.433]	[759.789]
	[7]	688.953[b]	1099.249[b]	832.636[b]	2880.674[b]	712.731[b]
10		688.953	1099.490	832.854	2880.681	713.173
		[688.953]	[1100.085]			

TABLE 7.2.5 (continued)

Flow Regime and Section	Boundary Length (Ft)	Helium Pressure (PSI)	Temperature (F)	Tube Temperature (F)	Steam/Water Pressure (PSI)	Temperature (F)
Evaporator II						
9	121.212^b	688.950^b	1069.430^b	790.749^b	2932.123^b	691.879^b
	121.046	688.950	1069.639	790.782	2931.580	691.851
	[120.786]				[2928.502]	[691.693]
[6]						
8		688.947^b	1038.940^b	785.666^b	2938.788^b	692.221^b
		688.947	1038.977	785.641	2938.304	692.196
		[688.947]	[1038.394]			
Evaporator 1						
7	103.896^b	688.944^b	1003.329^b	738.178^b	2945.357^b	692.557^b
	103.617	688.944	1002.844	738.081	2944.903	692.533
	[103.013]				[2942.094]	[692.390]
[5]						
6		688.941^b	968.676^b	734.646^b	2951.188^b	692.854^b
		688.940	968.501	734.616	2950.816	692.835
		[688.940]	[968.751]			
Economizer II						
5	81.918^b	688.938^b	951.338^b	733.180^b	2955.943^b	693.097^b
	81.363	688.938	950.326	733.014	2955.586	693.078
	[81.071]				[2952.583]	[692.925]
[4]						
4		688.936^b	932.173^b	727.883^b	2957.657^b	684.356^b
		688.936	930.982	727.559	2957.316	683.955
		[688.935]	[931.248]			

TABLE 7.2.5 (continued)

Flow Regime and Section		Boundary Length (Ft)	Helium		Tube Temperature (F)	Steam/Water	
			Pressure (PSI)	Temperature (F)		Pressure (PSI)	Temperature (F)
Economizer I							
3	[3]		688.925[b]	846.098[b]	725.021[b]	2959.550[b]	670.453[b]
			688.925	845.327	725.905	2959.229	669.786
			[688.925]	[845.658]		[2956.217]	[669.553]
2	[2]	68.598[b]	688.918[b]	744.189[b]	602.132[b]	2966.658[b]	567.891[b]
		67.867	688.918	743.760	601.613	2966.248	567.357
		[67.598]	[688.918]	[744.180]		[2963.201]	[567.237]
Water inlet section							
1	[1]					2972.583[b]	403.000[b]
						2972.107	403.000
						[2969.036]	[403.000]

[a] [ ]: Transient responses for the lumping case with two sections in the subcooled convective region and one section in each of the remaining flow regions.

[b] Value obtained from the steady state calculations using 300 sections with the input conditions after perturbation. Values without any mark are the transient responses for the lumping case with two sections in each of the flow regions.

$\Delta PG_o = -0.001$ [-0.001] $\Delta e_{PG_o} \leq 10^{-3}$ [< 10^{-3}]

$\Delta TG_o = 3.483$ [3.903] $\Delta e_{TG_o} = -0.429$ [-0.009]

$\Delta PS_{in} = 8.519$ [5.448] $\Delta e_{PS_{in}} = -0.476$ [-3.547]

$\Delta TS_o = 16.375$ [15.108] $\Delta e_{TS_o} = -0.369$ [-1.638]
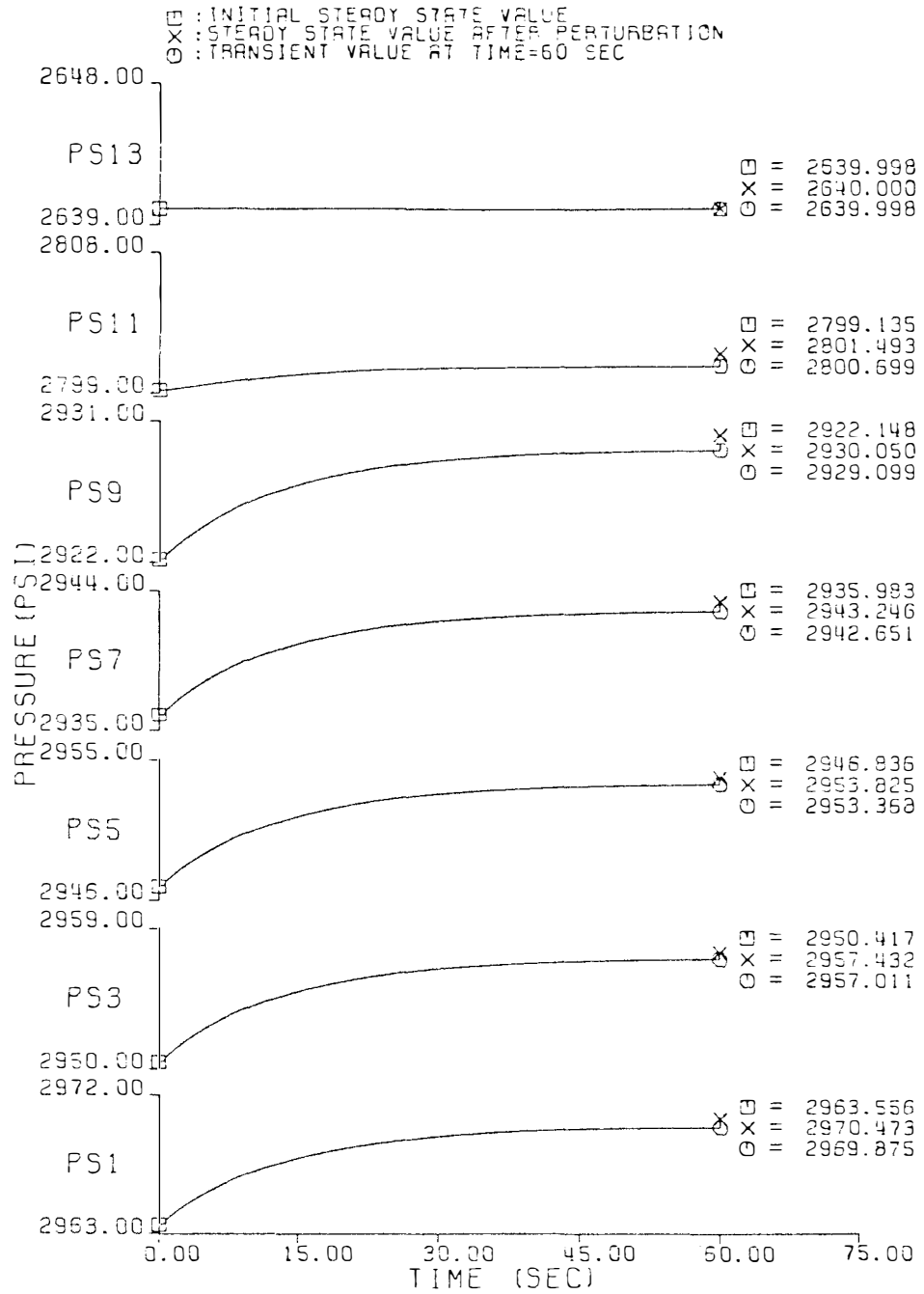
Figure 7.2.5. Transient Responses to 1 Lbm/Sec per Module Step Increase in Helium Inlet Mass Flow Rate.
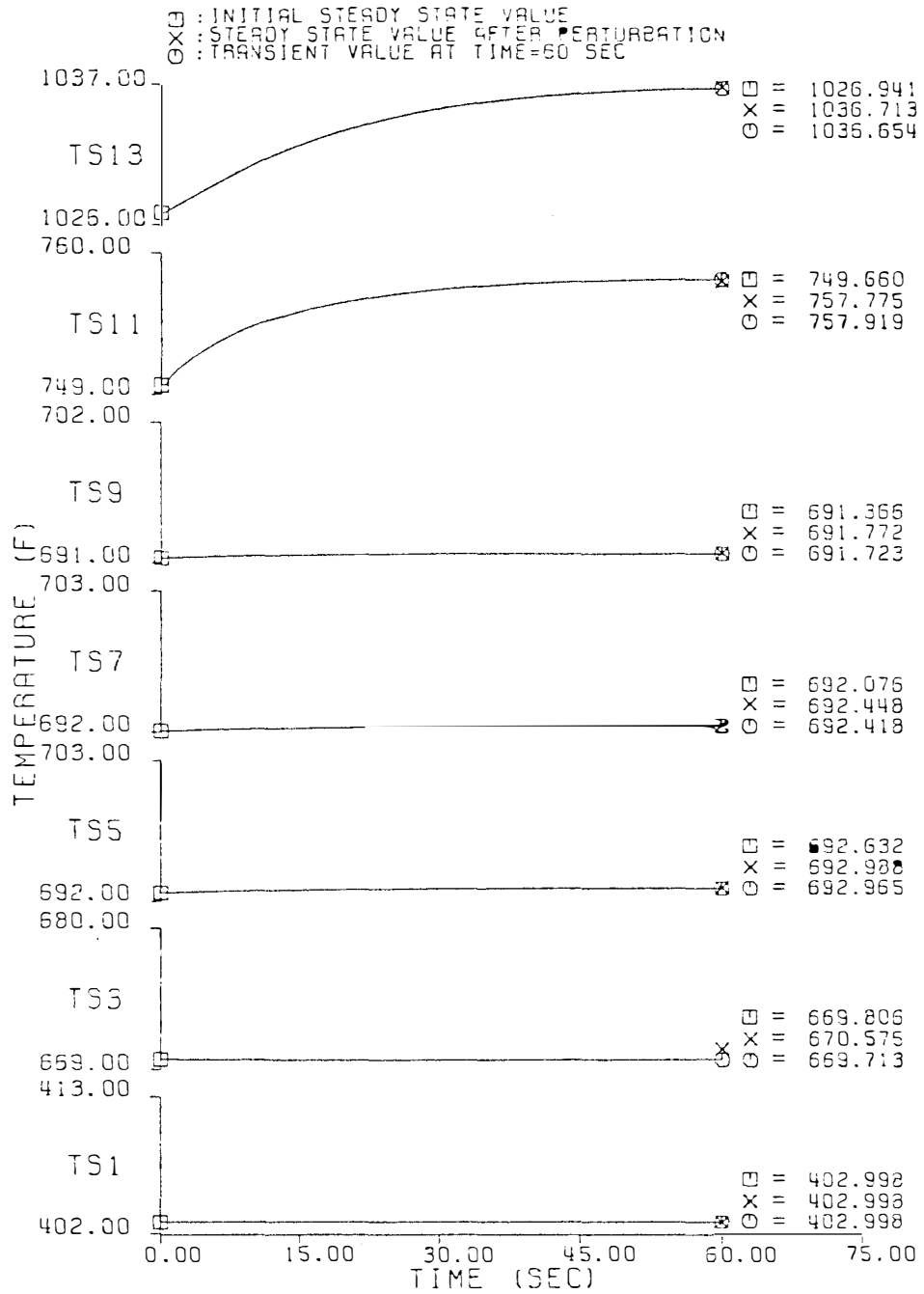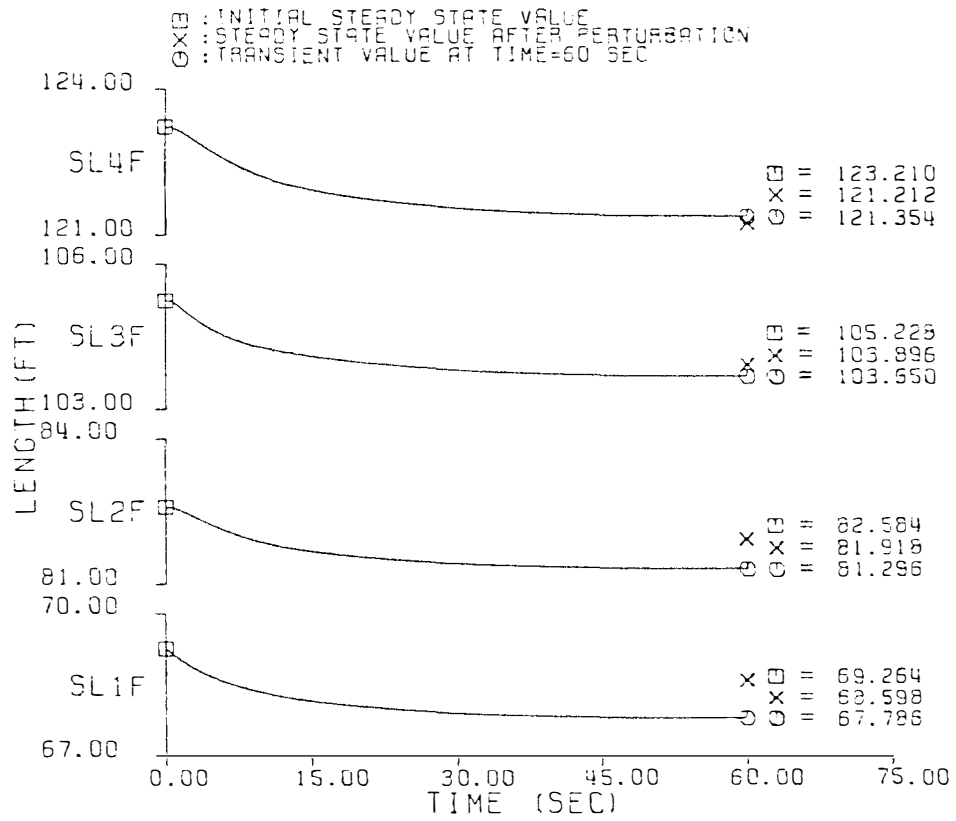
Figure 7.2.5 (continued)
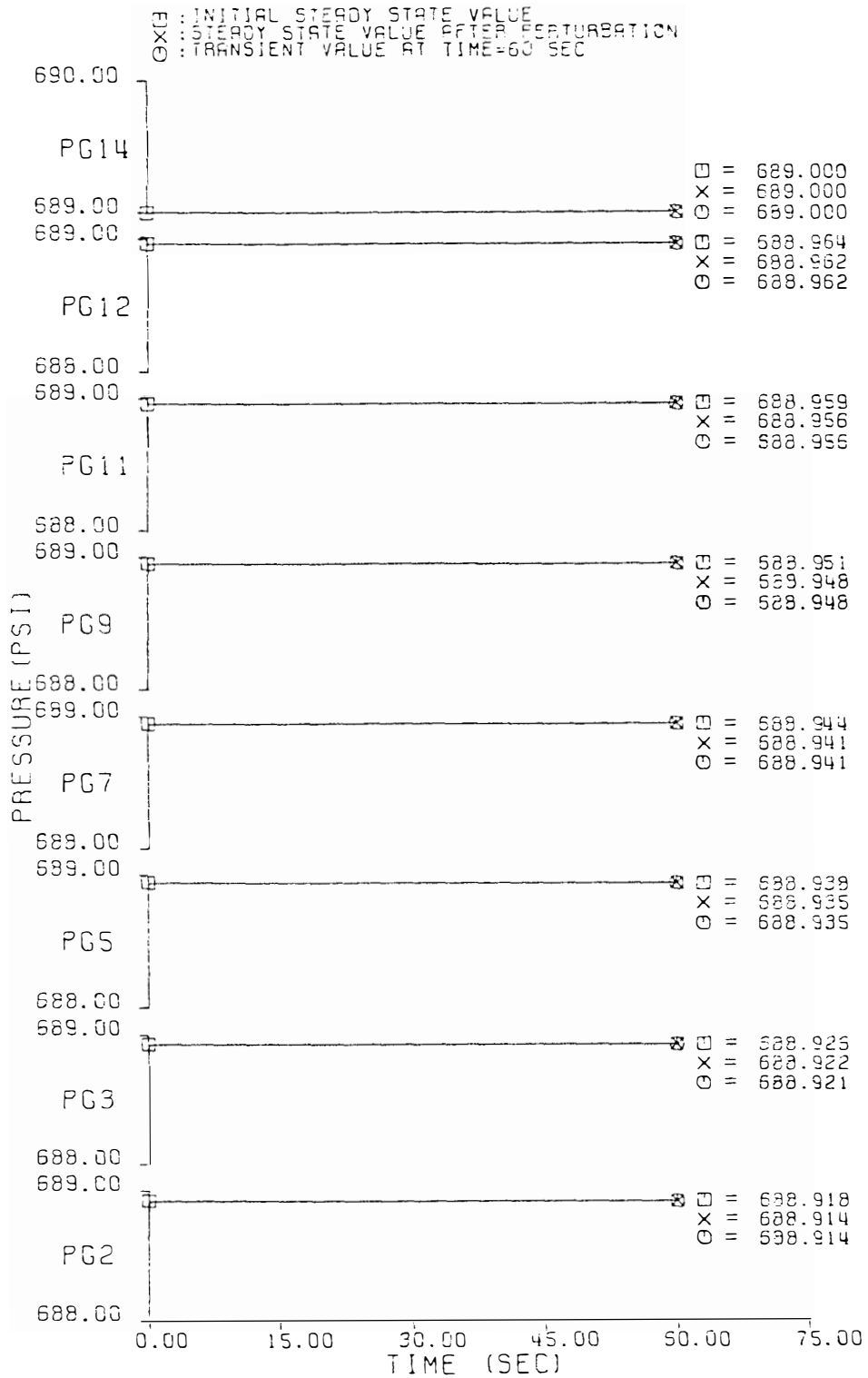
134

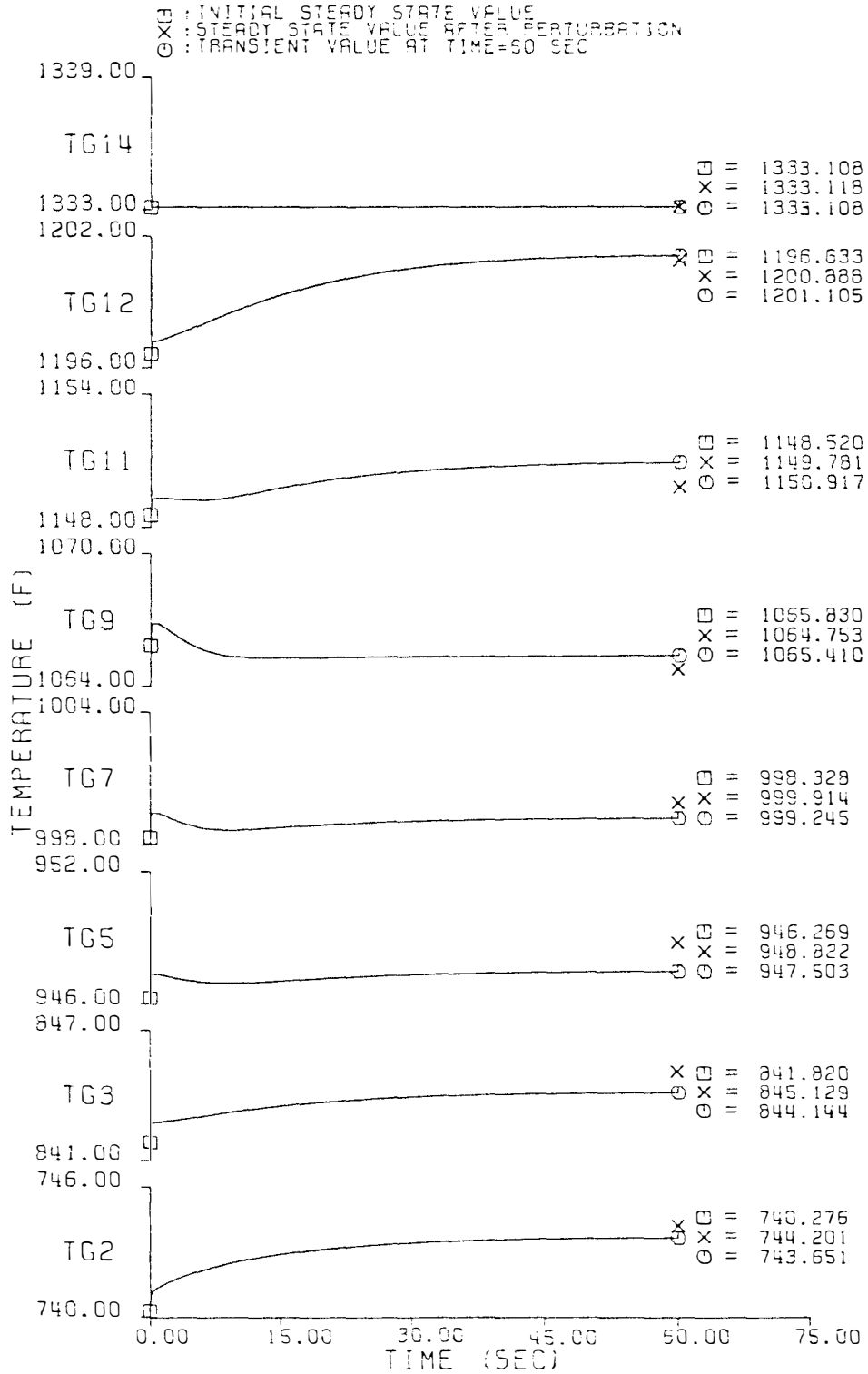Figure 7.2.5 (continued)

Figure 7.2.5 (continued)
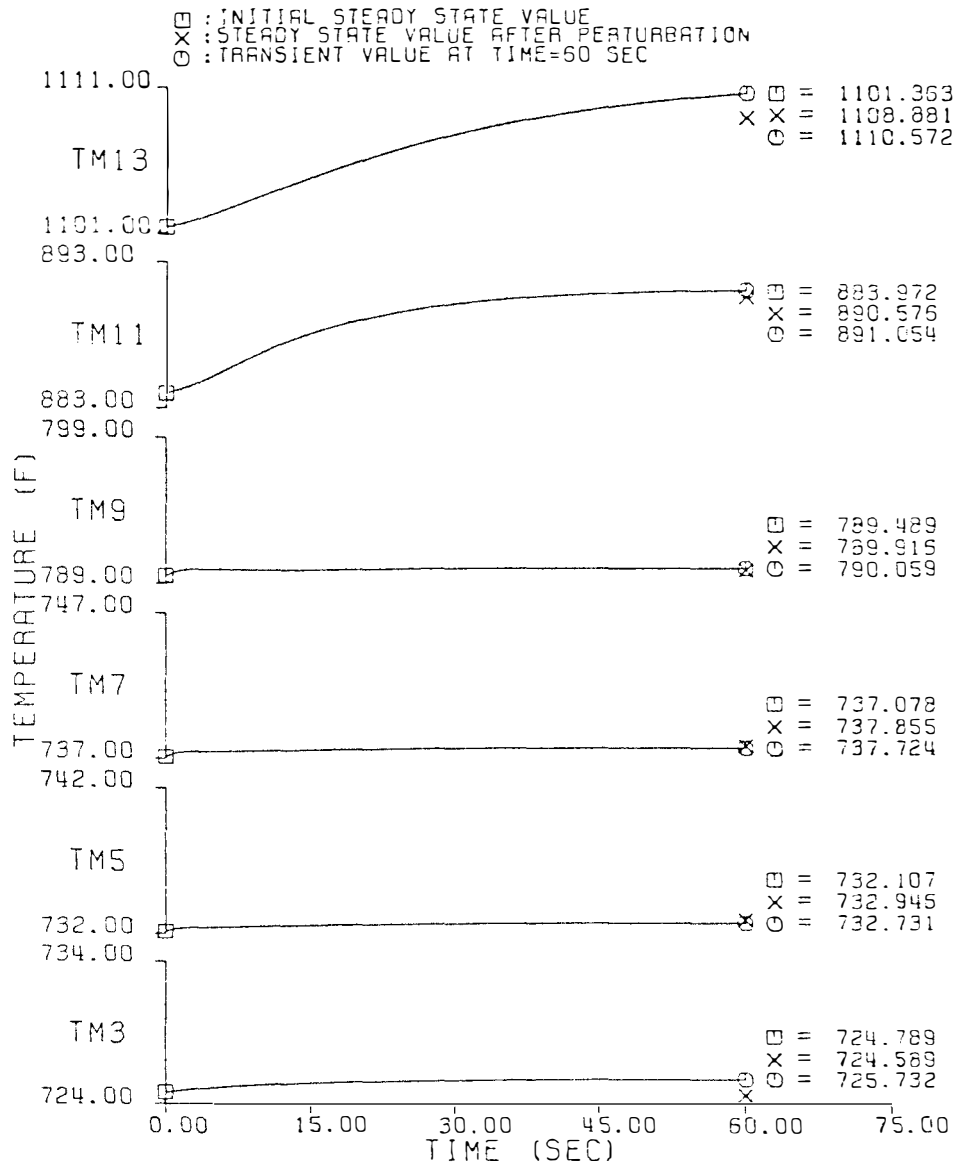
136

Figure 7.2.5 (continued)

Figure 7.2.5 (continued)

energy of helium. Both the heat transfer coefficient and the internal energy of helium are increased as its mass flow rate is increased. The former leads to a helium temperature drop and the latter leads to a rise. The slight decrease in TG9 is consistent with the resultant value from the steady state code. The increased mass flow rate also increases the pressure drop in each section which decreases the pressure at each section such as PG2 through PG12 (PG14 is an input condition). The increased heat transfer rate from the helium to the tube metal sections drive up the tube temperature as shown in TM3 through TM13. Additional heat flows into the secondary side and causes the steam/water temperature increases as indicated in TS3 through TS13. The additional heat can also increase the evaporation of water, which leads to the drop of each regime boundary as shown in SL1F, SL2F, SL3F and SL4F. The steam/water pressures, PS1 through PS11 increase due to the effects of thermal expansion and regime boundaries moving (PS13 is an input condition).

Numerical comparison between the transient state at 60 sec and the steady state after perturbation is given in Table 7.2.6. The comparison shown in Table 7.2.6 shows that the deviations of the transient state from the steady state after perturbation are small. In the outputs of the steam generator, the changes in the helium outlet temperature, the water inlet pressure and the steam outlet temperature are significant but with small deviations in Δe_{SV_k}.

7.2.6 Responses to a Step Change in the Helium Inlet Pressure

No significant responses are observed for a 29 psi (or 2 bars) step increase in the helium inlet pressure except that the helium pressure

TABLE 7.2.6

COMPARISON OF TRANSIENT RESPONSES AT 60 SEC AND STEADY STATE VALUES
AFTER 1 LBM/SEC PER MODULE STEP INCREASE IN HELIUM
INLET MASS FLOW RATE[a]

Flow Regime and Section	Boundary Length (Ft)	Helium		Tube Temperature (F)	Steam/Water	
		Pressure (PSI)	Temperature (F)		Pressure (PSI)	Temperature (F)
Helium inlet section						
14	[9]	689.000[b] 689.000 [689.000]	1333.109[b] 1333.109 [1333.109]			
Superheater II						
13		688.984[b] 688.984	1247.040[b] 1248.339	1108.881[b] 1110.573	2640.000[b] 2640.000 [2640.000]	1036.713[b] 1036.654 [1035.818]
12	[8]	688.962[b] 688.962 [688.962]	1200.890[b] 1201.106 [1201.112]	1016.831[b] 1013.624	2729.749[b] 2729.588	920.126[b] 917.761
Superheater I						
11		688.957[b] 688.956	1149.781[b] 1150.918	890.576[b] 891.054	2801.494[b] 2800.700 [2800.404]	757.776[b] 757.919 [757.667]
10	[7]	688.952[b] 688.951 [688.951]	1095.015[b] 1095.164 [1095.608]	830.946[b] 831.750	2878.914[b] 2878.097	711.662[b] 712.371

TABLE 7.2.6 (continued)

Flow Regime and Section	Boundary Length (Ft)	Helium Pressure (PSI)	Temperature (F)	Tube Temperature (F)	Steam/Water Pressure (PSI)	Temperature (F)
Evaporator II						
9	121.212[b] 121.354 [121.116]	688.949[b] 688.948	1064.755[b] 1065.411	789.917[b] 790.060	2930.051[b] 2929.100 [2926.634]	691.773[b] 691.724 [691.596]
[6]						
8		688.945[b] 688.945 [688.945]	1034.873[b] 1034.872 [1034.241]	784.975[b] 784.909	2936.694[b] 2935.944	692.113[b] 692.075
Evaporator I						
7	103.896[b] 103.650 [103.083]	688.942[b] 688.942	999.915[b] 999.246	737.856[b] 737.724	2943.247[b] 2942.652 [2940.446]	692.449[b] 692.418 [692.305]
[5]						
6		688.938[b] 688.938 [688.938]	965.682[b] 965.374 [965.610]	734.355[b] 734.303	2949.070[b] 2948.584	692.746[b] 692.721

TABLE 7.2.6 (continued)

Flow Regime and Section		Boundary Length (Ft)	Helium		Tube Temperature (F)	Steam/Water	
			Pressure (PSI)	Temperature (F)		Pressure (PSI)	Temperature (F)
Economizer II							
5		81.918[b]	688.936[b]	948.822[b]	732.946[b]	2953.826[b]	692.989[b]
		81.296	688.935	947.504	732.731	2953.369	692.966
		[81.060]				[2950.958]	[692.842]
	[4]						
4			688.933[b]	929.970[b]	727.723[b]	2955.539[b]	684.405[b]
			688.933	928.472	727.308	2955.099	683.880
			[688.933]	[928.700]			
Economizer I							
3	[3]	68.598[b]	688.922[b]	845.129[b]	724.590[b]	2957.433[b]	670.576[b]
		67.786	688.922	844.145	725.733	2957.012	669.713
		[67.563]	[688.922]	[844.424]		[2954.600]	[669.524]
2	[2]		688.915[b]	744.202[b]	602.683[b]	2964.546[b]	568.335[b]
			688.915	743.651	602.026	2964.021	567.660
			[688.914]	[744.002]		[2961.575]	[567.561]

TABLE 7.2.6 (continued)

Flow Regime and Section	Boundary Length (Ft)	Helium Pressure (PSI)	Helium Temperature (F)	Tube Temperature (F)	Steam/Water Pressure (PSI)	Steam/Water Temperature (F)
Water inlet section						
					2970.474[b]	403.000[b]
1 [1]					2969.875	403.000
					[2967.400]	[403.000]

[a][ ]: Transient responses for the lumping case with two sections in the subcooled convective region and one section in each of the remaining flow regions.

[b]Values obtained from the steady state calculations using 300 sections with the input conditions after perturbation. Values without any mark are the transient responses for the lumping case with two sections in each of the flow regions.

ΔPG_o = -0.004 [-0.005] Δe_{PG_o} = 0.001 [-0.001]

ΔTG_o = 3.374 [3.725] Δe_{TG_o} = -0.551 [-0.2]

ΔPS_{in} = 6.317 [3.842] $\Delta e_{PS_{in}}$ = -0.599 [-3.074]

ΔTS_o = 9.712 [8.876] Δe_{TS_o} = -0.059 [-0.895]

itself rises in each section. Since there is no significant change in the temperature differences between the helium and the tube metal and between the tube metal and the steam/water, the secondary fluid system is not affected. Responses are shown in Figure 7.2.6.

7.3 Effects of Changing the Number of Sections in the Dynamic Model

Transient responses for Case 2 with the same perturbations used for Case 1 are studied and compared with those responses of Case 1. As noted in the beginning of this chapter, page 77, Case 2 has one section in each of the flow regimes except the subcooled convective region (two sections) while Case 1 has two sections in each of the flow regions. Because of a different number of sections used in the two cases, only the output response comparisons are of interest. This is shown in Figure 7.3.1 through Figure 7.3.6. Numerical comparisons of the responses at the final observation time between Case 2 and Case 1 are given in Table 7.2.2 through Table 7.2.6, page 96 through page 142. From the overall point of view, the case with fewer lumps is less accurate in comparison with the steady state values after perturbation. However the differences of the responses between the two lumping cases are small except that the secondary pressure has a large difference. This can be seen from Table Table 7.2.2 through Table 7.2.6 and Figure 7.3.1 through Figure 7.3.6 for all perturbations. The large difference in the secondary pressure between two lumping cases may arise from the approximation of the local pressure at the geometry change by using equation (3-14). In a few section moving boundary model, the estimation of a pressure from two
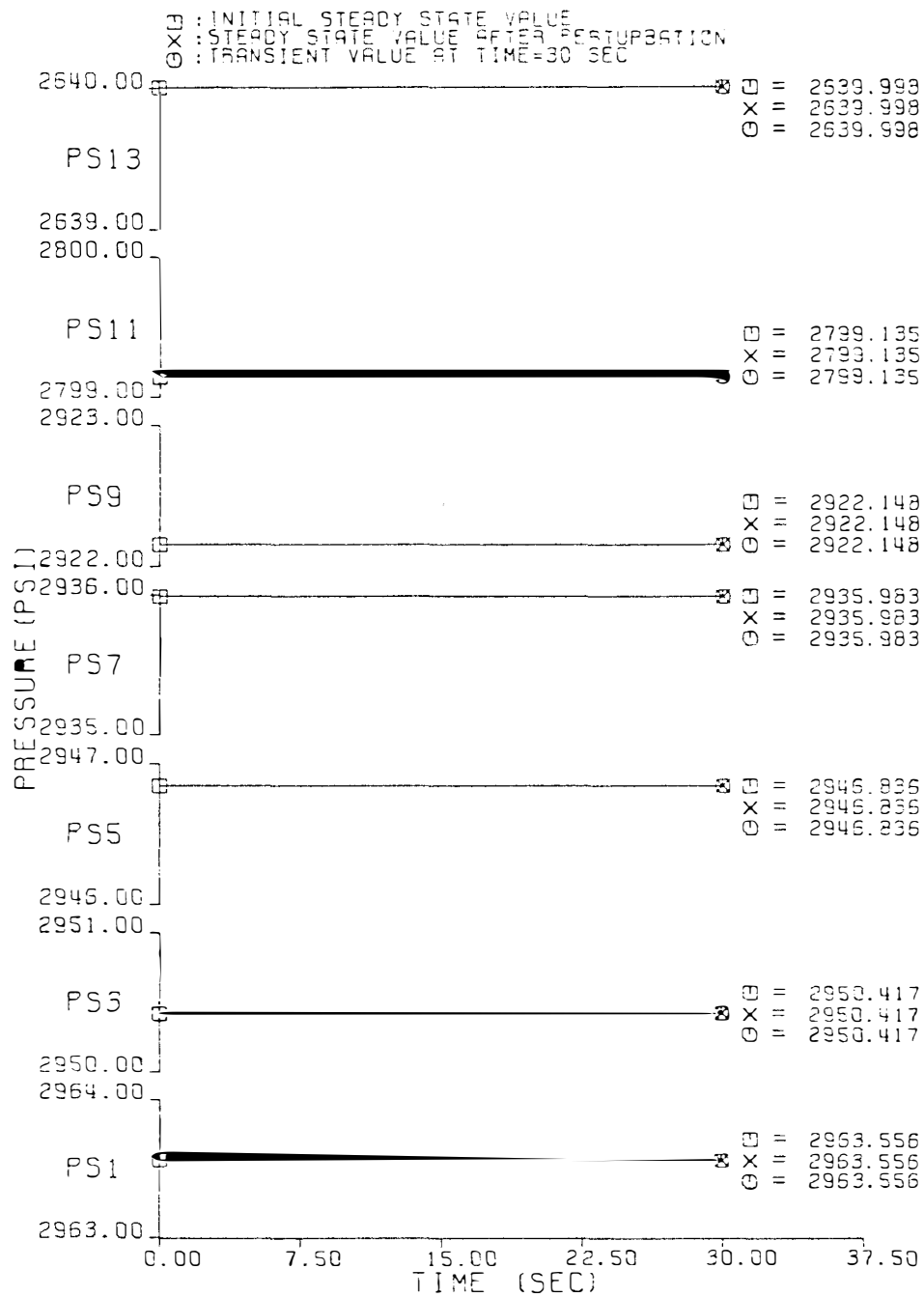
Figure 7.2.6. Transient Responses to 29 Psi Step Increase in Helium
Inlet Pressure.

Figure 7.2.6 (continued)
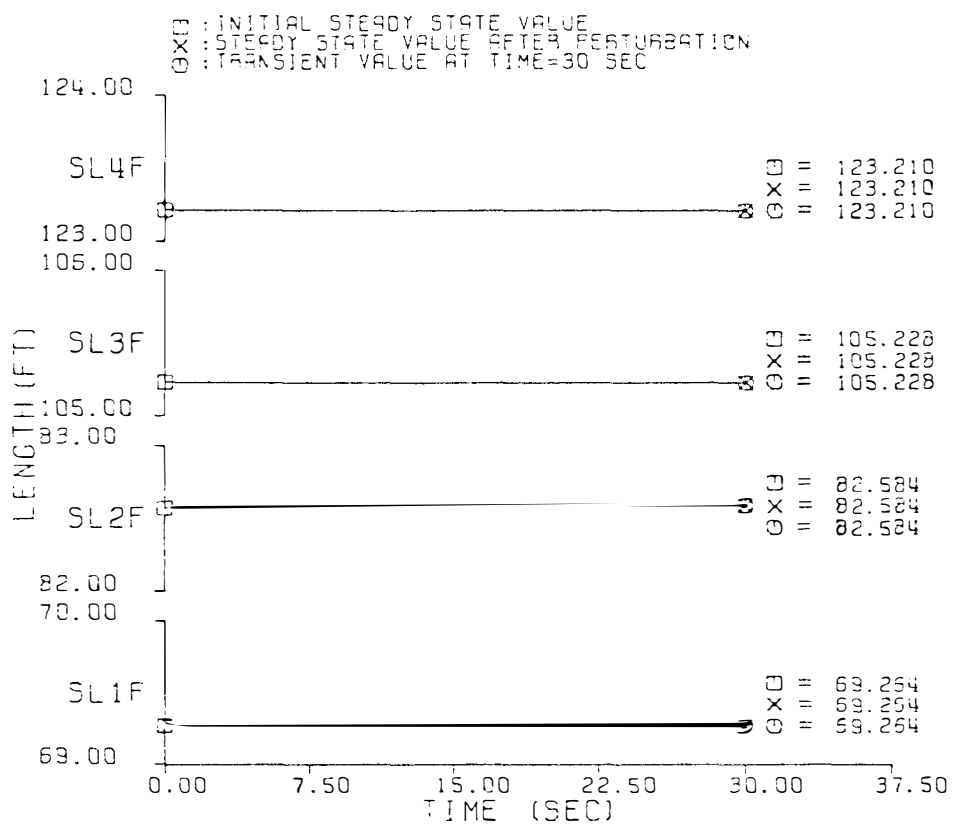
146
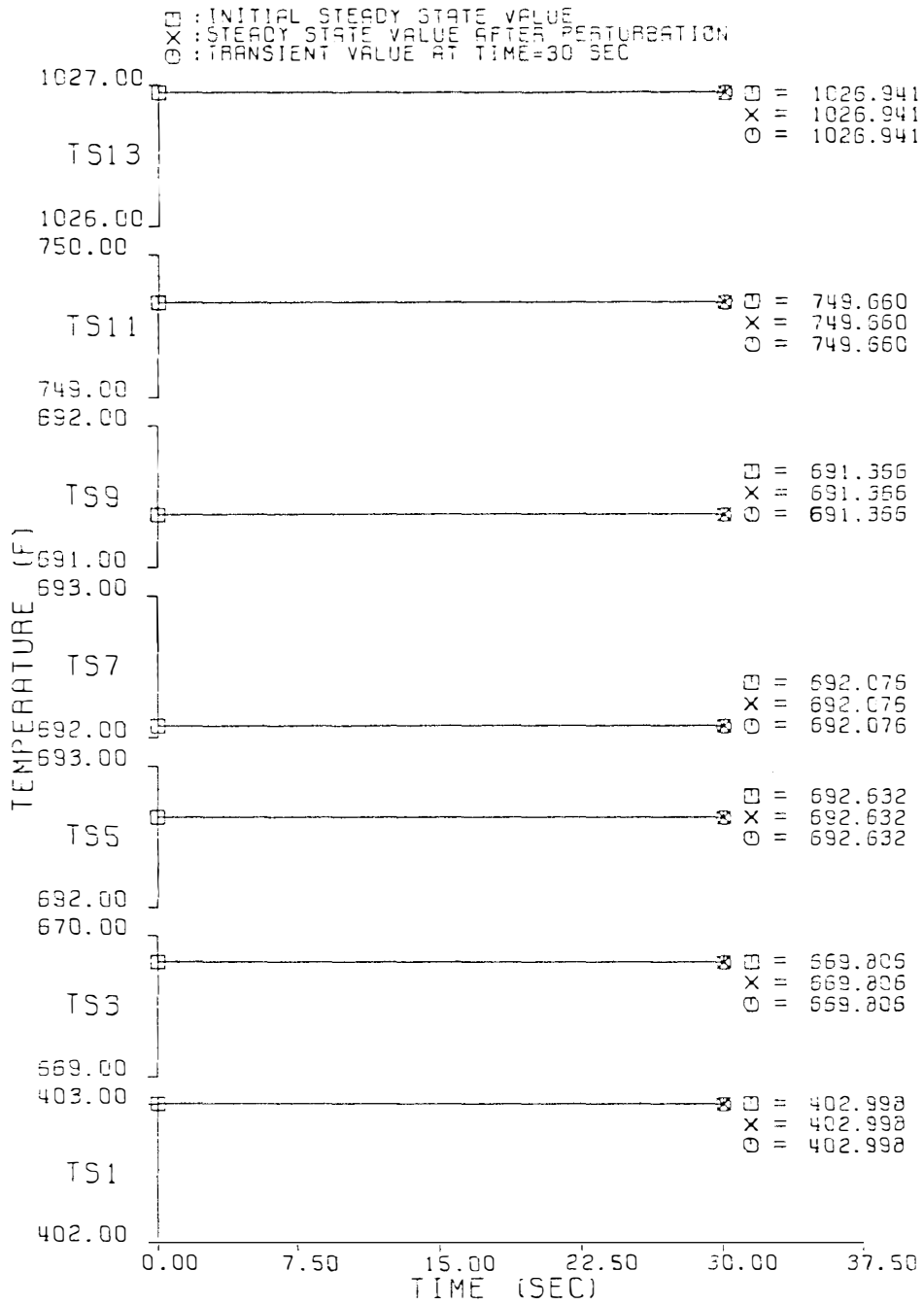

Figure 7.2.6 (continued)

Figure 7.2.6 (continued)

Figure 7.2.6 (continued)

Figure 7.2.6 (continued)

150
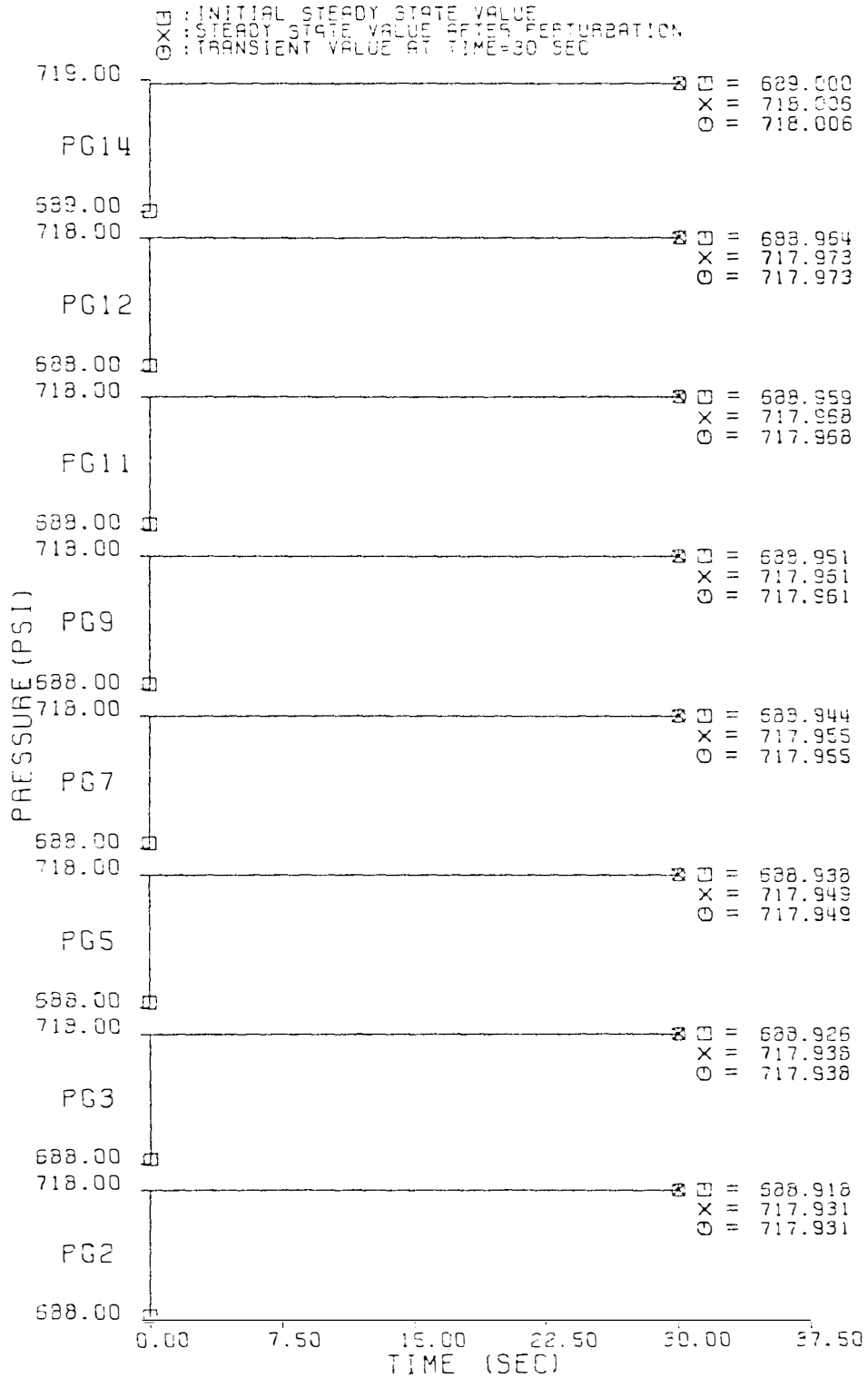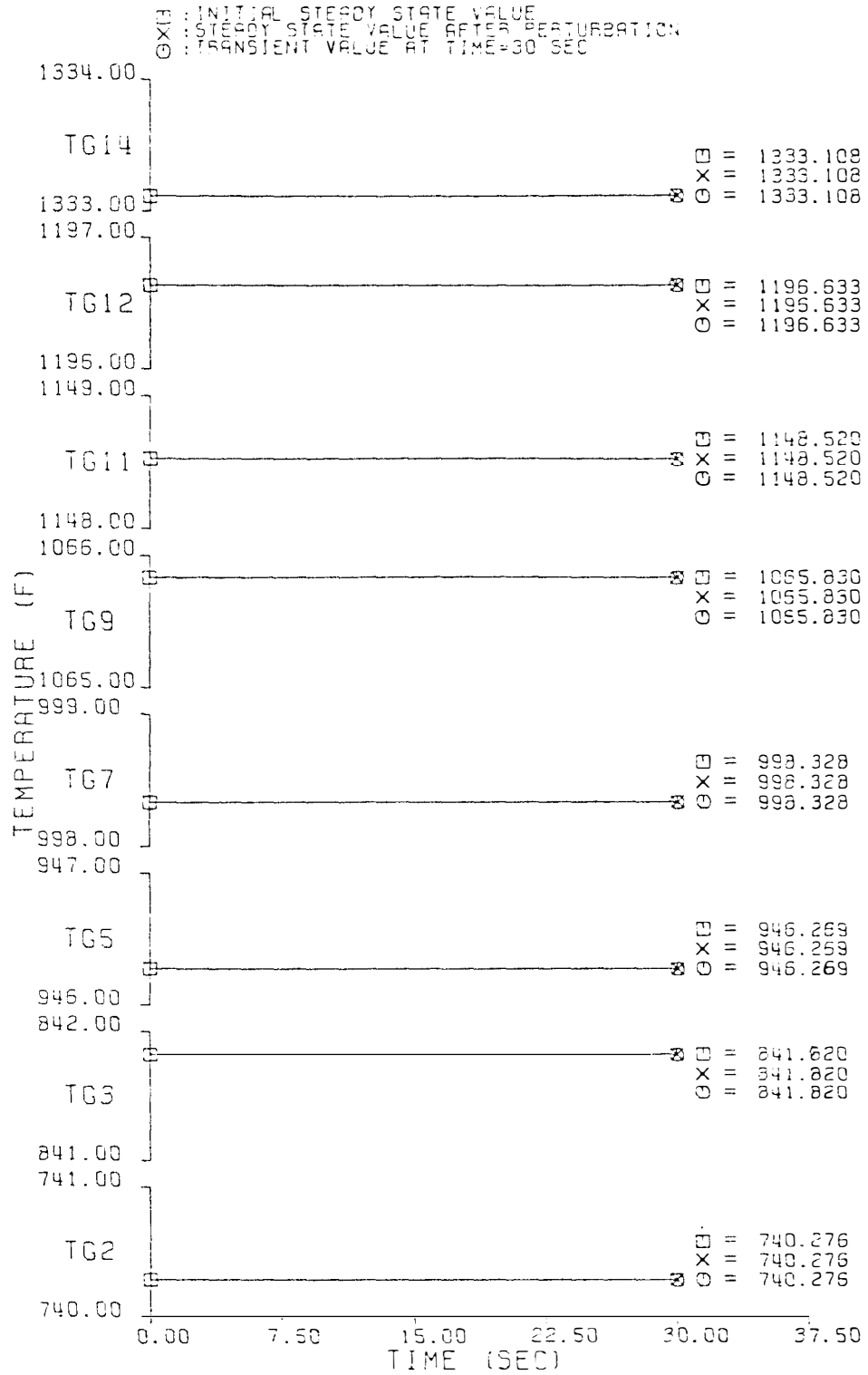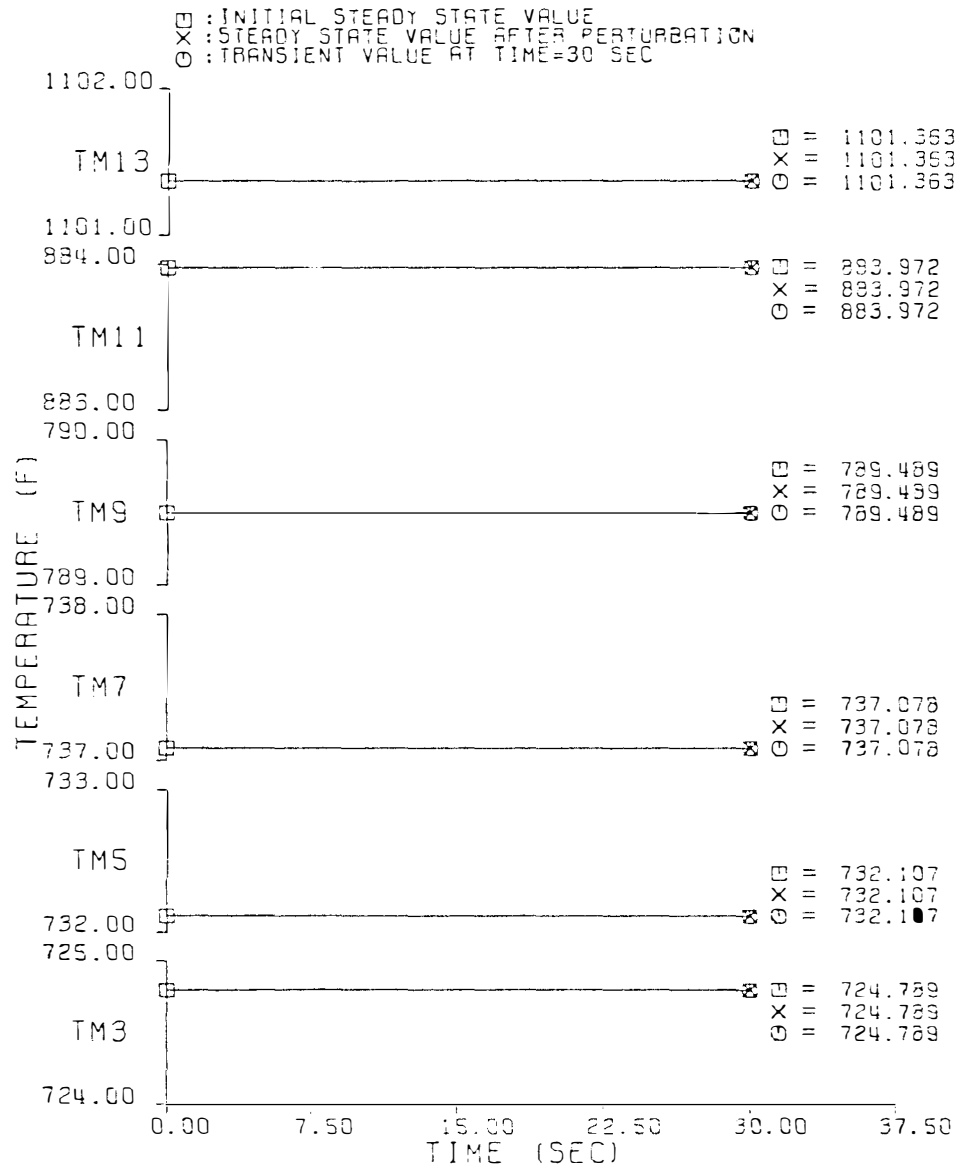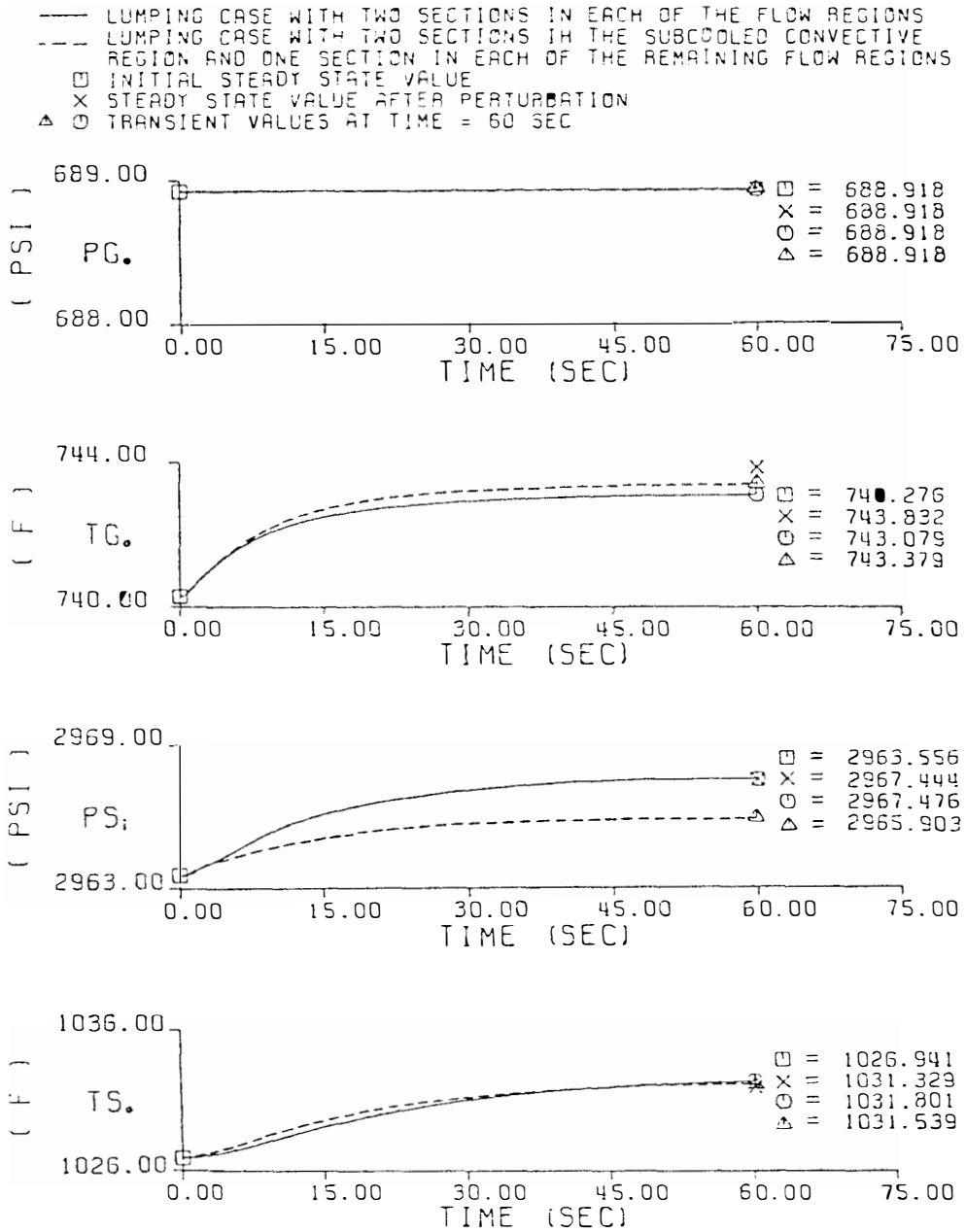
Figure 7.3.1.   Comparison of Transient Responses to 9°F Step Increase
in Feedwater Temperature for Two Lumping Cases.
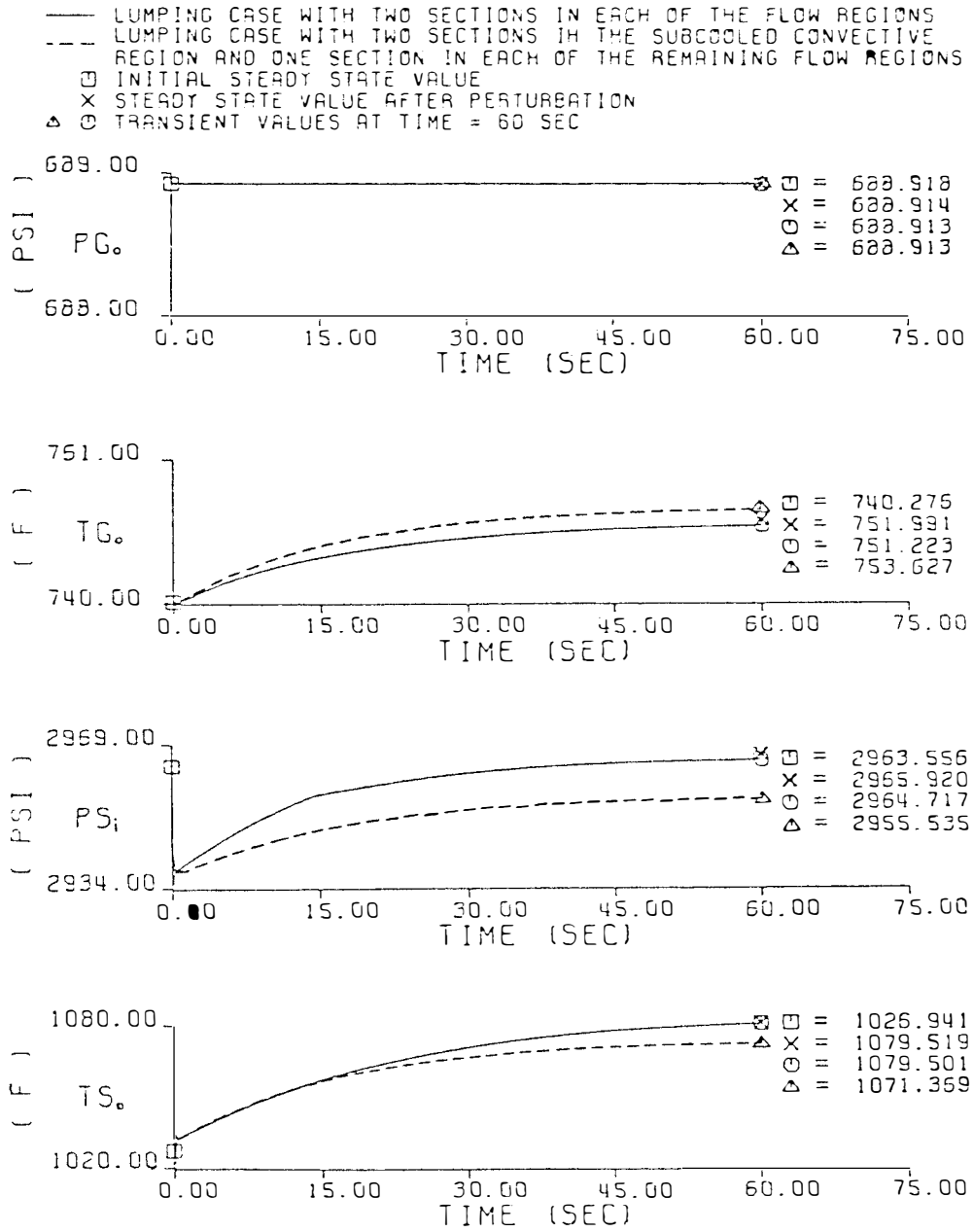
Figure 7.3.2. Comparison of Transient Responses to 0.05 Lbm/Sec per Tube Step Decrease in Feedwater Mass Flow Rate for Two Lumping Cases.

Figure 7.3.3. Comparison of Transient Responses to 58 Psi Step Decrease
in Steam Outlet Pressure for Two Lumping Cases.

Figure 7.3.4.   Comparison of Transient Responses to 10°F Step Increase in Helium Inlet Temperature for Two Lumping Cases.

Figure 7.3.5.   Comparison of Transient Responses to 1 Lbm/Sec per Module Step Increase in Helium Mass Flow Rate for Two Lumping Cases.
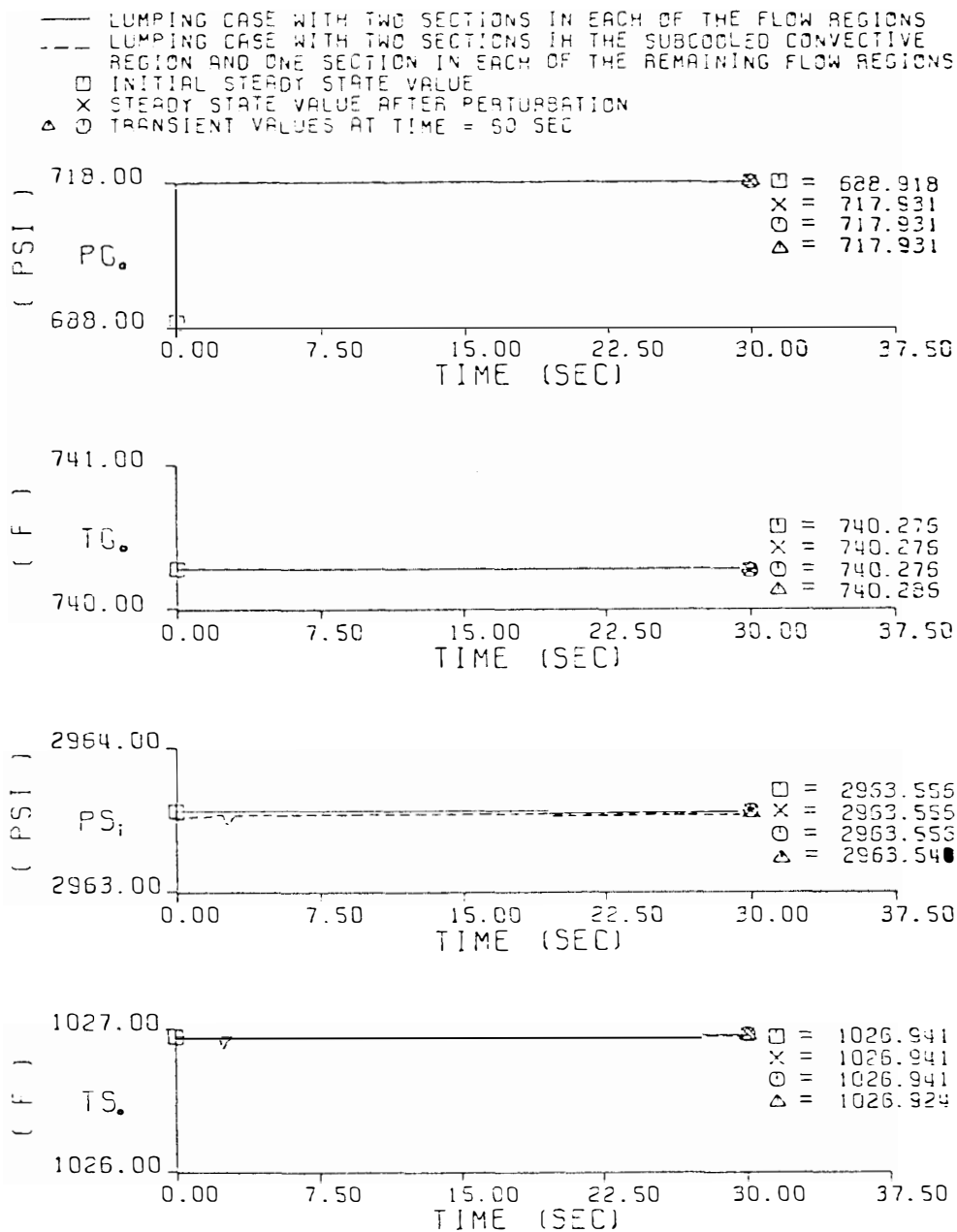
Figure 7.3.6. Comparison of Transient Responses to 29 Psi Step Increase in Helium Inlet Pressure for Two Lumping Cases.

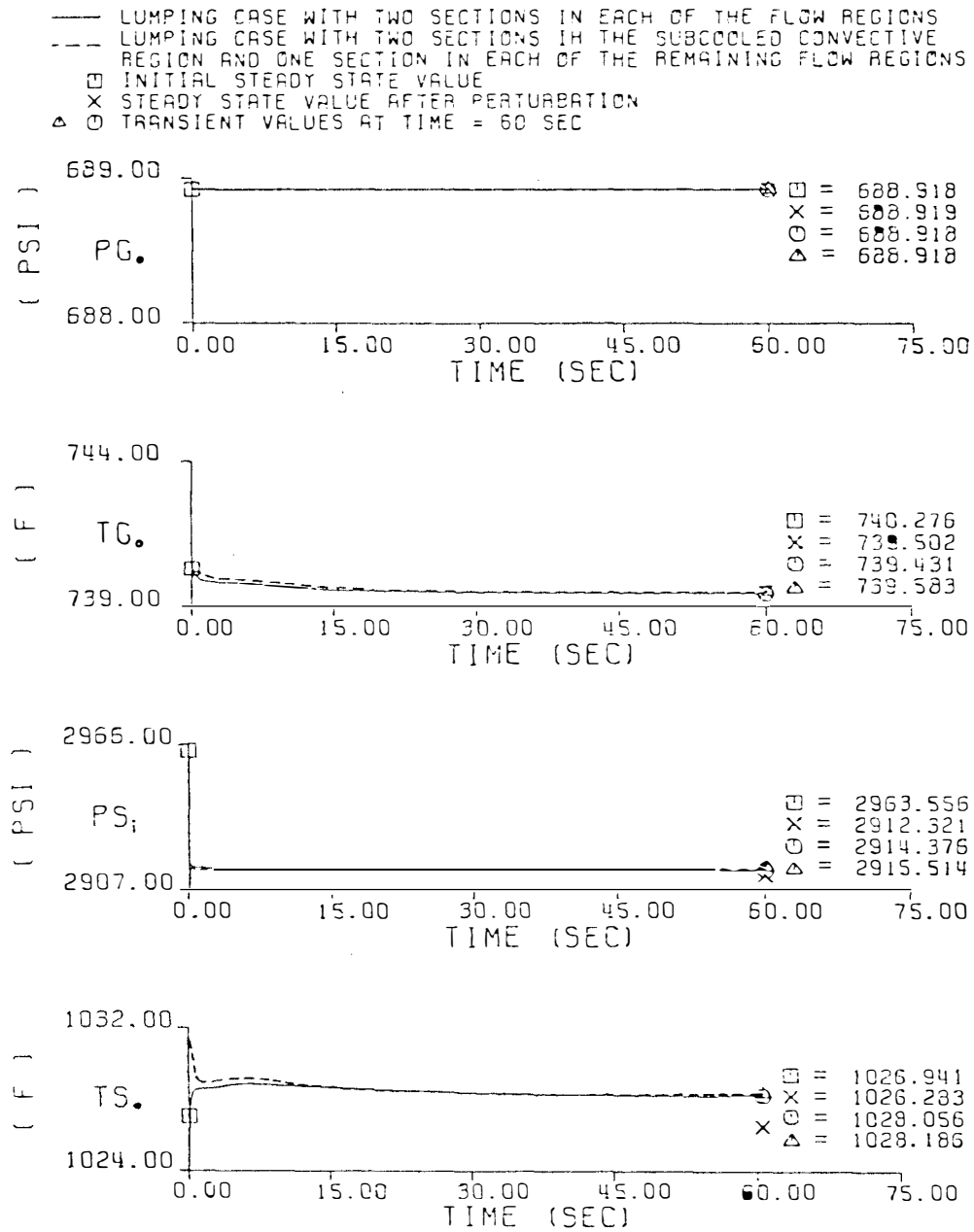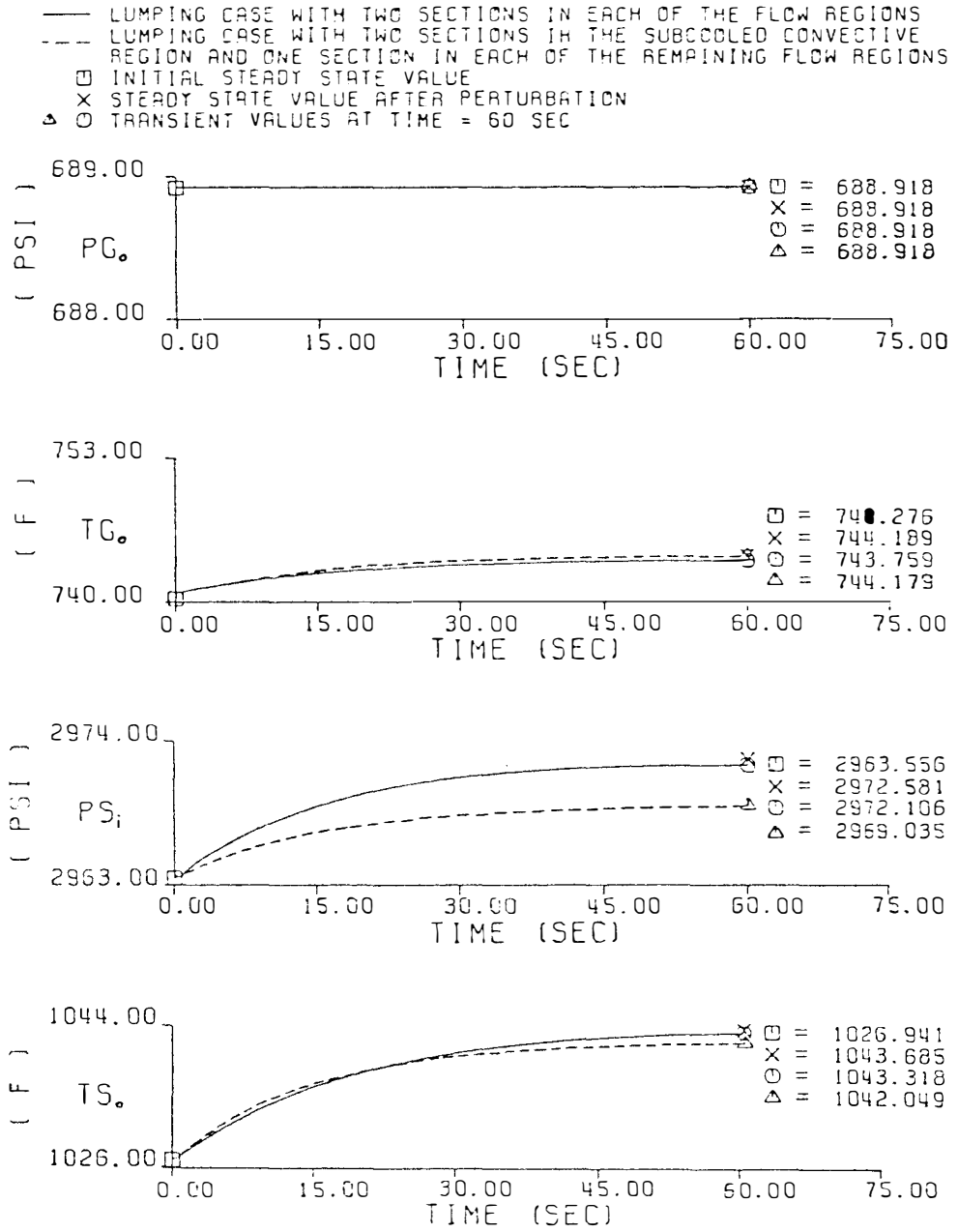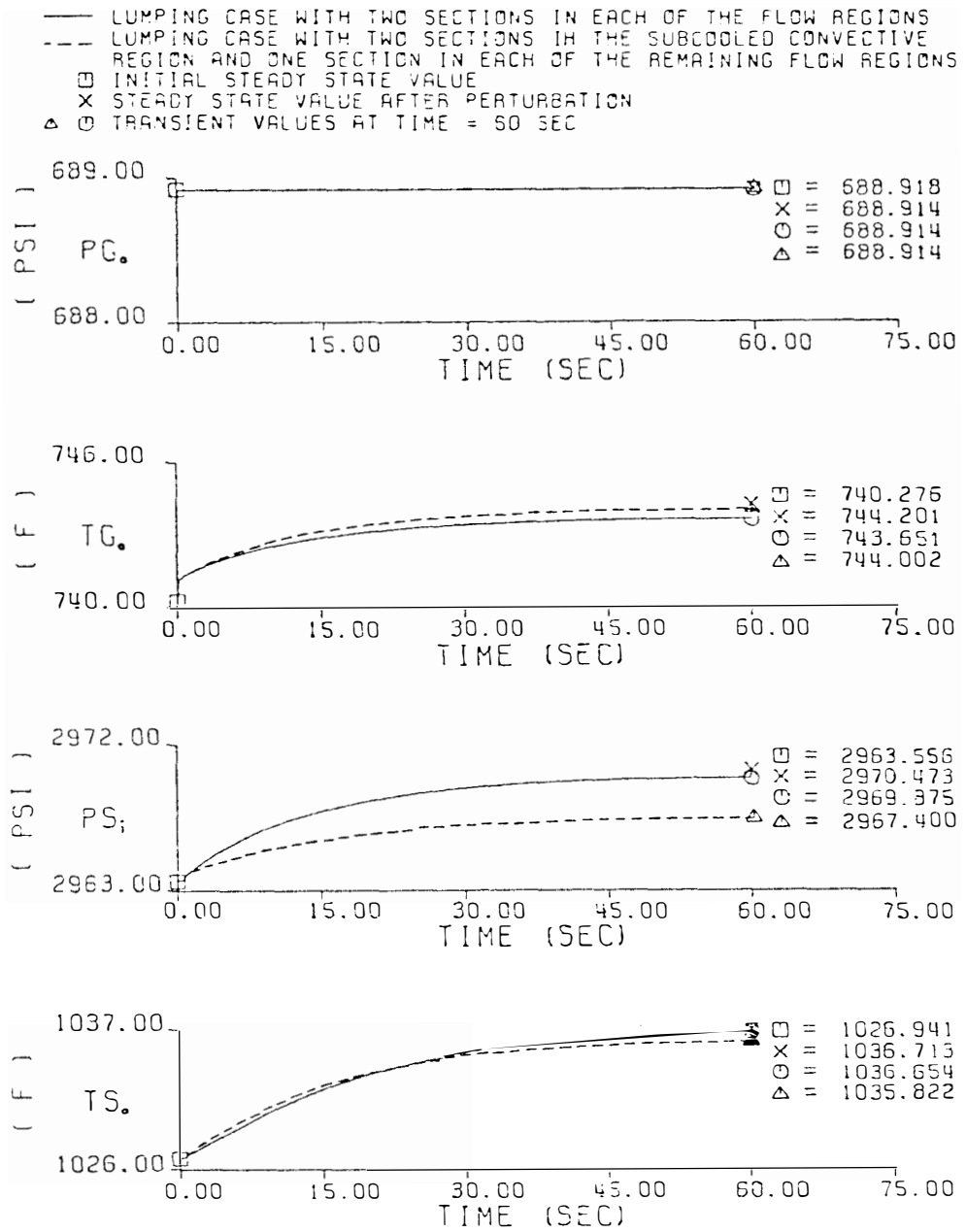other pressures at the locations far from each other is accompanied by an inaccuracy due to the nonlinearities of the steam generator system properties.

7.4 Effects of Changing the Calculational Time Step

To survey the applicable range and the optimal order of magnitude of the calculational time step, the transient code was run for two intervals, 10^{-1} sec and 10^{-3} sec respectively in addition to the 10^{-2} sec used in previously discussed results. The optimal time step is based on the consideration of minimum calculation time but good accuracy. It is found that with 10^{-1} sec, some numerical values are not in the domain of some functions in the code. With 10^{-3} sec, the results are in good agreement with those using 10^{-2} sec. This suggests that a time step of the order of 10^{-2} sec is the best for this dynamic modeling.

Numerical comparison between results obtained with 10^{-2} and 10^{-3} sec is given in Table 7.4.1 through Table 7.4.3. The comparison shows good agreement.

7.5 Nonlinearity of the Steam Generator Outputs

The steam generator responses to the variations of the inputs were studied in order to get a better understanding of the nonlinear effects in the once-through steam generator. This was done by using the steady state code since it provided sufficient information for the selection between the linear and the nonlinear model. Three hundred nodes along the tube coordinate were used. The distributed parameter property was therefore included in the calculations. The output variables including

TABLE 7.4.1

COMPARISON OF TRANSIENT RESPONSES AT 3 SEC AFTER 9°F STEP INCREASE
IN FEEDWATER TEMPERATURE BETWEEN CASES OF USING 10^{-2} SEC
AND 10^{-3} SEC AS CALCULATIONAL TIME STEP

Flow Regime and Section	Boundary Length (Ft)	Helium Pressure (PSI)	Helium Temperature (F)	Tube Temperature (F)	Steam/Water Pressure (PSI)	Steam/Water Temperature (F)
Helium inlet section						
14		689.000 689.000[a]	1333.109 1333.109[a]			
Superheater II						
13		688.985 688.985[a]	1244.546 1244.546[a]	1101.389 1101.389[a]	2640.000 2640.000[a]	1027.113 1027.112[a]
12		688.964 688.964[a]	1196.659 1196.659[a]	1007.649 1007.648[a]	2728.731 2728.731[a]	909.150 909.149[a]
Superheater I						
11		688.959 688.959[a]	1148.418 1148.418[a]	883.955 883.955[a]	2799.169 2799.169[a]	750.207 750.206[a]
10		688.955 688.955[a]	1096.086 1096.087[a]	831.653 831.653[a]	2870.059 2870.057[a]	709.535 709.535[a]

TABLE 7.4.1 (continued)

Flow Regime and Section	Boundary Length (Ft)	Helium Pressure (PSI)	Helium Temperature (F)	Tube Temperature (F)	Steam/Water Pressure (PSI)	Steam/Water Temperature (F)
Evaporator II						
9	123.1279	688.952	1065.323	789.372	2922.519	691.385
	123.1284[a]	688.952[a]	1065.324[a]	789.372[a]	2922.518[a]	691.385[a]
8		688.948	1033.773	783.421	2929.584	691.749
		688.948[a]	1033.774[a]	783.420[a]	2929.582[a]	691.749[a]
Evaporator I						
7	104.9675	688.945	997.742	737.014	2936.482	692.102
	104.9679[a]	688.945[a]	997.743[a]	737.014[a]	2936.481[a]	692.102[a]
6		688.941	963.550	733.592	2942.463	692.409
		688.941[a]	963.550[a]	733.592[a]	2942.461[a]	692.409[a]
Economizer II						
5	82.4187	688.939	945.617	731.980	2947.283	692.655
	82.4191[a]	688.939[a]	945.618[a]	731.980[a]	2947.282[a]	692.655[a]
4		688.937	926.537	726.622	2949.012	683.741
		688.937[a]	926.539[a]	726.622[a]	2949.010[a]	683.741[a]

TABLE 7.4.1 (continued)

Flow Regime and Section	Boundary Length (Ft)	Helium Pressure (PSI)	Helium Temperature (F)	Tube Temperature (F)	Steam/Water Pressure (PSI)	Steam/Water Temperature (F)
Economizer I						
3	68.8650 68.8656[a]	688.926 688.926[a]	841.483 841.483[a]	724.562 724.562[a]	2950.926 2950.925[a]	670.018 670.018[a]
2		688.919 688.919[a]	740.994 740.993[a]	602.364 602.363[a]	2958.056 2958.054[a]	569.319 569.318[a]
Water inlet section						
1					2964.015 2964.014[a]	412.000 412.000[a]

[a] 10^{-3} sec calculational time step. Otherwise, 10^{-2} sec calculational time step.

TABLE 7.4.2

COMPARISON OF TRANSIENT RESPONSES AT 3 SEC AFTER 0.05 LBM/SEC PER TUBE STEP
DECREASE IN FEEDWATER MASS FLOW RATE BETWEEN CASES OF USING
10^{-2} SEC AND 10^{-3} SEC AS CALCULATIONAL TIME STEP

Flow Regime and Section	Boundary Length (Ft)	Helium Pressure (PSI)	Helium Temperature (F)	Tube Temperature (F)	Steam/Water Pressure (PSI)	Steam/Water Temperature (F)
Helium inlet section						
14		689.000	1333.109			
		689.000[a]	1333.109[a]			
Superheater II						
13		688.985	1245.947	1105.145	2640.000	1037.400
		688.985[a]	1245.946[a]	1105.142[a]	2640.000[a]	1037.391[a]
12		688.964	1199.204	1014.984	2720.670	924.214
		688.964[a]	1199.201[a]	1014.973[a]	2720.669[a]	924.197[a]
Superheater I						
11		688.958	1148.747	887.891	2785.462	763.378
		688.958[a]	1148.754[a]	887.882[a]	2785.460[a]	763.361[a]
10		688.953	1093.405	832.202	2856.585	715.392
		688.953[a]	1093.425[a]	832.206[a]	2856.562[a]	715.388[a]

TABLE 7.4.2 (continued)

Flow Regime and Section	Boundary Length (Ft)	Helium Pressure (PSI)	Helium Temperature (F)	Tube Temperature (F)	Steam/Water Pressure (PSI)	Steam/Water Temperature (F)
Evaporator II						
9	121.4923 121.4998[a]	688.950 688.950[a]	1061.025 1061.044[a]	788.862 788.867[a]	2905.042 2905.024[a]	690.483 690.483[a]
8		688.947 688.947[a]	1027.653 1027.669[a]	779.451 779.451[a]	2911.917 2911.898[a]	690.838 690.838[a]
Evaporator I						
7	102.1080 102.1153[a]	688.944 688.944[a]	993.633 993.646[a]	735.768 735.770[a]	2918.661 2918.643[a]	691.186 691.186[a]
6		688.940 688.940[a]	961.177 961.188[a]	732.593 732.595[a]	2923.872 2923.855[a]	691.454 691.454[a]
Economizer II						
5	80.5761 80.5826[a]	688.938 688.938[a]	943.007 943.010[a]	730.682 730.683[a]	2928.079 2928.062[a]	691.671 691.670[a]
4		688.935 688.935[a]	923.738 923.734[a]	725.705 725.704[a]	2929.645 2929.628[a]	683.394 683.397[a]

TABLE 7.4.2 (continued)

Flow Regime and Section	Boundary Length (Ft)	Helium Pressure (PSI)	Helium Temperature (F)	Tube Temperature (F)	Steam/Water Pressure (PSI)	Steam/Water Temperature (F)
Economizer I						
3	66.7589	688.925	840.758	723.129	2931.400	688.301
	66.7599[a]	688.925[a]	840.755[a]	723.128[a]	2931.384[a]	688.301[a]
2		688.918	741.907	601.293	2937.573	566.956
		688.918[a]	741.904[a]	601.290[a]	2937.556[a]	566.954[a]
Water inlet section						
1					2942.761	403.000
					2942.744[a]	403.000[a]

[a] 10^{-3} sec calculational time step. Otherwise, 10^{-2} sec calculational time step.

TABLE 7.4.3

COMPARISON OF TRANSIENT RESPONSES AT 3 SEC AFTER 10°F STEP INCREASE IN HELIUM
INLET TEMPERATURE BETWEEN CASES OF USING 10^{-2} SEC AND
10^{-3} SEC AS CALCULATIONAL TIME STEP

Flow Regime and Section	Boundary Length (Ft)	Helium		Tube Temperature (F)	Steam/Water	
		Pressure (PSI)	Temperature (F)		Pressure (PSI)	Temperature (F)
Helium inlet section						
14		689.000 689.000[a]	1343.107 1343.107[a]			
Superheater II						
13		688.985 688.985[a]	1251.157 1251.157[a]	1102.637 1102.637[a]	2640.000 2640.000[a]	1029.243 1029.241[a]
12		688.965 688.965[a]	1202.604 1202.603[a]	1011.179 1011.178[a]	2728.895 2728.895[a]	912.388 912.386[a]
Superheater I						
11		688.959 688.959[a]	1159.380 1153.381[a]	885.191 885.190[a]	2799.652 2799.652[a]	751.623 751.620[a]
10		688.955 688.955[a]	1100.062 1100.064[a]	832.534 832.534[a]	2871.262 2871.259[a]	710.268 710.267[a]

TABLE 7.4.3 (continued)

Flow Regime and Section	Boundary Length (Ft)	Helium Pressure (PSI)	Helium Temperature (F)	Tube Temperature (F)	Steam/Water Pressure (PSI)	Steam/Water Temperature (F)
Evaporator II						
9	122.9782	688.952	1069.230	790.193	2923.722	691.447
	122.9789[a]	688.952[a]	1069.231[a]	790.193[a]	2923.719[a]	691.447[a]
8		688.949	1037.587	784.269	2930.709	691.806
		688.949[a]	1037.588[a]	784.269[a]	2930.706[a]	691.806[a]
Evaporator I						
7	104.9891	688.946	1001.161	737.485	2937.536	692.157
	104.9896[a]	688.946[a]	1001.162[a]	737.485[a]	2937.553[a]	692.157[a]
6		688.942	966.592	734.019	2943.502	692.464
		688.942[a]	966.593[a]	734.019[a]	2943.549[a]	692.464[a]
Economizer II						
5	82.4599	688.940	948.589	732.416	2948.378	692.711
	82.4603[a]	688.940[a]	948.589[a]	732.416[a]	2948.375[a]	692.711[a]
4		688.937	929.425	727.040	2950.094	683.724
		688.937[a]	929.426[a]	727.040[a]	2950.091[a]	683.724[a]

TABLE 7.4.3 (continued)

Flow Regime and Section	Boundary Length (Ft)	Helium Pressure (PSI)	Helium Temperature (F)	Tube Temperature (F)	Steam/Water Pressure (PSI)	Steam/Water Temperature (F)
Economizer I						
3	69.0193 69.0197[a]	688.926 688.926[a]	843.215 843.215[a]	725.005 725.005[a]	2951.994 2951.991[a]	669.791 669.791[a]
2		688.919 688.919[a]	741.329 741.329[a]	601.077 601.077[a]	2959.130 2959.128[a]	567.307 567.307[a]
Water inlet section						
1					2965.086 2965.084[a]	403.000 403.000[a]

[a] 10^{-3} sec calculational time step. Otherwise, 10^{-2} sec calculational time step.

the helium outlet temperature, water inlet pressure and the steam outlet
temperature with respect to the variations in the feedwater mass flow
rate and helium inlet temperature are shown in Figure 7.5.1 and
Figure 7.5.2 respectively. In Figure 7.5.1, the nonlinear property is
shown in the water inlet pressure, the helium outlet temperature and in
the steam outlet temperature for the feedwater mass flow rate ranging
from 80% to 100% of the full load (the full load mass flow rate is
0.988220 lbm/sec/tube). The deviation of the helium temperature at 80%
of the full load from the tangent line at the full mass flow rate is
approximately 24°F. The deviation of the steam outlet temperature at
80% of the full mass flow rate from the line tangent to the full load
point is approximately 18.5°F. The water inlet pressure has a pronounced
nonlinearity although the variation is small.

For the case of varying the helium inlet temperature as shown in
Figure 7.5.2, the nonlinearity in the water inlet pressure is significant.
AT 97.75% of the reference helium inlet temperature, (that is T_{gref}
= 1333.1°F), the deviation of the water inlet pressure from the line
tangent to the point at the reference helium inlet temperature is about
8 psia. Good linearity in the helium outlet temperature and the steam
outlet temperature is observed for the helium inlet temperature ranging
from 1301°F to 1341°F.

7.6 Comparison of Transient Responses for Three Models

The Fort St. Vrain 330 MW(e) steam generator design information was
used with the model developed in this research, KOLU(T) to compute
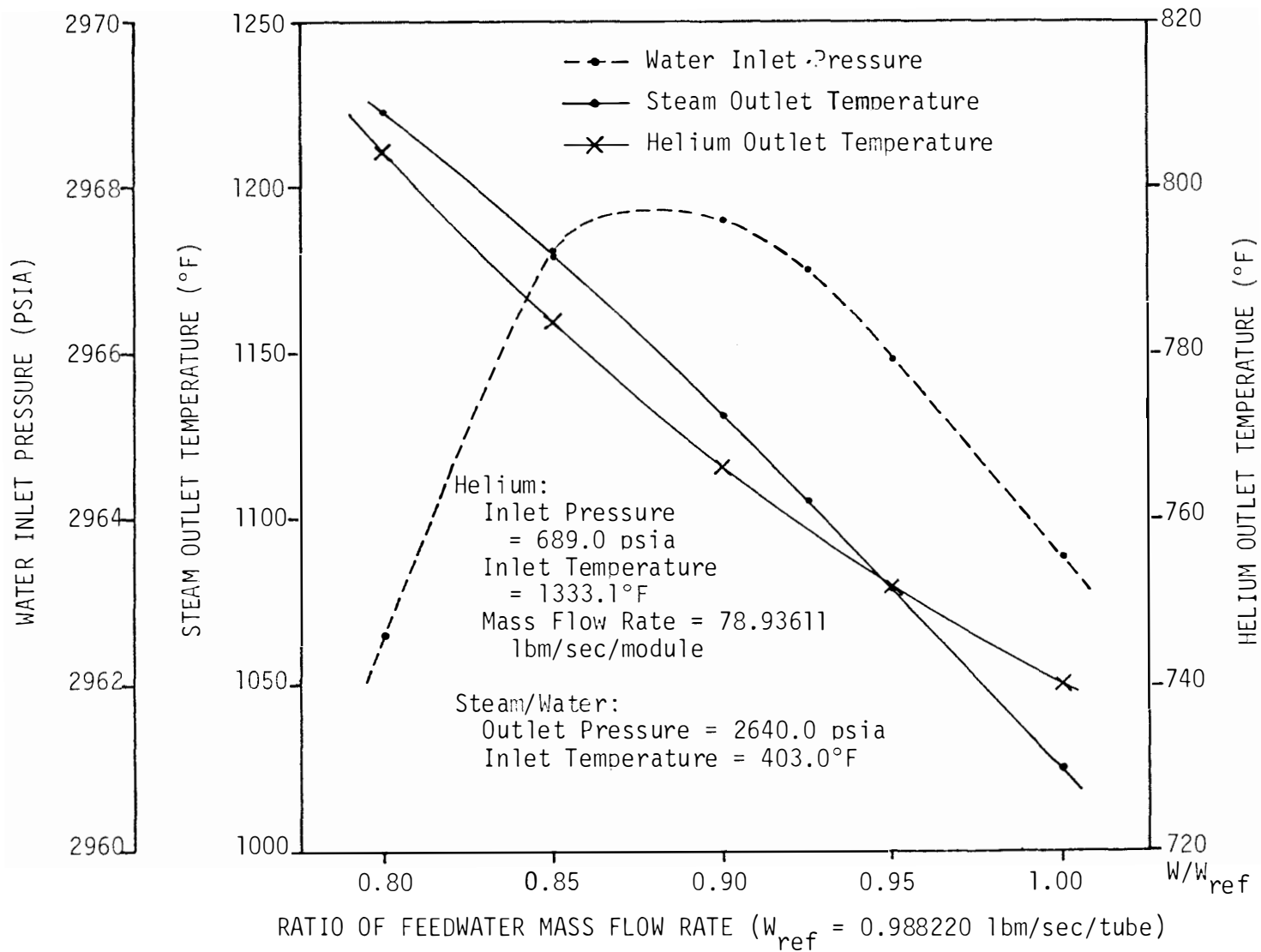transient responses. These responses are compared with those obtained

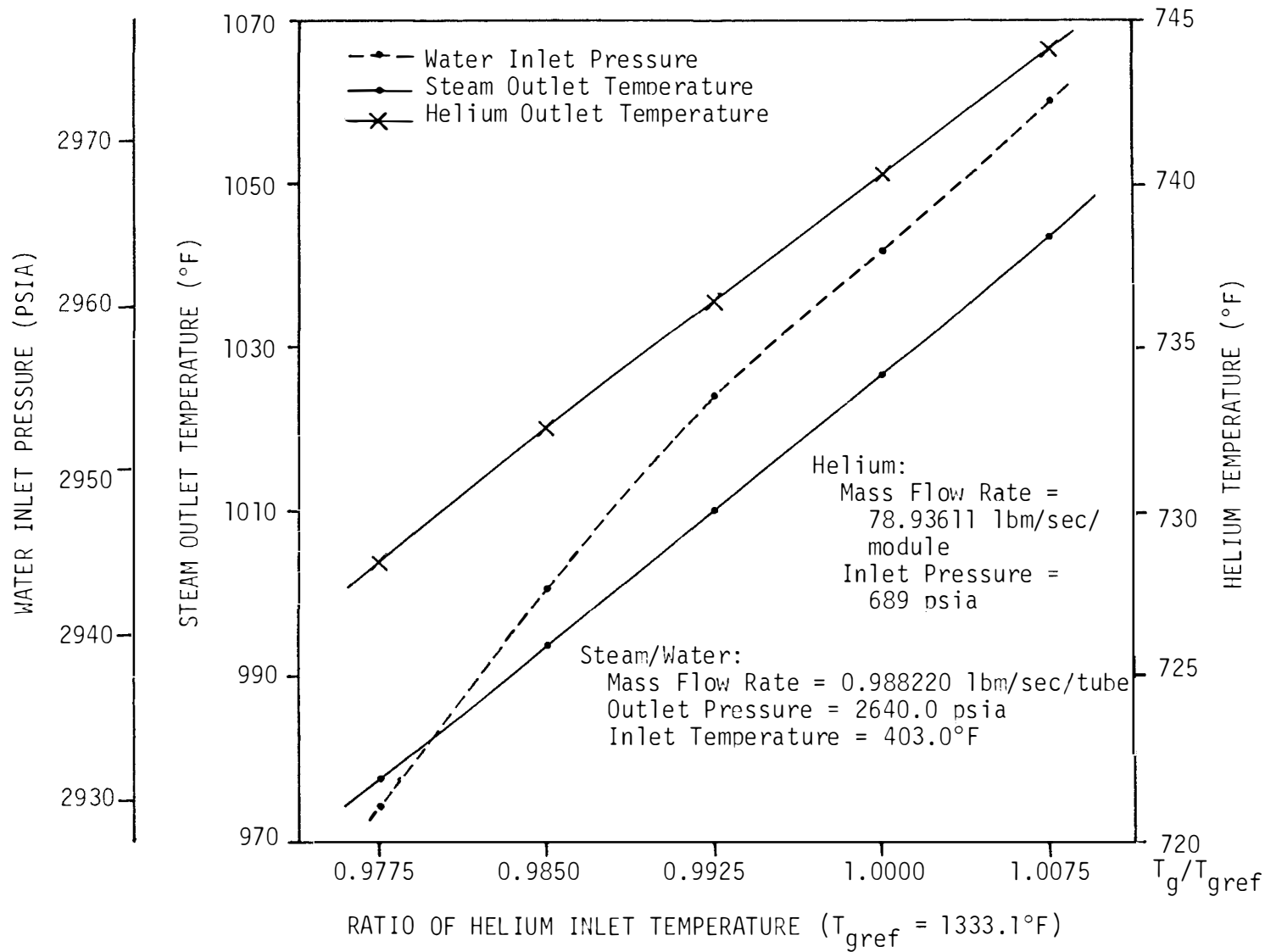Figure 7.5.1. Fort St. Vrain Steam Generator Outputs Due to Variation in Steam/Water Mass Flow Rate.

Figure 7.5.2. Fort St. Vrain Steam Generator Outputs Due to Variation in Helium Inlet Temperature.

168

employing two other models, namely BLAST[47] and UTSGRHM.[48] The
comparisons are shown in Figure 7.6.1, Figure 7.6.2 and Figure 7.6.3.
All of the three models shown are nonlinear.

KOLU(T) is a very detailed, multilump, moving boundary model. The
flow regimes employed include subcooled convection, subcooled nucleate
boiling, saturated nucleate boiling, film boiling and superheat convection
(including superheater I and superheater II). The results shown were
obtained by employing two sections in each flow region. In KOLU(T), the
conservation of energy equations for the working fluids and tube, and
the differential equations for moving boundaries are solved using the
explicit integration method. The mass flow rate variation is approximated
by a combination of the first order variation in mass and momentum
equations, which leads to a delay function in terms of sonic velocity,
Mach number and the length of the flow path. The momentum balance
equation is used to determine pressure. In the KOLU model a three
hundred node steady state calculation, KOLU(S), is included and used to
verify the transient responses at the final observation time.

BLAST is a multinode, fixed boundary model. The flow regimes
employed consist of subcooled forced convection, subcooled and saturated
nucleate boiling, transition boiling, film boiling and superheat forced
convection. Five sections on the helium fluid side, one section in the
evaporator I, two sections in the evaporator II, two sections in the
superheater I and one section in the superheater II were used. The
conservation of mass, momentum and energy equations for steam/water and
helium and conservation of energy equations for the tube (in nodal form)
are solved by employing the implicit integration technique.
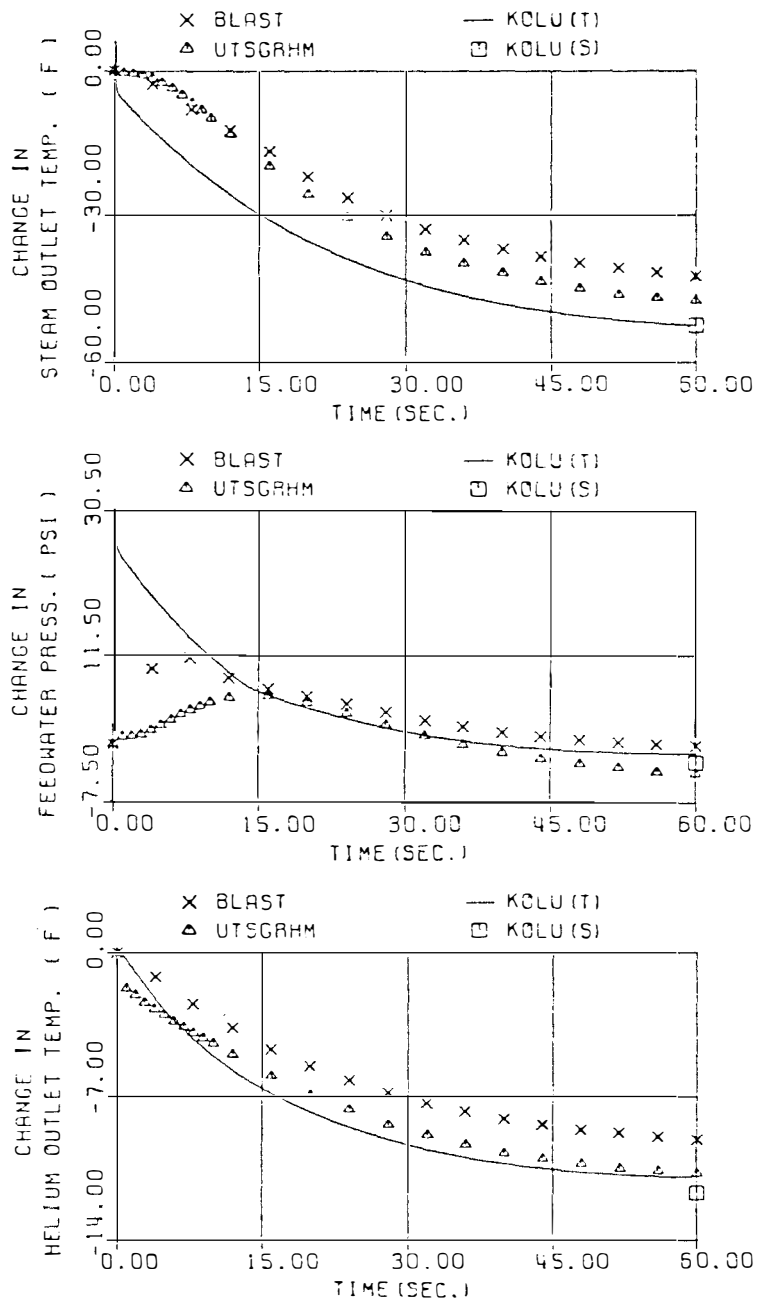
Figure 7.6.1. Comparison of Transient Responses to 0.05 Lbm/Sec per
Tube Step Increase in Feedwater Mass Flow Rate for
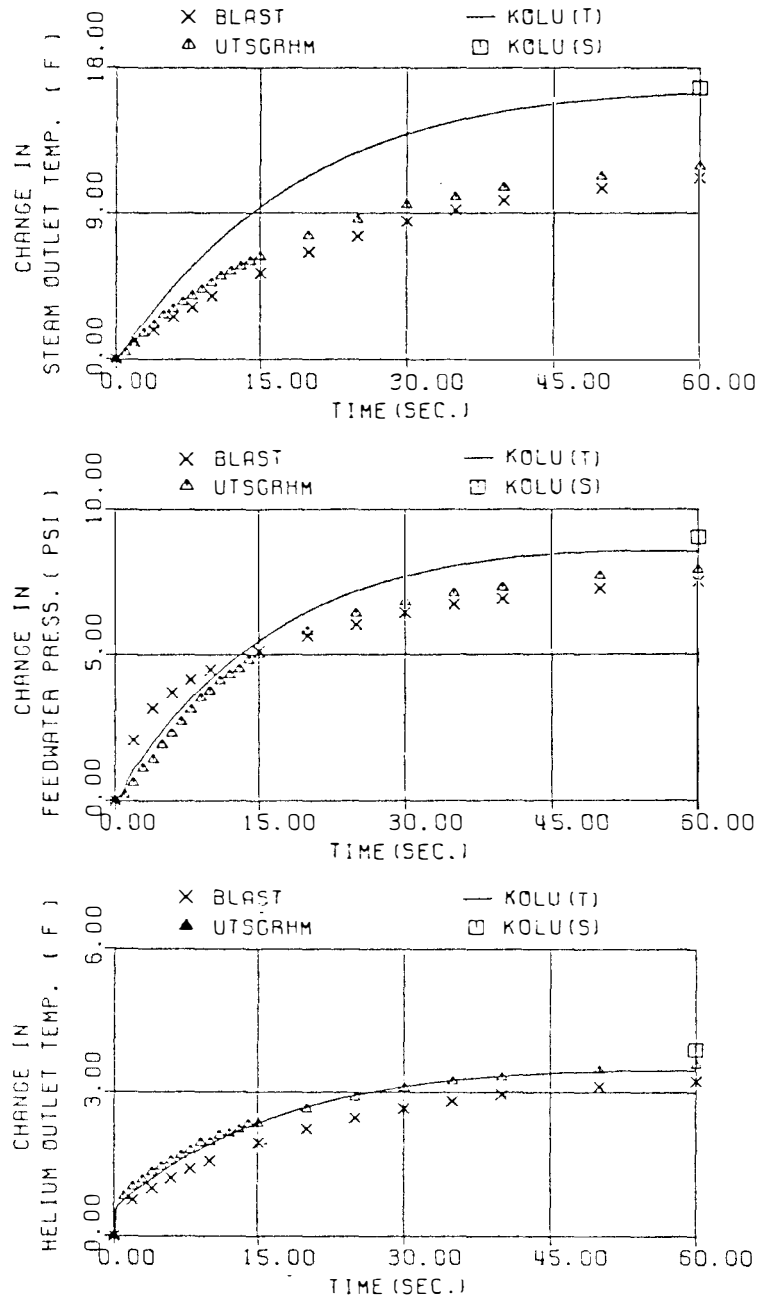Three Models.

Figure 7.6.2. Comparison of Transient Responses to 10°F Step Increase in Helium Inlet Temperature for Three Models.
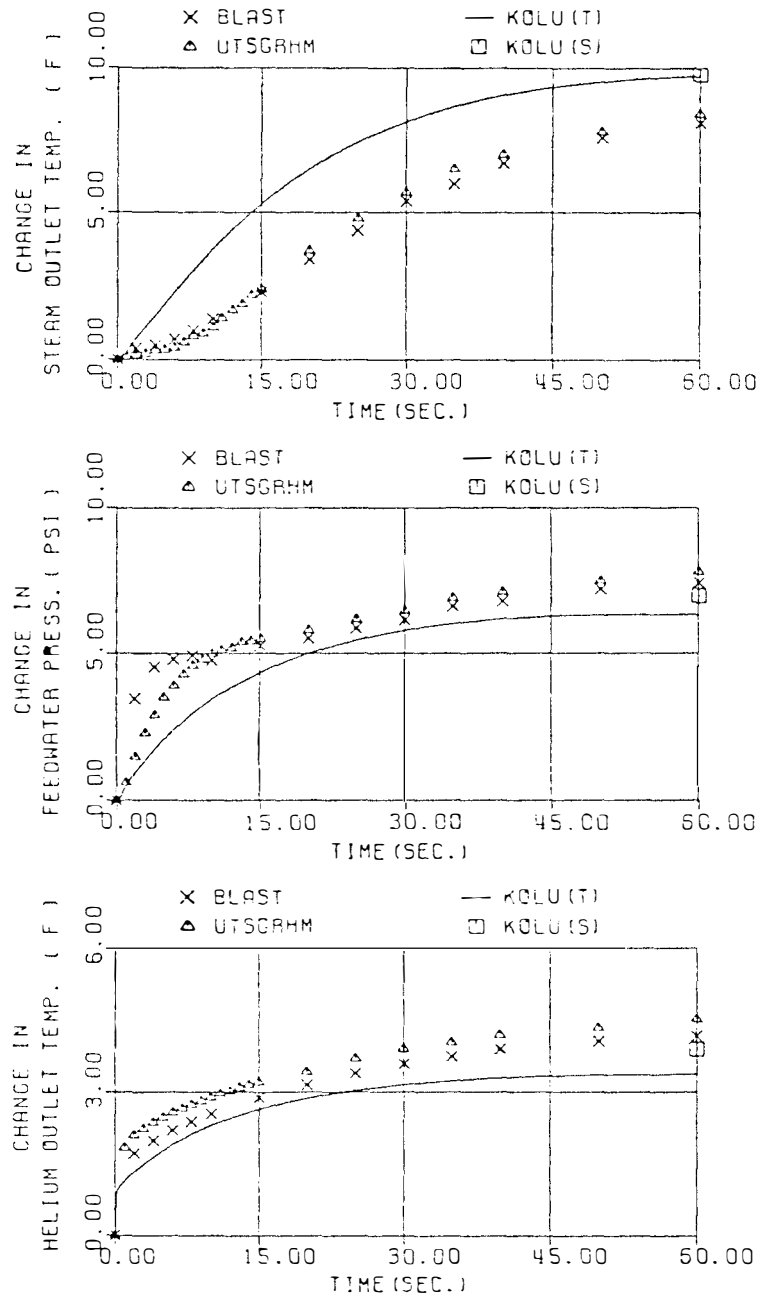
Figure 7.6.3. Comparison of Transient Responses to 1 Lbm/Sec per Module Step Increase in Helium Mass Flow Rate for Three Models.

UTSGRHM is a model with fewer sections. It employs one section for the economizer, two sections for the evaporator and one section for superheater I and superheater II each. The flow regimes used include subcooled convection, nucleate boiling, film boiling and superheat convection.

On the steam/water side, UTSGRHM solves the conservation of energy by using an explicit integration method and assuming the quasistatic form for the evaporator region. The pressure is calculated by employing the quasistatic form of the momentum equation or the thermodynamic equation for the saturation region. The mass flow rate in regions except the subcooled convection is calculated by using the orifice equation.

On the helium side, a constant pressure and a constant mass flow rate along the axial direction is assumed.

Responses for three perturbations are given for comparison.

1. 0.05 lbm/sec per tube step increase in the feedwater mass flow rate

As shown in Figure 7.6.1, the comparison indicates that KOLU(T) has larger responses (in the sense of absolute value) in the steam outlet temperature, helium outlet temperature and the feedwater pressure than BLAST and UTSGRHM have. In the response of feedwater pressure, KOLU displays a fast pressure change while both BLAST and UTSGRHM show slower pressure changes. However, the steady state predictions of these three state variables by KOLU(S) are quite close to KOLU(T).

2. 10°F step increase in the helium inlet temperature

In Figure 7.6.2, the changes in the helium outlet temperature are quite consistent for all three models. But the changes in the steam outlet temperature and feedwater pressure are larger in KOLU(T) than those in BLAST and UTSGRHM. This difference may be due to the effects of using different parameters, correlations and model structures in each model, since the steady state values predicted by KOLU(S) are close to the final observed responses in KOLU(T).

3. 1 lbm/sec per module step increase in the helium mass flow rate

In Figure 7.6.3, the change in the steam outlet temperature obtained in KOLU(T) is larger than those obtained by BLAST and UTSGRHM. But the steady state value predicted by KOLU(S) is in good agreement with the final observed value in KOLU(T). In the feedwater pressure and helium outlet temperature responses, the values predicted by KOLU(S) are close to those obtained in BLAST and UTSGRHM. However the differences in responses among the three models are small.

It is concluded from the comparisons shown in Figure 7.6.1 through Figure 7.6.3, that the transient responses obtained with KOLU are consistent with the responses obtained with BLAST and UTSGRHM.

CHAPTER 8

CONCLUSIONS AND RECOMMENDATIONS

A detailed, nonlinear, many lump once-through steam generator model was developed. It was run successfully and gave plausible results.

It is concluded from the model testing and discussions that the detailed, nonlinear transient model with the lumping case of two sections in each flow regime developed in this research is practical and suitable for representing the distributed-parameter dynamics for the Fort St. Vrain once-through steam generator. The steady state calculation presented in this research is reliable and useful in supplementing the dynamic study. The most suitable working range of the model is in high mass velocity (greater than 1.0×10^6 lbm/ft^2-hr) since the homogeneous model in the two phase flow is assumed.

To extend the use of the model to low mass velocity, it is necessary to include the separated flow model in the two phase flow system so that the state variables, the correlations used and properties are within the range of interest.

For a complicated geometry and a large spatial variation of state variables, it is inadequate to use a small number of sections to study steam generator dynamics. This is shown in the results for two lumping cases. To select the adequate number of sections for dynamic modeling, it is suggested first to perform the steady state calculations. Then from the resultant steady state distributions, one determines the number of sections to be used. In general, for situations with high slopes of

state variables and/or with complicated geometry, the model correction factors for momentum [i.e. C_{6i} in equation (3-23) and C_{6gi} in equation (3-27)] and the model correction factors for energy [i.e. C_{7gi} in equation (3-30) and C_{7i} in equation (3-31)] will deviate significantly from unity if a small number of sections is employed in the model. It is best to select the number of sections for each flow regime such that both the correction factors for momentum and the model correction factors for energy are close to one for the flow distributions change during the transient. The range of the correction factors used in this model is from 0.83 to 2.1. Most of them are close to unity.

The study of the nonlinearity of the steam generator outputs in Section 7.5, provides some information about the difference in the outputs between the linear and the nonlinear model for the Fort St. Vrain once-through steam generator. As discussed in Section 7.5, the difference in the helium outlet temperature between the calculated curve (which is nonlinear) and the linear curve is 24°F for a 20% change in the feedwater mass flow rate and for the same amount of change in the feedwater mass flow rate, the difference in the steam outlet temperature is found as 18.5°F. In both cases of a 20% reduction in feedwater mass flow rate and a decrease of 30°F helium inlet temperature, the water inlet pressure displays significant nonlinearity. Therefore, it is concluded, that for large perturbations like a 10% change in the feedwater mass flow rate and/or 30°F change in the helium inlet temperature, only the nonlinear model is adequate.

Applications of the nonlinear model developed here to very large transient analysis and safety analysis require verification of the

validity of property functions and correlations for the state variable

variations encountered. Furthermore, the nonstationary system

correlations should be used if it is necessary.

LIST OF REFERENCES

LIST OF REFERENCES

1. Boure, J. A., A. E. Bergles, and L. S. Tong, "Review of Two-Phase Flow Instability," Nuclear Engineering and Design, Vol. 25, pp. 65-192 (1973).

2. Aritomi, Masanovi, Shigebumi Aoki, and Akira Inoue, "Instabilities in Parallel Channel of Forced-Convection Boiling Upflow System, (II) Experimental Results," Journal of Nuclear Science and Technology, Vol. 14, No. 2, pp. 88-96 (February 1977).

3. Black, D. L., G. E. Klinzing and J. W. Tierney, "Temperature—Viscosity Induced Laminar Instabilities in a Gases Heated Channel," Nuclear Engineering and Design, Vol. 40, pp. 225-233 (1977).

4. Ramshaw, J. D., and J. A. Trapp, "Characteristics, Stability, and Short-Wavelength Phenomena in Two-Phase Flow Equation Systems," Nuclear Science and Engineering, Vol. 66, No. 1, pp. 93-102 (1978).

5. Kerlin, T. W., G. C. Zwingelstein, and B. R. Upadhyaya, "Identification of Nuclear Systems," Nuclear Technology, Vol. 36, No. 1, pp. 7-38 (1977).

6. Kerlin, T. W., and B. R. Upadhyaya, "System Identification in Nuclear Power Plants," Proceedings of the 1977 Joint Automatic Control Conference, Vol. 1, pp. 310-317 (1977).

7. Savery, C. W., W. Kujawa, and H. G. Kwatny, "Nuclear Once-Through Steam Generator Modeling and Simulation, A Review," Mechanical Engineering and Mechanics Department, Drexel University, Philadelphia, Pennsylvania (April 1974).

8. Ray, A., and H. F. Bowman, "A Nonlinear Dynamic Model of a Once-Through Subcritical Steam Generator," Transaction of the ASME, Journal of Dynamic Systems, Measurement, and Control, pp. 332-339 (September 1976).

9. Chen, A. T., "A Digital Simulation for Nuclear Once-Through Steam Generators," Ph.D. Dissertation, The University of Tennessee, Knoxville, Tennessee (1976).

10. Kwatny, H. G., and W. A. Konopacki, "The Modeling of a Once-Through Steam Generator for System Dynamics and Control Studies," Proceedings of the 1977 Joint Automatic Control Conference, Vol. 1, pp. 323-331 (1977).

11. Bruens, N. W. S., J. F. L. M. Brux, D. G. H. Latzko, and B. Vriesema, "Modeling of Nuclear Steam Generator Dynamics," Proceedings of the

Second Power Plant Dynamics, Control and Testing Symposium,
pp. 23-37 (September 1975).

12. Hedrick, R. A., and J. C. Cleveland, "Blast: A Digital Computer
    Program for the Dynamic Simulation of the High Temperature Gas
    Cooled Reactor Reheater—Steam Generator Module," ORNL/NUREG/TM-38,
    Oak Ridge National Laboratory, Oak Ridge, Tennessee (August 1976).

13. Ibid., pp. 13-16.

14. Porsching, T. A., J. H. Murphy, J. A. Redfield, et al., "FLASH-4:
    A Fully Implicit Fortran IV Program for the Digital Simulation of
    Transients in a Reactor Plant," WAPD-TM-840, Bettis Atomic Power
    Laboratory, Pittsburgh (March 1969).

15. Porsching, T. A., J. H. Murphy, and J. A. Redfield, "Stable
    Numerical Integration of Conservation Equations for Hydraulic
    Networks," _Nuclear Science and Engineering_, Vol. 43, pp. 218-225
    (1971).

16. Schuetzenduebel, W. G., "GGA Technology Course on the Fort St. Vrain
    Steam Generators," GAMD-10457, Gulf General Atomic Company,
    San Diego, California (1971).

17. "NRC Information Item 14.11-4; Part I Steam Generator and Reheater
    Physical Characteristics," Information obtained from Oak Ridge
    National Laboratory, Oak Ridge, Tennessee.

18. Schultz, G. M., "Large HTGR Steam Generator Design Verification and
    Support Program—Heat Transfer, Fluid Flow, and Stability,"
    Gulf-GA-A 12808, Vol. II (GA-LTR-5) (1973).

19. Schuetzenduebel, W. G., p. 34.

20. Duchatelle, L., L. DeNucheze, and M. G. Robin, "Departure from
    Nucleate Boiling in Helical Tubes of Liquid Metal Heated Steam
    Generators," Paper 73-HT-57, ASME AIChE Heat Transfer Conference,
    Atlanta, Georgia (August 1973).

21. Collier, J. G., _Convective Boiling and Condensation_, (New York:
    McGraw-Hill, 1972), p. 47.

22. Whitaker, S., _Introduction to Fluid Mechanics_, (Englewood Cliffs:
    Prentice-Hall, 1968), p. 403.

23. Porsching, T. A., et al., "Stable Numerical Integration of
    Conservation Equations for Hydraulic Networks," p. 225.

24. Lee, Ming-Huei, "Dynamic Modeling of Gas-Cooled Fast Breeder Reactor
    (GCFR) Core," Internal Report, Department of Nuclear Engineering,
    The University of Tennessee, pp. 110-113 (August 1974).

25. Bein, M., and R. Yahalom, "Dynamic Simulation of an LMFBR Steam Generator," Proceedings of the Second Power Plant Dynamics, Control and Testing Symposium, pp. 24-1-24-18 (September 1975).

26. Lee, Ming-Huei, pp. 13-20.

27. Srinivasan, P. S., S. S. Nandapurkar, and F. A. Holland, "Pressure Drop and Heat Transfer in Coils," The Chemical Engineer, pp. 113-119 (May 1968).

28. Ito, H., "Friction Factors for Turbulent Flow in Curved Pipes," Journal of Basic Engineering, pp. 123-134 (June 1959).

29. Seban, R. A., and E. F. McLaughlin, "Heat Transfer in Tube Coils with Laminar and Turbulent Flow," Int. J. Heat Mass Transfer, Vol. 6, pp. 387-395 (1963).

30. Owhadi, A., K. J. Bell, and B. Crain, Jr., "Forced Convection Boiling Inside Helically-Coiled Tubes," Int. J. Heat Mass Transfer, Vol. 11, pp. 1779-1793 (1968).

31. Crain, B., Jr., and K. J. Bell, "Forced Convection Heat Transfer to a Two-Phase Mixture of Water and Steam in a Helical Coil," Heat Transfer: Fundamental and Industrial Applications, AIChE Symposium Series, Vol. 69, No. 131 (1973).

32. Gilli, P. V., "Heat Transfer and Pressure Drop for Cross Flow Through Banks of Multistart Helical Tubes with Uniform Inclinations and Uniform Longitudinal Pitches," Nuclear Science and Engineering, Vol. 22, pp. 298-314 (1965).

33. Schultz, G. M., pp. 3-7—3-8.

34. Moody, L. F., "Friction Factors for Pipe Flow," Transactions of the American Society of Mechanical Engineers, Vol. 66, pp. 671-684 (1944).

35. Grimison, E. D., "Correlation and Utilization of New Data on Flow Resistance and Heat Transfer for Cross Flow of Gases Over Tube Banks," Transactions of the American Society of Mechanical Engineers, Vol. 59, pp. 583-594 (1937).

36. El-Wakil, M. M., Nuclear Heat Transport, (Toronto: International Textbook, 1971), p. 252.

37. Miropolskiy, Z. L., "Heat Transfer in Film Boiling of a Steam-Water Mixture in Steam-Generating Tubes," Teploenergetika, Vol. 10, pp. 49-52 (1963), AEC-tr-6252.

38. Chen, J. C., "Correlation for Boiling Heat Transfer to Saturated Fluids in Convective Flow," <u>I&EC Process Design and Development</u>, Vol. 5, No. 3, pp. 322-329 (1966).

39. Schultz, G. M., p. 3-7.

40. Duchatelle, L., et al.

41. Sanders, J. P., "Physical and Thermodynamic Properties of Helium to be Used in Performance Evaluation of Gas-Cooled Reactors," Intra-Laboratory Correspondence, Oak Ridge National Laboratory, Oak Ridge, Tennessee (November 1972).

42. Wilson, Jr., M. P., "Thermodynamic and Transport Properties of Helium," GA-1355, General Dynamics (January 1960).

43. <u>UK Steam Tables in SI Units 1970</u>, (London: Edward Arnold, 1970) pp. 138-155.

44. Bruges, E. A. and M. R. Gibson," Dynamic Viscosity of Compressed Water to 10 Kilobar and Steam to 1500°C," <u>Journal Mechanical Engineering Science</u>, Vol. 11, No. 2, pp. 189-205 (1969).

45. Information provided by Oak Ridge National Laboratory, Oak Ridge, Tennessee.

46. Schuetzenduebel, W. G., p. 34.

47. Hedrick, R. A. and J. C. Cleveland, Personal Communication, Oak Ridge National Laboratory, 1977.

48. J. G. Thakkar, "Development of Identification Technique and Nonlinear Models of the HTGR Plant Components," A Ph.D. Dissertation, Department of Nuclear Engineering, The University of Tennessee (to be published).

VITA

Ming-Huei Lee was born in Taya, Taiwan, Republic of China, on January 2, 1946. His parents are Ho-Tien Lee and the former Yueh-Chin Liao. He attended Taiping Elementary School in Taichung and was graduated from Taiwan Provincial Taichung First Middle School in 1964. The following fall he entered the National Tsing Hua University and received a Bachelor of Science degree in Nuclear Engineering in 1968. In 1970, he received a Master of Science degree in Nuclear Engineering from the Institute of Nuclear Science in National Tsing Hua University. He taught a course in Yuan Pei Medical School in 1970.

He came to the United States in October 1971 and studied solid state dosimetry in Oak Ridge National Laboratory for one year. In 1972, he entered the Graduate School at the University of Tennessee and received the Doctor of Philosophy degree in Nuclear Engineering in August 1978.

He is married to the former Szu-ching Ou of Taichung, Taiwan, Republic of China.